

INCIPIENT MOTION OF COARSE SOLITARY PARTICLES

A THESIS SUBMITTED TO
THE GRADUATE SCHOOL OF NATURAL AND APPLIED SCIENCES
OF
MIDDLE EAST TECHNICAL UNIVERSITY

BY

BESİM GÜLCÜ

IN PARTIAL FULFILLMENT OF THE REQUIREMENTS
FOR
THE DEGREE OF MASTER OF SCIENCE
IN
CIVIL ENGINEERING

FEBRUARY 2009

Approval of the thesis:

INCIPIENT MOTION OF COARSE SOLITARY PARTICLES

submitted by **BESİM GÜLCÜ** in partial fulfillment of the requirements for the degree of **Master of Science in Civil Engineering Department, Middle East Technical University** by,

Prof. Dr. Canan Özgen
Dean, Graduate School of **Natural and Applied Sciences**

Prof. Dr. Güney Özcebe
Head of Department, **Civil Engineering**

Prof. Dr. Mustafa Göğüş
Supervisor, **Civil Engineering Dept., METU**

Examining Committee Members:

Assoc. Prof. Dr. İsmail Aydın
Civil Engineering Dept., METU

Prof. Dr. Mustafa Göğüş
Civil Engineering Dept., METU

Assoc. Prof. Dr. A. Burcu Altan Sakarya
Civil Engineering Dept., METU

Assoc. Prof. Dr. M. Ali Kökpınar
TAKK Dept., DSI

Inst. Dr. Mete Köken
Civil Engineering Dept., METU

Date: 09.02.2009

I hereby declare that all information in this document has been obtained and presented in accordance with academic rules and ethical conduct. I also declare that, as required by these rules and conduct, I have fully cited and referenced all material and results that are not original to this work.

Name, Last name: Besim Gülcü

Signature :

ABSTRACT

INCIPIENT MOTION OF COARSE SOLITARY PARTICLES

Gülcü, Besim

M.Sc., Department of Civil Engineering

Supervisor: Prof. Dr. Mustafa Göğüş

February 2009, 120 pages

In this study the incipient motion of coarse solitary particles having different specific weights and shapes was investigated. A tilting flume of rectangular cross-section having a net working length of 12 m was used through the experiments. The slope of the channel and the discharge in the channel are the two basic variable parameters that determine the initiation of motion. Particles made of cement and mixture of cement and iron dust in certain ratios were used in the experiments with an obstructing element of various heights right behind the particles. Dimensionless hydraulic parameters determined from theoretical analysis were related to each other. Velocity profiles over the flow depths were measured and flow conditions corresponding to critical conditions were evaluated in terms of critical velocities and shear velocities. The findings of this study were compared with the results of similar studies given in the literature.

Keywords: Incipient motion, sediment transport, particle shape, particle size, coarse particles

ÖZ

İRİ KATI MADDELERİN AKIM İÇERİSİNDE İLK HAREKETE GEÇİŞİ

Gülcü, Besim

Yüksek Lisans, İnşaat Mühendisliği Bölümü

Tez Yöneticisi: Prof. Dr. Mustafa Göğüş

Şubat 2009, 120 sayfa

Bu çalışmada farklı özgül ağırlık ve şekillere sahip iri katı maddelerin akım içerisinde ilk harekete geçişleri incelenmiştir. Deneysel boyunca net çalışma uzunluğu 12 m olan, eğimi değiştirilebilen, dikdörtgen kesitli bir kanal kullanılmıştır. Kanalin eğimi ve kanaldaki debi harekete geçişi belirleyen temel değişkenlerdir. Deneysel, çimento ve çimento - demir tozunun belirli oranlarda karıştırılmasıyla elde edilmiş taneler ve bunların hemen arkasına yerleştirilen çeşitli yüksekliklerde hareketi engelleyici elemanlar kullanılmıştır. Teorik analizlerden elde edilen boyutsuz hidrolik parametreler arasında ilişkiler kurulmuştur. Akım derinlikleri boyunca hız profilleri ölçülmüş ve kritik duruma karşı gelen akım şartları, kritik akım hızı ve kritik kayma gerilmesi hızı cinsinden ifade edilmiştir. Bu çalışmada elde edilen neticeler literatürdeki benzer çalışmaların sonuçları ile karşılaştırılmıştır.

Anahtar Kelimeler: İlk harekete geçiş, katı madde hareketi, dane şekli, dane büyüklüğü, iri maddeler

To My Wife and Parents

ACKNOWLEDGEMENTS

This research has been carried out under the supervision of Prof. Dr. Mustafa GÖĞÜŞ in the Hydromechanics Laboratory of the Department of Civil Engineering in the Middle East Technical University.

The author wishes to express his sincere appreciation to Prof. Dr. Mustafa GÖĞÜŞ for his guidance and helpful advice throughout the research.

The technical assistance of author's colleagues and the effort of laboratory staff are gratefully acknowledged.

The author offers sincere thanks to his family for their unshakable faith in him, their patience and confidence in him. They receive many indebted thanks.

TABLE OF CONTENTS

ABSTRACT	iv
ÖZ	v
ACKNOWLEDGEMENTS	vii
TABLE OF CONTENTS	viii
LIST OF TABLES	x
LIST OF FIGURES	xi
LIST OF SYMBOLS.....	xv
CHAPTERS	
I. INTRODUCTION.....	1
I.1. INTRODUCTORY REMARKS	1
I.2. REVIEW OF RELEVANT LITERATURE.....	2
II. THEORY AND THE METHODOLOGY	13
II.1. DIMENSIONAL ANALYSIS	13
II.2. DETERMINATION OF THE EQUIVALENT SEDIMENT DIAMETER.....	18
II.3. ANALYTICAL FORMULATION AND BRAHMS EQUATION.....	20
II.4. ANALYTICAL FORMULATION AFTER GOGUS (1980).....	21
II.5. USE OF THE NEW SHAPE FACTOR	26
III. THE EXPERIMENTAL INVESTIGATIONS	28
III.1. EXPERIMENTAL SETUP	28
III.1.1. Determination of the Flow Rate	30
III.1.2. The Obstructing Element.....	31
III.1.3. Particle Shapes and Sizes	31
III.2. EXPERIMENTAL PROCEDURE.....	36
III.3. ANALYSIS OF EXPERIMENTAL DATA, COMPARISON WITH PREVIOUS STUDY AND DISCUSSION OF RESULTS.....	37

III.3.1. Relationship Between the Entrainment Function and the Grain Reynolds Number	37
III.3.2. Relationship Between the Entrainment Function and the Dimensionless Grain Size	51
III.3.3. Determination and Application of the Equivalent Sediment Diameter	57
III.3.4. Re-analysis of Brahms Equation	66
III.3.5. Determination of the Critical Condition from the Height to Length Ratio of the Particle	70
III.3.6. Evaluation of the Relationship Between the Critical Velocity and the Grain Size	73
III.3.7. Comparison of Present Study with the Study of Novak and Nalluri.....	78
IV. THE EXPERIMENTAL INVESTIGATIONS WITH THE SECOND GROUP OF PARTICLES	84
IV.1. Relationship Between the Entrainment Function and the Grain Reynolds Number	84
IV.2. Relationship Between the Entrainment Function and the Dimensionless Grain Size	87
IV.3. Determination of the Equivalent Sediment Diameter	87
IV.4. Re-analysis of Brahms Equation	96
IV.5. Determination of the Critical Condition from the Height to Length Ratio of the Particle	100
V. CONCLUSIONS AND THE FURTHER RECOMMENDATIONS.....	103
REFERENCES	106
APPENDICES	
A. SIDE-WALL CORRECTION PROCEDURE.....	109
B. EXPERIMENTAL RESULTS	110

LIST OF TABLES

TABLES

Table I-1: f_1 and f_2 coefficients for equations of incipient motion (Novak and Nalluri, 1984).	9
Table III-1: Shapes and dimensions of particles used in the experiments.	34
Table III-2: Defining lengths for particles used in the experiments.....	35
Table B-1: Experimental data.....	111
Table B-2: Experimental data.....	116

LIST OF FIGURES

FIGURES

Figure I-1: Shields diagram (Simons and Senturk, 1992)	3
Figure I-2: Entrainment function versus particle Reynolds number (Novak and Nalluri, 1975).....	5
Figure I-3: $\frac{(V_{cc})_r}{\sqrt{g \cdot d_s \cdot (S_s - 1)}}$ against d_s/R_b (Novak and Nalluri, 1984).....	7
Figure I-4: τ_* against Re_* for single particles and constant d_s/k values (Novak and Nalluri, 1984).....	8
Figure I-5: $(V_{cc})_r/(V_{cc})_s$ against d_s/k (Novak and Nalluri, 1984).....	9
Figure I-6: Shields parameter τ_* as a function of slope for different grain sizes	11
Figure I-7: Critical entrainment function vs. grain Reynolds number for different values of R_b/d_s (Shvidchenko and Pender, 2000).....	11
Figure II-1: Parameters related to the condition of incipient motion	14
Figure II-2: Definition sketches for determination of the equivalent sediment diameter	19
Figure II-3: Definition sketch for present analysis.....	22
Figure II-4: Illustrative sketch for particle dimensions	27
Figure III-1: Experimental setup	29
Figure III-2: Dimensions of the rectangular sharp crested weir.....	30
Figure III-3: Particles used in the experiments.....	32
Figure III-4: τ_* vs. Re_* for cubic particles ($SF= 1.000$, $t/b=1.5/5$, $\gamma_s=1.96 \text{ g/cm}^3$)....	37
Figure III-5: τ_* vs. Re_* for spherical particles ($SF= 0.806$, $t/b=1.5/5$, $\gamma_s = 1.96 \text{ g/cm}^3$)	38
Figure III-6: τ_* vs. Re_* for rectangular prismatic particles ($SF= 1.025 \sim 1.250$, $t/b=1.5/5$, $\gamma_s = 1.96 \text{ g/cm}^3$).....	38

Figure III-7: τ^* vs. Re^* for rectangular prismatic particles ($SF= 0.375 \sim 0.720$, $t/b=1.5/5$, $\gamma_s = 1.96 \text{ g/cm}^3$).....	39
Figure III-8: τ^* vs. Re^* for irregular shaped particles ($SF= 0.905 \sim 1.077$, $t/b=1.5/5$, $\gamma_s = 1.96 \text{ g/cm}^3$).....	39
Figure III-9: R_b/d_s values on τ^* vs. Re^* plane for solitary particles ($SF=0.375\sim$ 1.250 , $t/b=1.5/5$, $\gamma_s = 1.96 \text{ g/cm}^3$).....	41
Figure III-10: τ^* vs. Re^* for solitary particles ($SF= 0.375 \sim 1.250$, $t/b=1.5/5$, $\gamma_s=1.96 \text{ g/cm}^3$).....	42
Figure III-11: Comparison of τ^* vs. Re^* of Defne's Study and Present Study ($SF= 0.375 \sim 1.250$, $\gamma_s=1.96 \text{ g/cm}^3$).....	44
Figure III-12: R_b/d_s versus Re^* as a function of shape factor, SF ($\gamma_s=1.96 \text{ g/cm}^3$)....	45
Figure III-13: τ^* vs. slope for solitary particles, size group 1 ($d_s = 1.24 \text{ cm}$)	46
Figure III-14: τ^* vs. slope for solitary particles, size group 2 ($d_s = 2.48 \text{ cm}$)	46
Figure III-15: τ^* vs. slope for solitary particles, size group 3 ($d_s = 3.72 \text{ cm}$)	47
Figure III-16: τ^* vs. slope for solitary particles, size group 4 ($d_s = 4.96 \text{ cm}$)	47
Figure III-17: τ^* vs. slope for solitary particles, size group 5 ($d_s = 6.20 \text{ cm}$)	48
Figure III-18: Shape factor correction for τ^* vs. slope for $d_s = 1.24 \text{ cm}$	49
Figure III-19: Shape factor correction for τ^* vs. slope for $d_s = 2.48 \text{ cm}$	49
Figure III-20: Shape factor correction for τ^* vs. slope for $d_s = 3.72 \text{ cm}$	50
Figure III-21: Shape factor correction for τ^* vs. slope for $d_s = 4.96 \text{ cm}$	50
Figure III-22: Shape factor correction for τ^* vs. slope for $d_s = 6.20 \text{ cm}$	51
Figure III-23: τ^* vs. d^* for solitary particles.....	52
Figure III-24: Critical entrainment function τ^* vs. dimensionless grain size d^* for different slopes.....	53
Figure III-25: Shape factor correction for τ^* vs. d^* for different slopes.....	55
Figure III-26: Critical entrainment function τ^* vs. dimensionless grain size d^* together with results of Shvidchenko and Pender.....	56

Figure III-27: Equivalent sediment diameters determined from the relationship of hydraulic radius and bed slope ($t/b=1.5/5$).....	58
Figure III-28: τ_* versus Re_* in terms of $(d_s)_e$ ($t/b=1.5/5$).....	59
Figure III-29: $R_b/(d_s)_e$ versus Re_* ($t/b=1.5/5$).....	61
Figure III-30: Comparison of $R_b/(d_s)_e$ versus Re_* curves obtained in present study and Defne's Study.....	62
Figure III-31: $(d_s)_e$ versus d_s and shape factors ($t/b=1.5/5$).....	63
Figure III-32: Critical cross-sectional velocity, V_{cc} vs. $(d_s)_e$	64
Figure III-33: Critical velocity in the vertical, V_{vc} vs. $(d_s)_e$	65
Figure III-34: Critical bottom velocity, V_{bc} vs. $(d_s)_e$	65
Figure III-35: V_{bc} versus $W^{1/6}$ for particles of different shape factors.....	67
Figure III-36: Empirical constant, K , of Brahms equation versus shape factor, SF ...	68
Figure III-37: Comparison of relation between K and shape factor, SF	68
Figure III-38: K versus product of shape factor and relative depth.....	69
Figure III-39: Comparison of relation between K and product of shape factor and relative depth.....	70
Figure III-40: $(Fr_v)_b/\sqrt{\cos\theta}$ versus b/c	71
Figure III-41: $(Fr_v)_b/\sqrt{\cos\theta}$ versus $(SF)(b/c)$	72
Figure III-42: Comparison of $(Fr_v)_b/\sqrt{\cos\theta}$ versus $(SF)(b/c)$	73
Figure III-43: Critical cross-sectional velocity versus grain size.....	74
Figure III-44: Critical velocity in the vertical versus grain size.....	76
Figure III-45: Critical bottom velocity versus grain size.....	77
Figure III-46: Variation of τ_* and Re_* based on $(d_s)_e$ as a function of d_s/k	79
Figure III-47: τ_c versus grain size.....	80
Figure III-48: Densimetric Froude number in terms of cross-sectional velocity versus relative depth.....	81
Figure III-49: The relationship between $(SF)^{0.5}(Fr_v)_d$ and d_s/R_b	82
Figure IV-1: Comparison of τ_* vs. Re_* for particles with $\gamma_s=1.96 \text{ g/cm}^3$ and $\gamma_s=2.36 \text{ g/cm}^3$	85

Figure IV-2: Comparison of R_b/d_s versus Re^* as a function of shape factor, SF for particles with $\gamma_s=1.96 \text{ g/cm}^3$ and $\gamma_s=2.36 \text{ g/cm}^3$	86
Figure IV-3: Comparison of trend lines for particles with $\gamma_s=1.96 \text{ g/cm}^3$ and $\gamma_s=2.36 \text{ g/cm}^3$	88
Figure IV-4: Equivalent sediment diameters determined from the relationship of hydraulic radius and bed slope.....	89
Figure IV-5: Comparison of $R_b/(d_s)_e$ versus Re^* curves obtained for both sediment groups having different specific weights	90
Figure IV-6: Variation of $(d_s)_e$ with d_s	92
Figure IV-7: Critical cross-sectional velocity, V_{cc} vs. $(d_s)_e$	93
Figure IV-8: Critical velocity in the vertical, V_{vc} vs. $(d_s)_e$	94
Figure IV-9: Critical bottom velocity, V_{bc} vs. $(d_s)_e$	95
Figure IV-10: V_{bc} versus $W^{1/6}$ for particles of different shape factors.....	97
Figure IV-11: V_{bc} versus $W^{1/6}$ for cubic and spherical particles of $\gamma_s=1.96 \text{ g/cm}^3$ and $\gamma_s=2.36 \text{ g/cm}^3$	98
Figure IV-12: Comparison of K vs SF values of particles with $\gamma_s=1.96 \text{ g/cm}^3$ and $\gamma_s=2.36 \text{ g/cm}^3$	99
Figure IV-13: Comparison of K vs $(SF)(d_s/R_b)$ values of particles with $\gamma_s=1.96 \text{ g/cm}^3$ and $\gamma_s=2.36 \text{ g/cm}^3$	100
Figure IV-14: Comparison of b/c vs $(Fr_v)_b/\sqrt{\cos\theta}$ values of particles with $\gamma_s=1.96 \text{ g/cm}^3$ and $\gamma_s=2.36 \text{ g/cm}^3$	101
Figure IV-15: Comparison of $(SF)(b/c)$ vs $(Fr_v)_b/\sqrt{\cos\theta}$ values of particles with $\gamma_s=1.96 \text{ g/cm}^3$ and $\gamma_s=2.36 \text{ g/cm}^3$	102

LIST OF SYMBOLS

a	: Maximum width of a grain perpendicular to flow direction and parallel to the channel bottom
a_l	: Length of the major axis of the particle used in the shape factor equation by Novak and Nalluri (1975).
A_d	: Drag area of the grain
A_f	: Surface area of the grain related with the frictional force
A_l	: Lift area of the grain
b	: Height of a grain resting on channel bed
b_l	: Length of the intermediate axis of the particle used in the shape factor equation by Novak and Nalluri (1975).
B	: Channel width
c	: Maximum length of a grain in flow direction parallel to channel bottom
c_l	: Length of the minor axis of the particle used in the shape factor equation by Novak and Nalluri (1975).
C_1, C_2, C_3	: Empirical coefficients in equation (2.33)
C_d	: Drag coefficient of grain
C_l	: Lift coefficient of grain
C_D, C_F	: Empirical coefficients in equation (2.30)
C_L, C_W	: Empirical coefficients in equation (2.30)
C_Q	: Discharge coefficient
D	: Triaxial diameter of particle
d	: Grain size, usually sieve diameter
d^*	: Dimensionless grain diameter
d_{16}, d_{84}	: Grain size for which 16 % and 84 % are finer, respectively
d_g	: Mean particle diameter based on granulometric curve for mixed-size grains
d_s	: Nominal diameter of sediment particle based on volume

$(d_s)_e$: Equivalent sediment diameter
f_1, f_2	: Empirical coefficients for the general form of the relationship between densimetric Froude number and relative depth
f_i	: Friction factor for flow around surface of grain
F_d	: Drag force acting on a grain
F_f	: Friction force acting on a grain
F_l	: Lift force acting on a grain
F_w	: Submerged weight of a grain
$(Fr_v)_b$: Densimetric Froude number in terms of average flow velocity and particle height
$(Fr_v)_d$: Densimetric Froude number in terms of average flow velocity and particle diameter
Fr_*	: Densimetric Froude number in terms of shear velocity
g	: Gravitational acceleration
h	: Depth of flow section
H	: Measured head above crest of weir, excluding velocity head.
I	: Intensity of sediment motion
k	: Roughness of bed.
K, K', K''	: Empirical constants for Brahms equation
L	: Characteristic length of a particle
L_l	: Effective length of crest of a weir
l_1, l_2, \dots, l_8	: Side lengths for the particles used in the experiments
m	: Number of particle displacements on area of interest in a time interval T
n	: Manning roughness coefficient
n_b	: Manning roughness coefficient of the bed
n_{eq}	: Equivalent Manning roughness coefficient
n_w	: Manning roughness coefficient of the channel walls
N	: Number of surface particles on area of interest
p	: Height of sharp crested weir

P	: Wetted perimeter
P_b, P_w	: Wetted perimeters of the bed and the walls, respectively
q_{s*}	: Einstein bed load parameter
Q	: Volumetric discharge over weir
R	: Hydraulic mean radius of conveyance
R_b	: Effective hydraulic radius corresponding to bed only
$(R_b)_c$: Critical effective hydraulic radius corresponding to bed only
Re^*	: Grain Reynolds number
S	: Slope of flow
S_c	: Critical slope
S_s	: Specific gravity of sediment
SF	: Shape factor for a sediment particle
t	: Height of obstructing element
T	: Time interval of observation in determining intensity of transport
$(u^*)_c$: Critical shear velocity
V	: Velocity of flow
V_{bc}	: Critical bottom velocity
V_{cc}	: Critical mean velocity in the cross-section
V_{vc}	: Critical mean velocity in the vertical
$(V_{cc})_r$: Critical velocity of single particle on rough fixed bed
$(V_{cc})_s$: Critical velocity of single particle on smooth fixed bed
W	: Weight of a sediment grain
α_d	: Correction coefficient for drag area of grain
α_f	: Correction coefficient for friction area of grain
α_l	: Correction coefficient for lift area of grain
α_v	: Correction coefficient for volume of grain
β_d	: Moment arm coefficient for drag force on exerted grain
β_f	: Moment arm coefficient for friction force exerted on grain
β_l	: Moment arm coefficient for lift force exerted on grain

β_w	: Moment arm coefficient for submerged weight of grain
$\Delta\rho$: Difference between ρ_s and ρ
ϕ	: Angle of repose
γ	: Specific weight of fluid
γ_s	: Specific weight of sediment particle
ν	: Kinematic viscosity of fluid
θ	: Angle of bed slope
ρ	: Density of fluid
ρ_s	: Density of sediment particle
σ	: Particle size distribution
τ^*	: Entrainment function, Shields parameter
$(\tau^*)_c$: Critical value of entrainment function for incipient motion
τ_0	: Bed shear stress
τ_c	: Critical bed shear stress
ξ	: Fraction indicating the part of the total area of the particle exposed to flow
\forall	: Volume of the grain

CHAPTER I

INTRODUCTION

I.1. Introductory Remarks

The beginning of particle motion has been one of the main questions in sediment transportation since very old times and has been named in many ways: Initiation of motion, inception of motion, incipient motion, threshold of motion... all explain the same critical condition. The earliest research about this critical condition has been made by Brahms in 1753 (Raudkivi, 1967), in which he resulted with the equation:

$$V_{bc} = K \cdot W^{1/6} \quad (1.1)$$

where W is the weight of the grain, K is an empirical constant and V_{bc} is the competent velocity of the flow at the particle level at which particle starts moving.

Even though many researchers have studied on the subject of incipient motion for more than two centuries after Brahms, the effect of particle shape has not been examined explicitly until the study of Gogus and Defne (2005). Defne (2002) has aimed to clarify the effect of shape and size of particles having constant specific weight on the threshold of motion. In his study, the effect of shape and size of solitary particles on the initiation of motion has been separately studied over smooth channel bed when the particles resting behind an obstruction of known height. Based on the earlier preliminary experiments conducted over various rough surfaces regarding the initiation of particle motion it was found that the coarse solitary particles resting over rough surfaces could be represented as if they were resting just behind an obstructing element having heights varying between 1/5 and 2/5 of the particle height. This obstruction height to particle height ratio used in Defne's study was 1/5.

The aim of this study is to investigate the effect of obstacle height behind the particle and specific weights of particles, as being two important parameters, on the initiation of particle motion. For these reasons a series of experiments were conducted with solitary particles of various shapes having specific weights of $\gamma_s = 1.96 \text{ g/cm}^3$ and 2.36 g/cm^3 and obstacle height to particle height ratios of 1/5 and 1.5/5.

Up to now, many researchers have dealt in the problem of determination of the critical condition for particle motion. A detailed review of the relevant literature is given in section I-2. Theory and methodology are explained in Chapter II. The experimental investigations on the effect of obstacle height is presented and discussed in details in Chapter III. In Chapter IV the results of experiments about the specific weight effect is discussed and finally, conclusion and further recommendations are given in Chapter V.

I.2. Review of Relevant Literature

At the topic of incipient motion of particles, Albert Frank Shields is one of the most reputable researcher. What Shields did was a dimensional analysis of the question. Since there are many variables concerned with the problem after the analysis, he simplified the problem for some certain conditions and he defined the parameters affecting the initiation of motion and resulted with the relation (Yalin, 1977):

$$\frac{\tau_c}{(\gamma_s - \gamma) \cdot d} = f\left(\frac{(u^*)_c \cdot d}{\nu}\right) \quad (1.2)$$

where:

- τ_c : critical bed shear stress
- γ_s : specific weight of the particle
- γ : specific weight of the fluid
- d : grain size
- $(u^*)_c$: critical shear velocity
- ν : kinematic viscosity of the fluid

The word “critical” and the subscript “c” are used to define the conditions at the initiation of motion. In general, bed shear stress is denoted by τ_0 and the term $\frac{\tau_0}{(\gamma_s - \gamma) \cdot d}$ is named as *Shields parameter* or *entrainment function*. It is equivalent to *densimetric Froude number* or *dimensionless shear stress* and it is usually denoted as τ^* or Fr^* . The term, $\frac{(u^*)_c \cdot d}{\nu}$, on the right hand side of above relation is named as *grain Reynolds number* or *boundary Reynolds number* and usually referred as Re^* . The graph that Shields obtained is given in Figure I-1. It is applicable to fully developed turbulent flow within the ranges of sediment sizes from 0.4 mm to 3.4 mm.

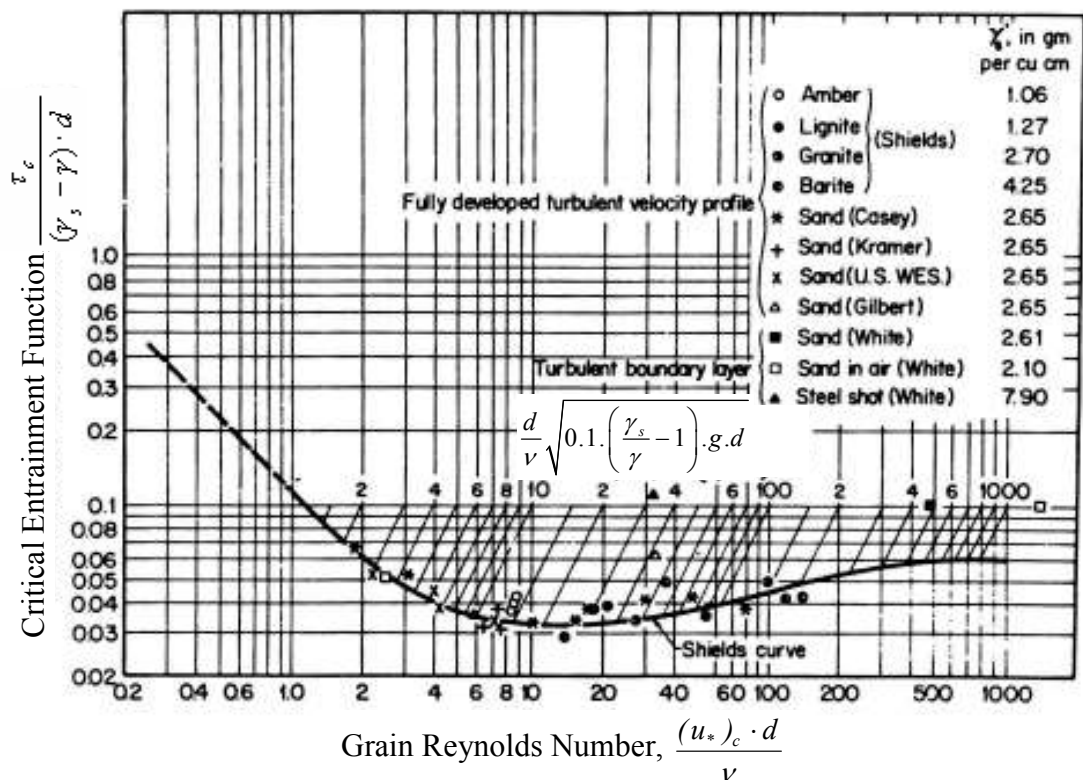


Figure I-1: Shields diagram (Simons and Senturk, 1992)

Novak and Nalluri (1975) have investigated the condition of incipient motion in circular conduits and rectangular flumes with fixed smooth beds and free surface

flow. They have used a tilting flume. The experiments were conducted in circular conduits of *152 mm* diameter and *305 mm* diameter, and in a rectangular flume of *305 mm* width. The lengths of the channels were *10 m*, *8 m* and *15 m* respectively. Novak and Nalluri have worked with sand, gravel, plastic, anthracite, and lead particles. The sand and gravel sizes ranged from *0.6 mm* to *50 mm*. The particle shape factor they have utilized was equal to $\frac{c_1}{\sqrt{a_1 \cdot b_1}}$, where c_1 is the minor axis and a_1 and b_1 are other two axes. The plastic particles had a shape factor varying between *0.6~ 0.95* while the shape of anthracite particles were quite comparable to natural sands. The lead particles were rather spherical with shape factors changing between *0.77~ 0.98*. Specific gravities of the particles were *1.18*, *1.6* and *11.74*, for plastic, anthracite and lead particles, respectively.

At the end of their research, Novak and Nalluri have obtained the relations for a range of $10 < Re_* < 1000$:

$$\tau_* = 0.065 \cdot (Re_*)^{-0.52} \quad (1.3)$$

$$\tau_* = 0.06 \cdot (Re_*)^{-0.61} \quad (1.4)$$

for the rectangular channel and for the channels with circular cross section, respectively. The comparison of their result with the Shields diagram is given in Figure I-2.

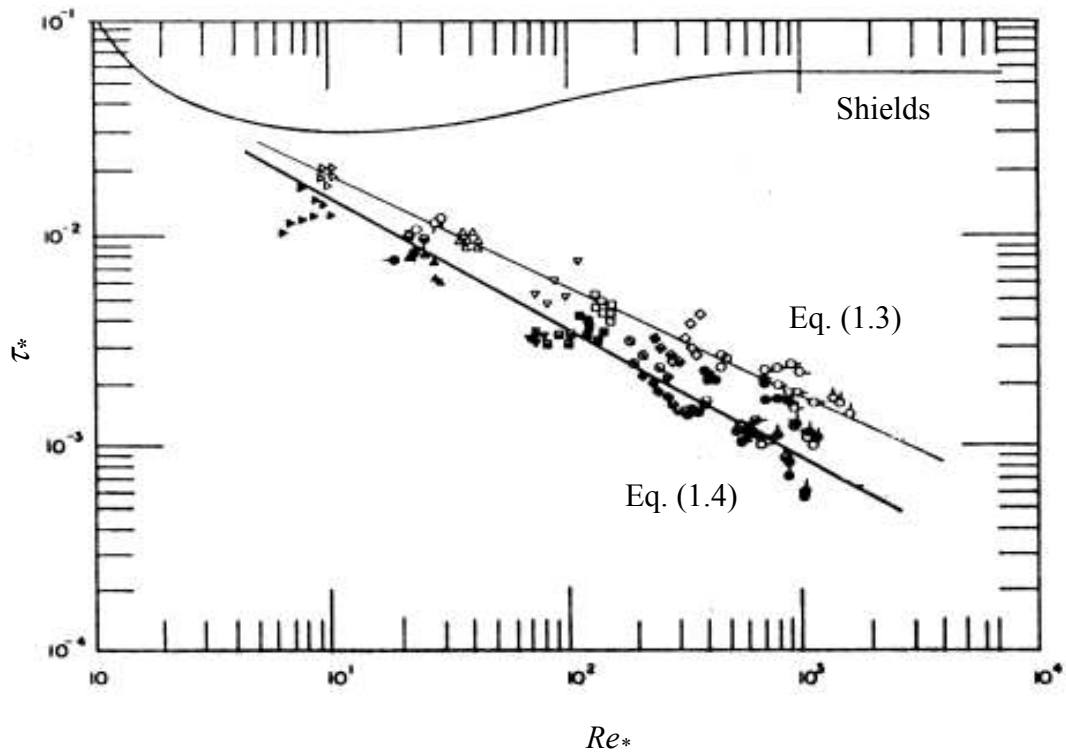


Figure I-2: Entrainment function versus particle Reynolds number
(Novak and Nalluri, 1975)

In terms of critical cross-sectional velocity of flow, V_{cc} , the equations are represented as:

$$V_{cc} = 0.17 \cdot (S_s - 1)^{1/2} \cdot d_s^{0.24} \quad (1.5)$$

$$V_{cc} = 0.16 \cdot (S_s - 1)^{1/2} \cdot d_s^{0.16} \quad (1.6)$$

for the rectangular channel and for the channels with circular cross section, respectively. Here S_s is the specific gravity of the sediment and d_s , is the nominal diameter of sediment particle.

In terms of critical shear stress, τ_c , the equations are given as:

$$\tau_c = 0.128 \cdot (S_s - 1) \cdot d_s^{0.4} \quad (1.7)$$

for rectangular channel, and

$$\tau_c = 0.104 \cdot (S_s - 1) \cdot d_s^{0.4} \quad (1.8)$$

for circular channels. Here τ_c is in N/m^2 and d_s is in mm.

In order to decrease the effect of channel shape, Novak and Nalluri proposed to analyze the results in terms of relative depth and presented the equation:

$$\frac{V_{cc}}{\sqrt{g \cdot d_s \cdot (S_s - 1)}} = 0.61 \cdot \left(\frac{d_s}{R} \right)^{-0.27} \quad (1.9)$$

where, relative depth d_s/R is the ratio of particle diameter to hydraulic mean radius of conveyance. The term, $\frac{V_{cc}}{\sqrt{g \cdot d_s \cdot (S_s - 1)}}$, on the left hand side is denoted as $(Fr_v)_d$

and it is the densimetric Froude number in terms of average flow velocity and particle diameter. This equation is valid for the range of $0.01 < d_s/R < 1$.

In their next study, Novak and Nalluri (1984) have studied on the incipient motion of single and grouped particles on smooth fixed and also rough fixed beds with roughness smaller than the particle size. The experiments were done in tilting flumes with circular and rectangular cross sections. The circular section flumes were of 300 mm diameter having length of 15 m and 6 m, respectively. Rectangular section flume was of 300 mm width and 15 m length. It was artificially roughened. The smaller roughness sizes (0.3 mm, 0.42 mm) were achieved by gluing waterproofed sand paper to the bed while the larger roughness sizes (1.44 mm, 2.2 mm, 4.2 mm) were achieved by sticking coarse gravel and sand particles to the bed. Equivalent diameter sizes of particles were from 0.6 mm to 50 mm and average relative density was 2.56. In each set of the experiments, particle sizes were always larger than the roughness sizes.

They analyzed the data from the investigation of incipient motion of discrete particles on beds with various roughness elements and presented the graph shown in

Figure I-3. Here, R_b is the effective hydraulic radius corresponding to bed only and $(V_{cc})_r$ is the critical cross-sectional velocity of flow for a single particle on a rough fixed bed. An average approximate relationship for the entire data suggests the following equation:

$$\frac{(V_{cc})_r}{\sqrt{g \cdot d_s \cdot (S_s - 1)}} = 0.54 \cdot \left(\frac{d_s}{R_b}\right)^{-0.38} \quad (1.10)$$

For comparison they have presented the graph shown in Figure I-3, in which the modified Shields equation (using the Strickler's equation for Manning roughness n) and Equation (1.9) applicable to single particles on a smooth bed were shown. As can be seen from Figure I-3 and the constants in Equations (1.9) and (1.10), the difference between these two cases of single particle on smooth or rough beds is not large particularly for relatively high values of d_s/R_b , with the critical velocity for a given set of values of d_s , S_s , and R_b always being bigger for the rough than the smooth bed.

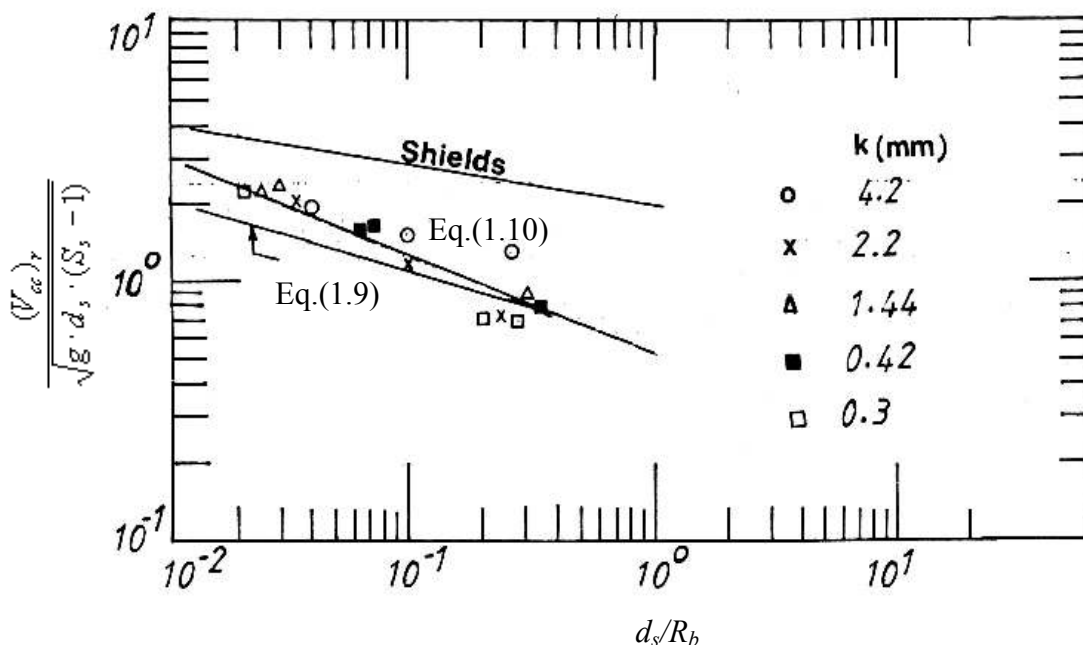


Figure I-3: $\frac{(V_{cc})_r}{\sqrt{g \cdot d_s \cdot (S_s - 1)}}$ against d_s/R_b (Novak and Nalluri, 1984)

In case of rough fixed beds and single particles, ratio of particle diameter to roughness height, k , plays an important role. Novak and Nalluri obtained the graph in Figure I-4, which is quite similar to the well-known Nikuradse graph showing the friction coefficient as a function of Reynolds number. The graph indicates that the value of τ_* will be a function of d_s/k for Re_* well above 1000.

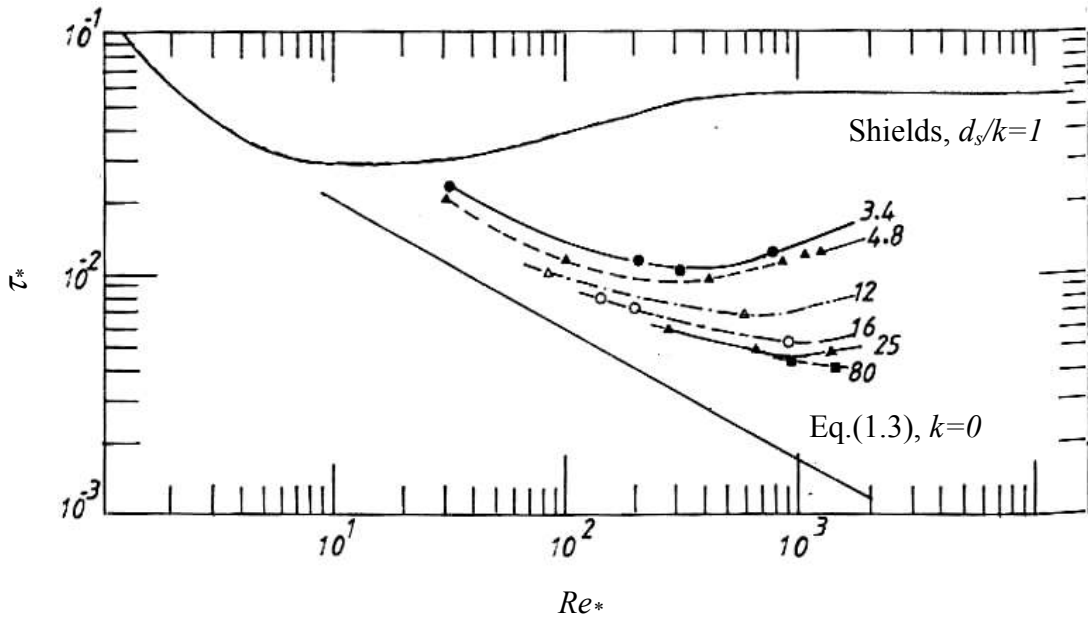


Figure I-4: τ_* against Re_* for single particles and constant d_s/k values
(Novak and Nalluri, 1984)

The effect of d_s/k ratio on the critical condition is given in Figure I-5. When the critical velocities of single particles on smooth fixed beds and on rough fixed beds are compared, a representative equation in the following form is obtained within the range of $75 > d_s/k > 2$

$$\frac{(V_{cc})_r}{(V_{cc})_s} = 1 + 1.43 \left(\frac{d_s}{k} \right)^{-0.4} \quad (1.11)$$

k : roughness of the bed

$(V_{cc})_s$: critical cross-sectional velocity of flow at which single particles on smooth beds move.

Figure I-5 shows this relation and indicates that the effect of d_s/k diminishes for d_s/k values greater than 100.

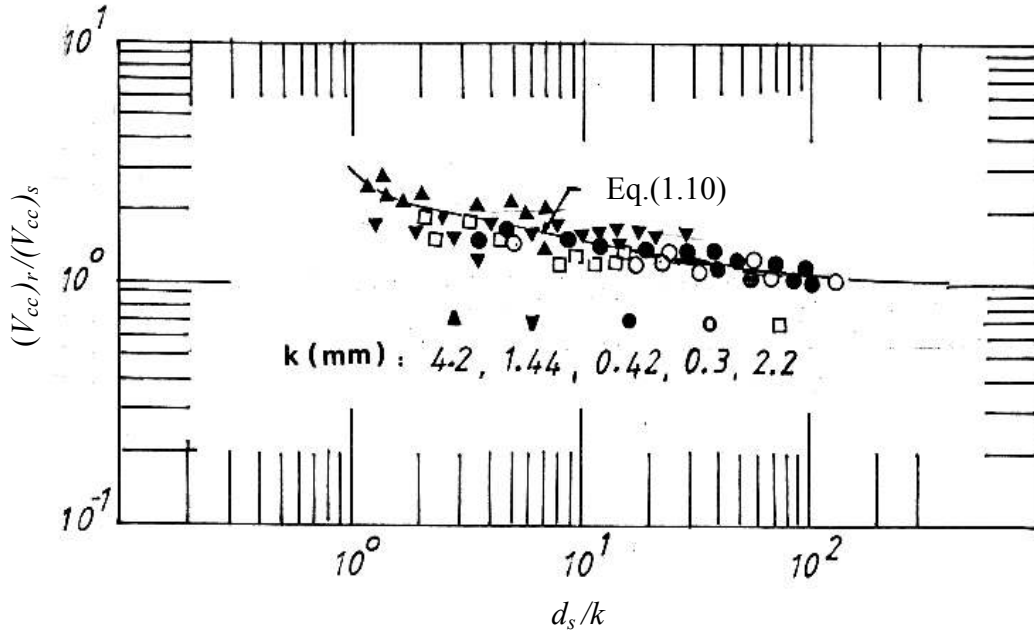


Figure I-5: $(V_{cc})_r / (V_{cc})_s$ against d_s / k (Novak and Nalluri, 1984)

When equations (1.9) and (1.10) are compared it is seen that all the equations are of the type:

$$\frac{V_c}{\sqrt{g \cdot d_s \cdot (S_s - 1)}} = f_1 \cdot \left(\frac{d_s}{R}\right)^{f_2} \quad (1.12)$$

Here, f_1 and f_2 are two empirical constants given in Table I-1.

Table I-1: f_1 and f_2 coefficients for equations of incipient motion (Novak and Nalluri, 1984).

	f_1	f_2	Eq.
Smooth bed single particles	0.61	-0.27	(1.9)
Rough bed single particles	0.54	-0.38	(1.10)
Rough and smooth bed touching particles	0.50	-0.40	-
Movable bed ($d_s = k$)	1.7 ~ 1.9	-0.095 ~ -0.167	-
Note: Range of experiments $0.01 < d_s / R < 0.3$, $3.5 < d_s / k \leq \infty$			

The ratio of flow depth to grain diameter plays an important role in critical conditions for sediment motion. Shvidchenko and Pender (2000) have studied the effect of relative depth on the incipient motion of coarse uniform sediments. Shvidchenko and Pender have conducted the experiments in a 0.3 m wide by 0.3 m deep tilting flume with a working length of 6.5 m . Coarse sand and gravel particles were grouped into eight uniform fractions ranging in size from 1 mm to 14 mm . Mean grain sizes were $1.5, 2.4, 3.4, 4.5, 5.65, 7.15, 9.0, 12.0$ with geometric standard deviation in-between $1.08\sim 1.26$. In each of the experiments, a sediment layer with 5 cm uniform thickness was laid and leveled prior to the experiment. After the flume was filled with water, flow was gradually increased to the desired value, besides ensuring the uniform flow conditions were always satisfied. The slope values varied between 0.0019 and 0.0287 , and flow depth varied between 0.006 and 0.136 m . Corresponding mean velocities and Froude numbers were within ranges $0.06\sim 1.07\text{ m/s}$ and $0.17\sim 1.17$, respectively. Sediment transport rates ranged from $0.0043\text{ gs}^{-1}\text{m}^{-1}$ up to $62.4\text{ gs}^{-1}\text{m}^{-1}$.

Shvidchenko and Pender deduced that the Shields parameter τ_* is dependent on the bed slope for uniform flow. They have stated that their deduction is also satisfied with the prior results obtained by Bathurst et al. in 1984 and by Graf and Suszka in 1987. This relation is given in Figure I-6. This effect has been explained by the effect of the relative depth, which is denoted as R_b/d_s for narrow channels with width to depth ratio less than about 10 .

Shvidchenko and Pender suggested a family of threshold curves corresponding to different values of R_b/d_s (See Figure I-7). From this figure, they conclude that critical Shields parameter depends on grain Reynolds number Re_* , even at high values of Re_* . This was against most of the previously made assumptions in the literature. If not deficient, this conclusion dethrones the modeling of coarse sediment transportation in reduced scale using sand size sediment. However, to clarify this case further studies with coarser materials at higher Re_* and larger values of R_b/d_s are required.

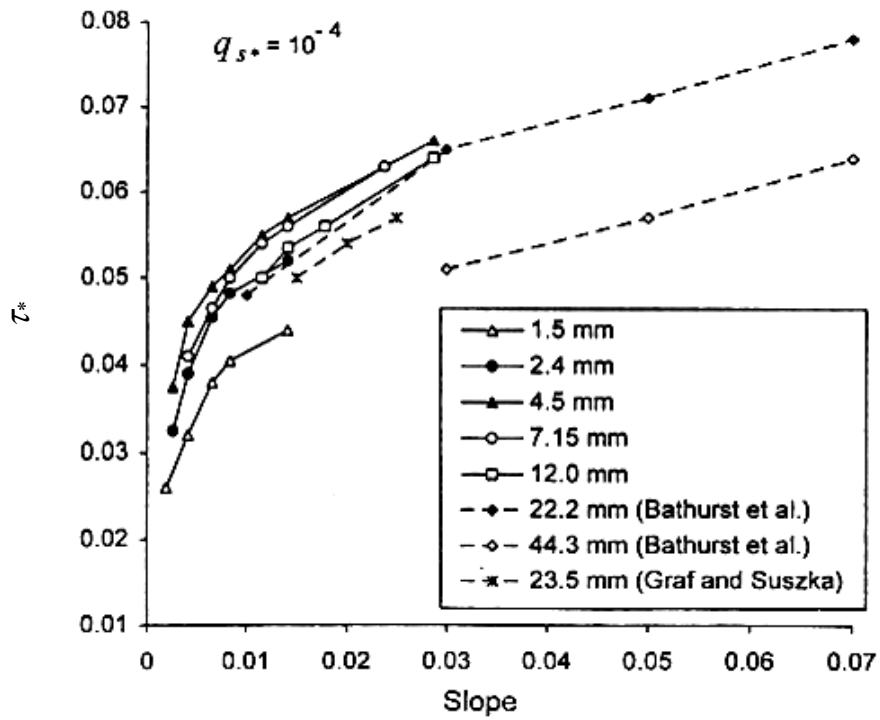


Figure I-6: Shields parameter τ^* as a function of slope for different grain sizes (Shvidchenko and Pender, 2000)

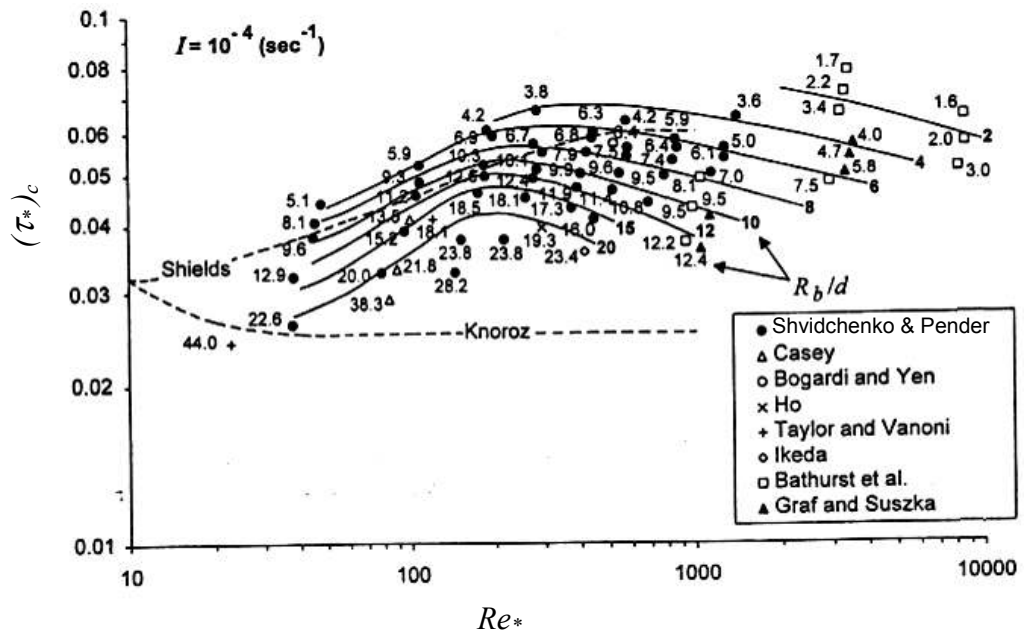


Figure I-7: Critical entrainment function vs. grain Reynolds number for different values of R_b/d_s (Shvidchenko and Pender, 2000)

Dependency of critical Shields parameter both on Re^* and R_b/d_s requires iterative calculations when dealing with the problem. Modifying the diagram proposed by Yalin in 1977, Shvidchenko and Pender related the critical Shields parameter to bed slope and dimensionless grain diameter, d^* . Dimensionless grain diameter, d^* , is determined with the equation:

$$d_* = d \cdot \left[\frac{g \cdot (S_s - 1)}{\nu^2} \right]^{1/3} \quad (1.13)$$

where d is the grain size, and S_s is the specific gravity of sediment particle.

CHAPTER II

THEORY AND THE METHODOLOGY

For incipient motion of sediment particles there are three considerations by means of theory. First one is the application of dimensional analysis to the critical condition of particle motion. This approach is similar to Shields' study on the subject, however, a few more dimensionless parameters are introduced in the present study to take into account more general cases. Second one is the use of *equivalent sediment diameter*, which was introduced by Gogus and Defne (2005). Third approach is based on analytical derivations from equilibrium of forces acting on a sediment grain resting on the bed. In analytical approach, previous researches of Brahm (Stelczer, 1981) and Gogus (1980) are taken as guidelines.

II.1. Dimensional Analysis

Since initiation of motion involves many measurable and non-measurable constraints, dimensional analysis is a good method to obtain a relation between the constraints. Parameters involved in the condition of incipient motion are classified below and are shown in Figure II-1.

Flow characteristics:

V : Velocity of the flow, [L/T],

h : Depth of flow section, [L],

B : Channel width, [L],

S : Slope of the flow,

g : Gravitational acceleration, [L/T²],

t : Height of the obstructing element, [L].

Properties of fluid:

ρ : Density of the fluid, $[M/L^3]$,

ν : Kinematic viscosity of the fluid, $[L^2/T]$.

Properties of the sediment particles:

a : Maximum width of a grain perpendicular to flow direction and parallel to the channel bottom, $[L]$,

b : Height of a grain resting on channel bed, $[L]$,

c : Maximum length of a grain in the flow direction parallel to the channel bottom, $[L]$,

ρ_s : Density of particle, $[M/L^3]$,

SF : Shape factor of particle.

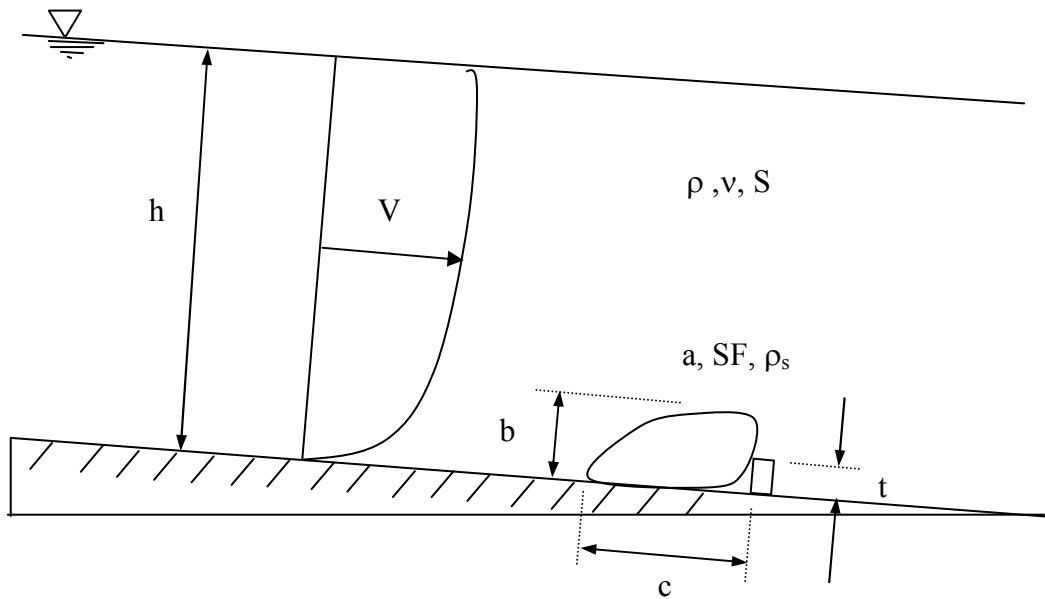


Figure II-1: Parameters related to the condition of incipient motion

The measurements are made under uniform flow conditions. Consequently the slope of the flow, S , is merely the slope of channel bottom. Functional relation between the involved parameters can be written as

$$f(V, g, a, b, c, v, h, B, t, \rho, \rho_s, SF, S) = 0 \quad (2.1)$$

The resulting dimensionless parameters are:

$$f\left(\frac{V}{\sqrt{g \cdot b}}, \frac{V \cdot b}{v}, \frac{b}{h}, \frac{b}{B}, \frac{b}{t}, \frac{b}{c}, \frac{b}{a}, \frac{\rho_s}{\rho}, SF, S\right) = 0 \quad (2.2)$$

$\frac{b}{a}$ and $\frac{b}{c}$ are parameters that are directly related to the shape of the particle and therefore, they are embedded into the shape factor, SF . The term $\frac{b}{t}$ is kept constant and identical in all of the experiments conducted in this study. Therefore the effect of $\frac{b}{t}$ can be overlooked among the other dimensionless parameters. The resulting parameters are

$$f\left(\frac{V}{\sqrt{g \cdot b}}, \frac{V \cdot b}{v}, \frac{b}{h}, \frac{b}{B}, \frac{\rho_s}{\rho}, SF, S\right) = 0 \quad (2.3)$$

In the studies related to the sediment particles, particle size is generally denoted with d , which is usually the sieve diameter of the grain. Another measure of size of particle is the triaxial diameter of the particle, which is denoted by D . It is simply the arithmetic mean of the dimensions of three primary axes of the particle. One more alternative is to use nominal diameter d_s , which is the diameter of a spherical particle having the same volume with the original particle. In expression (2.3), nominal diameter d_s , can be substituted instead of b , which is one of the defining lengths of the particle. This allows the final expressions to be arrived at to be in accordance with the previous studies on the subject of incipient motion.

$$f\left(\frac{V}{\sqrt{g \cdot d_s}}, \frac{V \cdot d_s}{v}, \frac{d_s}{h}, \frac{d_s}{B}, \frac{\rho_s}{\rho}, SF, S\right) = 0 \quad (2.4)$$

The term $\frac{V}{\sqrt{g \cdot d_s}}$ is known as *particle Froude number* and the term $\frac{V \cdot d_s}{\nu}$ is the *grain Reynolds number*. If shear velocity, u_* , is used instead of flow velocity, V ; the effect of slope, S , and flow depth, h , is taken into account implicitly.

$$u_* = \sqrt{\frac{\tau_0}{\rho}} \quad \text{and} \quad \tau_0 = \gamma \cdot h \cdot S \quad (2.5)$$

where τ_0 is the bed shear stress.

The particle Reynolds and Froude numbers can be rewritten in terms of shear velocity:

$$\left[\frac{V}{\sqrt{g \cdot d_s}} \right] \rightarrow \left[\frac{u_*}{\sqrt{g \cdot d_s}} \right] \xrightarrow{\rho \cdot u_*^2 = \tau_0} \left[\frac{\tau_0}{(\gamma_s - \gamma) \cdot d_s} \right] \quad (2.6)$$

$$\left[\frac{V \cdot d_s}{\nu} \right] \rightarrow \left[\frac{u_* \cdot d_s}{\nu} \right] \quad (2.7)$$

Final form of the particle Froude number in (2.6) is named as *densimetric Froude number in terms of shear velocity* and it includes the effect of ratio of sediment density to fluid density, $\frac{\rho_s}{\rho}$, implicitly. It is identical to *entrainment function*. For

the specific case of $B \gg d_s$, the influence of $\frac{d_s}{B}$ on the condition of incipient motion of particle can be neglected. However, the condition of $h \gg d_s$ is not satisfied in most of the experiments conducted in this present study. Therefore, it is not possible to drop the term $\frac{d_s}{h}$. Instead of this term, the use of parameter $\frac{d_s}{R_b}$ is

proposed in order to count for the effect of the side-walls. Here, R_b is the effective hydraulic radius corresponding to the bed only. R_b is obtained using side-wall correction procedure that is proposed by Shvidchenko and Pender (2000). Details of the correction procedure are given in Appendix A. Finally; dimensionless parameters

related to the incipient motion can be represented simply as

$$f\left(\frac{\tau_0}{(\gamma_s - \gamma) \cdot d_s}, \frac{u_* \cdot d_s}{\nu}, \frac{d_s}{R_b}, SF\right) = 0 \quad (2.8)$$

The relationship

$$\frac{u_* \cdot d_s}{\nu} = f\left(\frac{\tau_0}{(\gamma_s - \gamma) \cdot d_s}, \frac{d_s}{R_b}, SF\right) \quad (2.9)$$

is almost the same relationship with the one that Shields utilized in his experiments. However, this time, grain Reynolds number is expressed as a function of entrainment function together with a shape factor and including the effect of relative hydraulic radius.

Another dimensional analysis approach to the state of critical motion is obtained when depth of flow, h , and bed slope, S , are replaced with shear velocity, u_* , and $\frac{\gamma_s - \gamma}{\rho}$ is substituted instead of gravitational acceleration, g , and unit weight of sediment grain, ρ_s , among the involved parameters given in expression (2.1). The resulting parameters are

$$f\left(u_*, \frac{\gamma_s - \gamma}{\rho}, a, b, c, \nu, B, t, SF\right) = 0 \quad (2.10)$$

Imposing the simplifying conditions and following the steps similar to the ones explained in the above analysis; the resulting dimensionless parameters are acquired as

$$f\left(\frac{\rho \cdot u_*^2}{(\gamma_s - \gamma) \cdot d_s}, d_*, SF\right) = 0 \quad (2.11)$$

where d_* is the *dimensionless grain size* or *dimensionless grain diameter* and is explicitly given as

$$d_* = d_s \cdot \left(\frac{\frac{\gamma_s - \gamma}{\gamma} \cdot g}{v^2} \right)^{1/3} \quad (2.12)$$

At the end, entrainment function is represented as function of two parameters.

$$\frac{\tau_0}{(\gamma_s - \gamma) \cdot d_s} = f(d_*, SF) \quad (2.13)$$

II.2. Determination of the Equivalent Sediment Diameter

The term *equivalent sediment diameter* was introduced at a recent study made by Gogus and Defne (2005). They have defined this diameter for a given sediment particle having any arbitrary shape. Equivalent sediment diameter of a particle of certain shape, size and density is the diameter of a sphere having the same density with the particle that has incipient motion under the same flow and channel characteristics. In a rectangular channel of known width if the given particle moves at flow depth h_c and bed slope S_c , diameter of a sphere having the same density as the particle which moves in the same channel under these known flow conditions, h_c and S_c is defined as “*equivalent sediment diameter*” (See Figure II-2). To determine equivalent sediment diameter of a particle of known shape such as cubic particles, first, one should plot family of h_c versus S_c curves of spherical particles stating diameters of them on the curves. Each sphere tested should have at least three data. Then similarly h_c versus S_c curves of cubic particles are plotted following related experiments.

In case of narrow channels having different bed and side-wall characteristics, to consider the side-wall effect, instead of h_c versus S_c , bed hydraulic radius $(R_b)_c$ versus S_c curves should be used in the procedure described above.

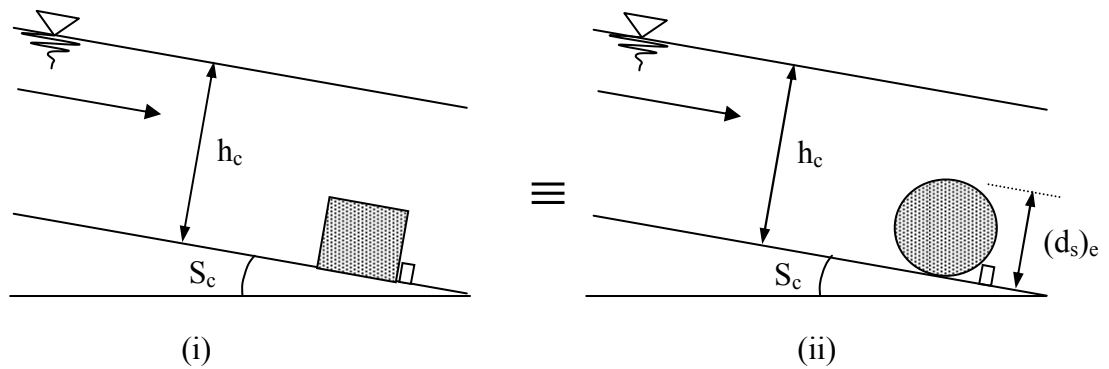


Figure II-2: Definition sketches for determination of the equivalent sediment diameter

- (i) Any arbitrarily shaped particle starting motion at slope S_c and corresponding depth h_c or $(R_b)_c$ in a rectangular channel of width B .
- (ii) Spherical particle starting motion under the same conditions in case (i). i.e. same slope, S_c , and same depth, h_c .

Equivalent sediment diameter of a grain of known specific weight can be expressed as a function of two parameters; nominal diameter and shape factor of the particle:

$$(d_s)_e = f(d_s, SF) \quad (2.14)$$

After the determination of equivalent sediment diameters for different shapes of grains, the relation between nominal diameter, d_s , and equivalent sediment diameter can be given as a function of shape factor, SF . Building up of a graph for such a relation is very important for practical use. It allows straightforward determination of the equivalent sediment diameter from nominal diameter and known shape of the particle.

At the end, the dimensionless relation given by equations (2.9) and (2.13) can be rewritten substituting equivalent sediment diameter, $(d_s)_e$, instead of nominal diameter, d_s .

$$\frac{u_* \cdot (d_s)_e}{\nu} = f\left(\frac{\tau_0}{(\gamma_s - \gamma) \cdot (d_s)_e}\right) \quad (2.15)$$

and

$$\frac{\tau_0}{(\gamma_s - \gamma) \cdot (d_s)_e} = f(d_*) \quad (2.16)$$

II.3. Analytical Formulation and Brahms Equation

The analytical formulation given below is similar to that presented by Brahms in 1753 and repeated for the sake of completeness. Equating the hydrodynamic force on the particle to the resisting force of the particle one obtains:

$$\xi \cdot \frac{\pi d_s^2}{4} \cdot \rho \cdot \frac{V_{bc}^2}{2} = \frac{\pi d_s^3}{6} \cdot (\gamma_s - \gamma) \cdot \tan \phi \quad (2.17)$$

in which, ρ and γ are density and specific weight of fluid respectively.

γ_s : specific weight of the sediment particle,

d_s : diameter of the particle,

V_{bc} : competent velocity of the flow, measured at the level of particle,

$\tan \phi$: friction coefficient,

ϕ : angle of repose,

ξ : fraction indicating the part of the total area of the particle exposed to flow.

$$V_{bc}^2 = \frac{4}{3} \cdot g \cdot \left(\frac{\rho_s}{\rho} - 1\right) \cdot \frac{\tan \phi}{\xi} \cdot d_s \quad (2.18)$$

$$V_{bc}^2 = K'' \cdot d_s \quad (2.19)$$

where $K'' = \frac{4}{3} \cdot g \cdot \left(\frac{\rho_s}{\rho} - 1\right) \cdot \frac{\tan \phi}{\xi}$

$$V_{bc}^6 = (K'' \cdot d_s)^3 \quad (2.20)$$

where d_s^3 is proportional to the weight of sediment particle, W . Then at the condition of incipient motion

$$V_{bc}^6 = K' \cdot W \quad (2.21)$$

Consequently, the critical velocity at threshold of motion is given as

$$V_{bc} = K \cdot W^{1/6} \quad (2.22)$$

where $K = f(d_s, \tan\phi, \rho, \rho_s, SF, R_b)$.

In the present study $\tan\phi$ can be replaced with the height of the obstructing element which is kept constant in all of the tests. Similarly, considering that ρ and ρ_s are constant throughout the experiments, the relationship given above for K can be simplified and expressed as

$$K = f\left(SF, \frac{d_s}{R_b}\right) \quad (2.23)$$

II.4. Analytical Formulation After Gogus (1980)

This analytical formulation is made in the light of Gogus' (1980) analysis, which is similar to that presented by Uzuner in 1977, of ice floe instability below a floating cover. The analogical similarity between the particles used and experimental procedure allows a parallelism in the derivation of the equations. The forces acting on a grain are described in Figure II-3.

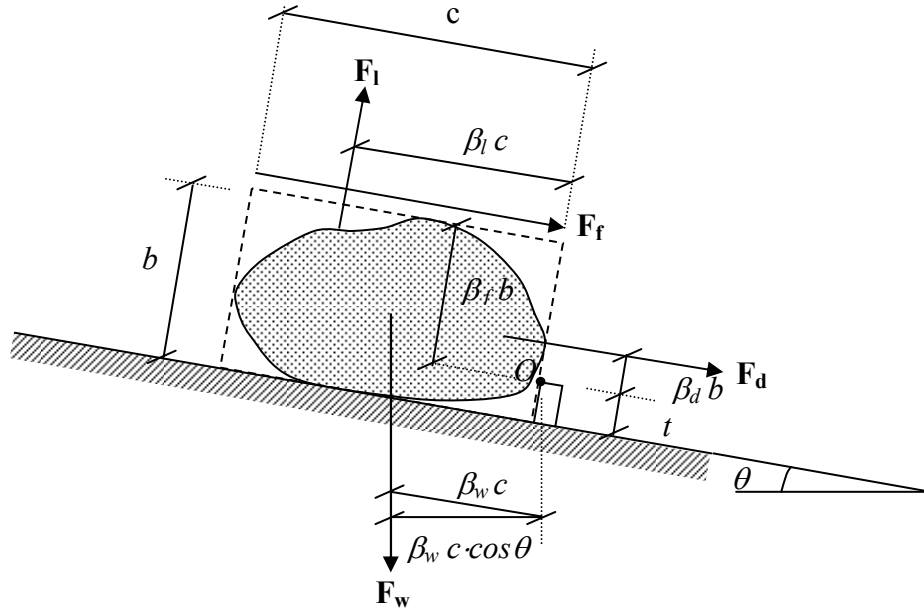


Figure II-3: Definition sketch for present analysis

Drag Force : Drag force is due to the pressure difference between upstream and downstream of the block and given as

$$F_d = C_d \cdot \rho \cdot \frac{V^2}{2} \cdot A_d \quad (2.24)$$

where C_d is the drag coefficient of the grain, ρ is density of fluid, and A_d is the drag area of the grain, which is the projected area of the grain perpendicular to the direction of flow.

Friction Force : Friction force is due to the shear stress acting on the surface of the grain. It is given as

$$F_f = f_i \cdot \rho \cdot \frac{V^2}{8} \cdot A_f \quad (2.25)$$

where f_i is the friction factor for the flow around the surface of the grain and A_f is the surface area of the grain related with the frictional force.

Submerged Weight of the Particle : Generally weight of the particle is a resisting force against the inception of motion of particle. Considering the effect of Buoyancy force together with the weight of the particle implicitly, the resulting force can be written as

$$F_w = (\rho_s - \rho) \cdot g \cdot \nabla \quad (2.26)$$

where g is gravitational acceleration and ∇ and ρ_s are volume and density of the grain, respectively.

Lift Force: Lift force is the force exerted on the block due the difference in pressure distribution normal to the flow direction. Lift force is expressed by

$$F_l = C_l \cdot \rho \cdot \frac{V^2}{2} \cdot A_l \quad (2.27)$$

where C_l is the lift coefficient of the grain and A_l is the lift area of the grain, which is the projected area of the grain parallel to the direction of flow.

As a matter of fact, all the coefficients introduced above, C_d, C_l, f_i may depend upon geometric characteristics of the grain and conditions of flow.

The threshold of motion and consequent rotation of the grain are reached when the sum of the moments of the above forces about a point O , the edge of obstruction that keeps the grain in a stable condition, is zero. This condition is represented by

$$\Sigma M_O = \begin{array}{l} \text{Pressure Drag moment} + \text{Lift moment} + \text{Frictional} \\ \text{Drag moment} + \text{Moment due to the Submerged} \\ \text{Weight of the Particle} \end{array} = 0 \quad (2.28)$$

Application points of the forces are, however, in question, except for the submerged weight. Therefore, as indicated in Figure II-3, the moment arms of these forces will be assumed proportional to either the thickness b of the grain or the length c of the

grain depending whether the force acts in the direction of the flow or normal to the direction of the flow, respectively. Thus the moment arms are; $\beta_d \cdot b$ for drag force, $\beta_l \cdot c$ for lift force, $\beta_f \cdot b$ for friction force and $\beta_w \cdot c \cdot \cos \theta$ for submerged weight, where $\beta_d, \beta_l, \beta_f$ and β_w are all less than 1.

The equations below are derived for rectangular prisms. Nevertheless, they are applicable to grains of all shapes, whether spherical or irregular, with shape factors for correcting the mentioned areas and the volume of the grain considered in the equations. Taking moments of all the forces described above about point O and substituting into Equation (2.28), we obtain the following equation

$$\begin{aligned} \Sigma M_O = & \mp C_d \cdot \rho \cdot \frac{V^2}{2} \cdot \alpha_d \cdot a \cdot b \cdot (\beta_d \cdot b) \\ & + C_l \cdot \rho \cdot \frac{V^2}{2} \cdot \alpha_l \cdot a \cdot c \cdot (\beta_l \cdot c) + f_i \cdot \rho \cdot \frac{V^2}{8} \cdot \alpha_f \cdot a \cdot c \cdot (\beta_f \cdot b) \\ & - (\rho_s - \rho) \cdot g \cdot \alpha_v \cdot a \cdot b \cdot c \cdot (\beta_w \cdot c \cdot \cos \theta) \end{aligned} = 0 \quad (2.29)$$

where $\alpha_d, \alpha_l, \alpha_f$ are correction coefficients for the related areas and α_v is the correction coefficient for the volume of the particle.

The sign of the pressure drag moment being (\mp) depends upon whether the point of application of the net pressure drag, F_d , is below (+) or above (-) point O . The multiplier β_w is the shape factor for correcting the computed volume of the grain. It is the ratio of real volume of the grain to the volume of surrounding rectangular prism. After substituting C_D, C_L, C_F, C_W instead of $\alpha_d \cdot \beta_d \cdot C_d, \alpha_l \cdot \beta_l \cdot C_l, f_i \cdot \alpha_f \cdot \beta_f / 4$ and $\alpha_v \cdot \beta_w$, respectively the above equation becomes

$$\begin{aligned} \Sigma M_O = & \mp C_D \cdot \rho \cdot \frac{V^2}{2} \cdot b^2 + C_L \cdot \rho \cdot \frac{V^2}{2} \cdot c^2 \\ & + C_F \cdot \rho \cdot \frac{V^2}{2} \cdot c \cdot b - C_W \cdot \Delta \rho \cdot g \cdot b \cdot c^2 \cdot \cos \theta \end{aligned} = 0 \quad (2.30)$$

where $\Delta \rho = \rho_s - \rho$. Rearranging the equation

$$\frac{V^2}{\frac{\Delta\rho}{\rho} \cdot g \cdot b} = \frac{2 \cdot C_w \cdot c^2 \cdot \cos\theta}{\mp C_D \cdot b^2 + C_F \cdot b \cdot c + C_L \cdot c^2} \quad (2.31)$$

or

$$\frac{V}{\sqrt{\frac{\Delta\rho}{\rho} \cdot g \cdot b}} = \sqrt{\frac{2 \cdot C_w \cdot \cos\theta}{\mp C_D \cdot \left(\frac{b}{c}\right)^2 + C_F \cdot \left(\frac{b}{c}\right) + C_L}} \quad (2.32)$$

It should be considered that the term on the left hand side of the above equation is the critical densimetric Froude number, $(Fr_v)_b$. It is based on the average flow velocity, at which the sediment particle becomes unstable, and one of the defining lengths that is b . Rearrangement of Equation (2.32) yields

$$(Fr_v)_b = \frac{V}{\sqrt{\frac{\Delta\rho}{\rho} \cdot g \cdot b}} = \sqrt{\frac{\cos\theta}{\mp C_1 \cdot \left(\frac{b}{c}\right)^2 + C_2 \cdot \left(\frac{b}{c}\right) + C_3}} \quad (2.33)$$

where $C_1 = C_D / (2 \cdot C_w)$, $C_2 = C_F / (2 \cdot C_w)$, $C_3 = C_L / (2 \cdot C_w)$. The relationship between $(Fr_v)_b$ and $\frac{b}{c}$ will be determined in the above form with no attempt at attributing physical interpretation to the coefficients C_1 , C_2 , C_3 . Final form of the equation gives the term $\frac{1}{(Fr_v)_b^2}$ expanded as a function of polynomial series in terms of $\frac{b}{c}$

truncated at the third term

$$\frac{1}{(Fr_v)_b^2} = \frac{1}{\cos\theta} \cdot \left[\mp C_1 \cdot \left(\frac{b}{c}\right)^2 + C_2 \cdot \left(\frac{b}{c}\right) + C_3 \right] \quad (2.34)$$

where

$$(Fr_v)_b^2 = \frac{V^2}{\frac{\Delta\rho}{\rho} \cdot g \cdot b} \quad (2.35)$$

Using trigonometric transformations and representing the term $\cos\theta$ in terms of channel bed slope, the final form of the equation is attained as

$$\frac{I}{(Fr_v)_b^2} = \frac{I}{\sqrt{I+S^2}} \cdot \left[\mp C_1 \cdot \left(\frac{b}{c}\right)^2 + C_2 \cdot \left(\frac{b}{c}\right) + C_3 \right] \quad (2.36)$$

II.5. Use of the New Shape Factor

The particle shape for each grain is expressed according to an imaginary rectangular prism including the whole volume of the grain within its body (Gogus and Defne, 2005; Defne, 2002). The crucial point is the determination of the defining lengths for this imaginary circumscribing rectangular prism. When determining the defining lengths, the most stable orientations of a particle on a horizontal plane are considered. Then the orientation of the particle that yields the minimum height is selected. Subsequently, the projected area of the particle perpendicular to the flow is selected as the frontal area. Note that this projected area changes according to the alignment of the particle with flow direction. In this study, two cases, most favorable and most unfavorable orientations, have been considered for rectangular prisms. The two defining lengths are the primary axes of the frontal projected area; the height of the particle, b , and the width of the particle, a . Finally the largest dimension that is parallel to the flow direction is the third defining length, which is the length of the particle and labeled as c . Moreover, a characteristic length is defined. The characteristic length, L , is the longest dimension on the projected area of the particle, perpendicular to the flow direction. For spherical particles it is merely the nominal diameter, d_s , and for other particles used in this study it is computed from the defining lengths a and b with the equation

$$L = \sqrt{a^2 + b^2} \quad (2.37)$$

An illustrative sketch on how the defining lengths are expressed for an arbitrarily shaped grain is given in Figure II-4.

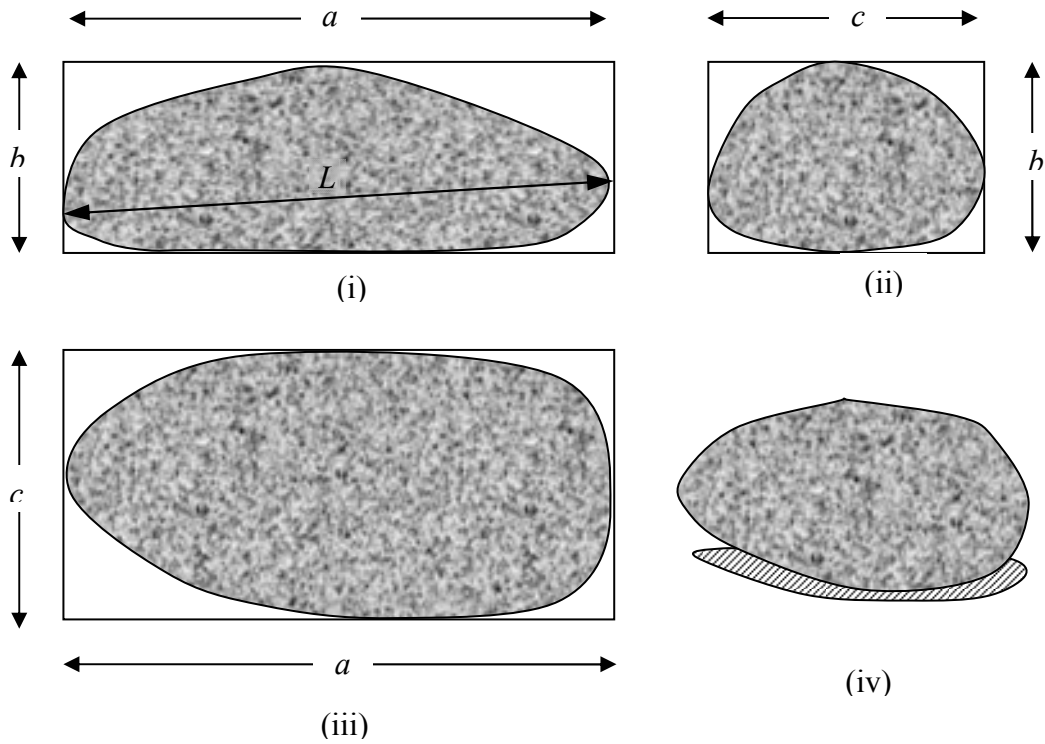


Figure II-4: Illustrative sketch for particle dimensions

- (i) Frontal projected area of the particle
- (ii) Side view and the projected area
- (iii) Top view and the projected area
- (iv) 3D view of the object

Defne (2002) has defined a new shape factor in the light of intuition obtained from previous studies (Gogus et al., 2001):

$$SF = \left(\frac{a+b}{2 \cdot c} \right) \cdot \left(\frac{\nabla}{a \cdot b \cdot c} \right)^{1/3} \quad (2.38)$$

where a , b , c are derived from the dimensions of the original particle and ∇ is the real volume of the particle. In this equation the first term is related to the orientation of the particle under fluid flow and in one respect is a measure of stability of the particle and the second term is the ratio of the volume of the original particle to the volume of enclosing imaginary rectangular prism.

CHAPTER III

THE EXPERIMENTAL INVESTIGATIONS

In this study, the inception of motion of totally 44 sedimentary particles of various shapes and densities was tested in a tilting flume at the Hydromechanics Laboratory of METU.

The specific properties of the experimental setup and details of the experimental procedure are explained in the following sections.

III.1. Experimental Setup

The experimental setup is a 12 m long tilting flume having a rectangular cross section. Net working length of the channel is 8 m. The depth of the cross section is 45 cm and the width is 50 cm. A detailed layout of the setup is given in Figure III-1.

The channel bottom is made up of concrete and the walls are made of glass. Tilting of the channel is maintained by a motor and screw combination. In each experiment with different slopes, uniform flow condition is always checked by monitoring the depth with the help of a mobile point gage attached to the channel.

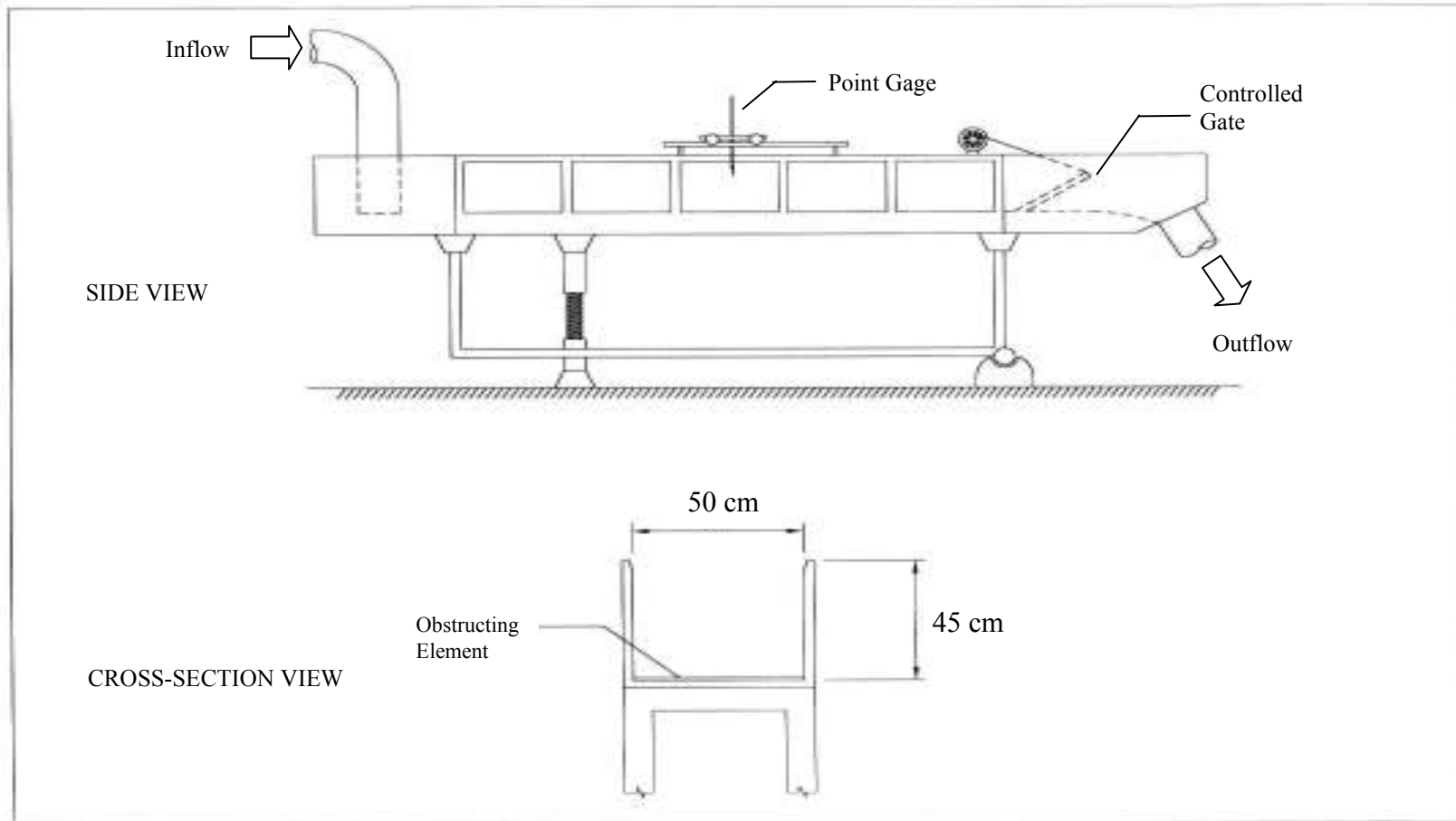


Figure III-1: Experimental setup

III.1.1. Determination of the Flow Rate

Water passing through the tilting flume discharges into another channel of 58 cm width and 70 cm depth. At the downstream of this channel a suppressed rectangular sharp-crested weir made of fiberglass is located to determine the flow rate. The dimensions of the weir and the channel are given in Figure III-2. The weir is aerated properly with the help of three pairs of ventilation holes. The diameter of each ventilation hole is 6 mm . Each pair consists of two holes that are drilled symmetrically on both sides of the channel.

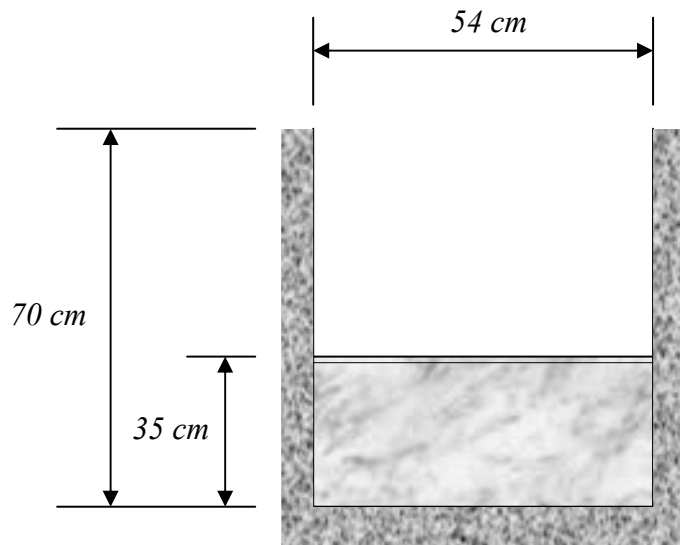


Figure III-2: Dimensions of the rectangular sharp crested weir

For a rectangular sharp crested weir, the discharge is computed from the equation (Henderson, 1966):

$$Q = C_Q \cdot \frac{2}{3} \cdot \sqrt{2g} \cdot L_l \cdot H^{3/2} \quad (3.1)$$

where Q is discharge, C_Q is the discharge coefficient, L_l is the effective length of the crest and H is the measured water head over the crest, excluding the velocity head.

The discharge coefficient, C_Q , in equation (3.1) is determined by the below equation introduced by Rehbock in 1929 (Addison, 1954 and King, 1954):

$$C_Q = 0.605 + \frac{l}{1000 \cdot H} + 0.08 \cdot \frac{H}{p} \quad (3.2)$$

where p is the height of the weir. This equation is valid up to $H/p = 5$ according to measurements by Rouse (Chow, 1959). The accuracy of the discharge measurements was found to be $\pm 2\%$ within this study.

III.1.2. The Obstructing Element

In order to be closer to real life conditions the interlocking of particles in a natural river is imitated with an obstructing element as mentioned in the preceding sections. For each particle dimension, a fiberglass rod of different height is embedded immediately downstream of the particle. The rod is placed crosswise the channel section. Height of the rod is always less than the size of the particle and it is increased with increasing size of particles. ***In each of the cases, a ratio of 1.5/5 is maintained between the height of the obstacle and the height of the particle.*** The heights of the rods used in the sets ranged in between *0.3 cm* and *1.86 cm*. The heights used were *0.3, 0.37, 0.6, 0.74, 0.9, 1.12, 1.49, 1.50* and *1.86 cm*. ***In the previous study performed by Defne (2002), same experiments were performed by using obstacles having a height ratio of 1/5 to the height of the particle.*** Results of that study and the present study will be compared in the preceding parts of this chapter in order to exhibit the effect of obstacle height.

III.1.3. Particle Shapes and Sizes

Particles of different shapes and sizes are mould from cement and mixture of cement and iron dust to model sediment grains. Specific weights of particles have been determined by weighing the particles on a digital balance having *0.01 g* accuracy and by measuring their volumes. The particles have been kept in water at least for one day

before the determination of their specific weight and before the experiments, allowing them to become fully saturated. *In the first part of the experiments, particles having specific weight ranging between 1.90 g/cm³ and 2.03 g/cm³ with an average specific weight of 1.96 g/cm³ are used. In the second part of experiments, particles with specific weights ranging between 2.29 g/cm³ and 2.43 g/cm³ with an average specific weight of 2.36 g/cm³ are used. By comparing the results of first and second part experiments, the effect of particle specific weight on initial motion of particles is demonstrated.*

The solitary particles are grouped into five categories according to their shapes and orientations with the flow. These are spheres, cubes, irregular particles and rectangular prisms (See Figure III-3).

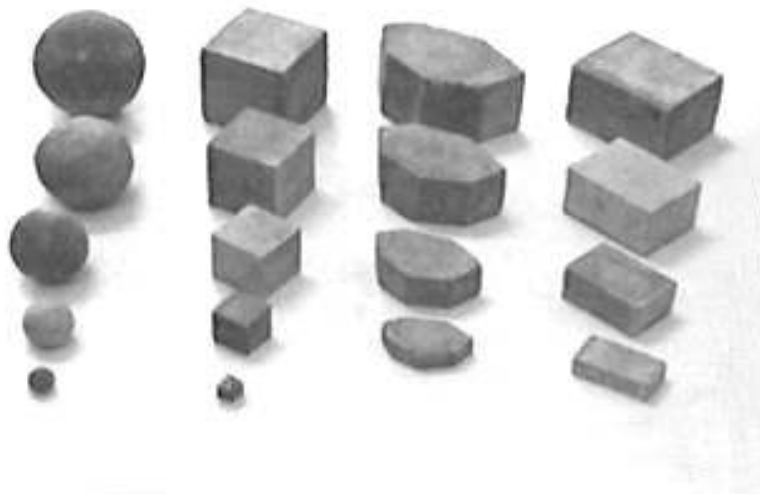


Figure III-3: Particles used in the experiments

Rectangular prisms are examined in two groups according to their orientation to the flow. The first group consists of particles laid down with their largest dimension perpendicular to the flow. In the second group, the largest dimension is aligned with the flow direction. All of the particles in each group are placed in a way that the shortest dimension is always the height of the grain. This is due to a reasonable assumption that a particle on the channel bed or riverbed should rest in a most stable

orientation when gravitational forces are considered. The particles that are not stable may start motion very earlier than establishment of a critical condition. This type of a threshold of motion is not taken as the incipient motion of the particle, since it is probable that the particle will immediately rearrange its orientation in order to be more stable under gravitational force.

Another classification of particles is due to their sizes. The size sets are labeled as 1, 2, 3, 4 and 5. These are equivalent to volume of cubes with one side 1 cm, 2 cm, 3 cm, 4 cm and 5 cm long, consequently the volumes are 1 cm^3 , 8 cm^3 , 27 cm^3 , 64 cm^3 and 125 cm^3 , respectively. Dimensions of each particle were measured with a compass having 0.1 cm accuracy. For size groups 2, 3, 4, and 5 there were particles from each shape groups. On the other hand, size group 1 was studied only with spherical and with cubic particles due to lacking of available moulds for this group of size. Geometrical properties, dimensional details, shape factors and symbols of the particles are also given in Table III-1 and Table III-2.

Table III-1: Shapes and dimensions of particles used in the experiments.

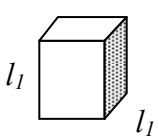
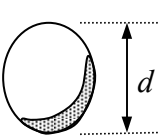
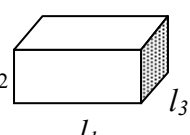
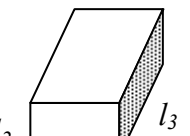
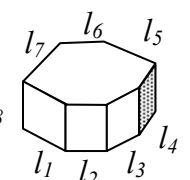
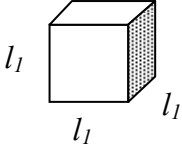
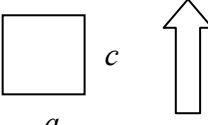
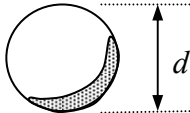
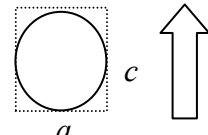
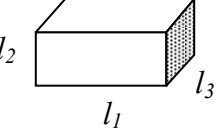
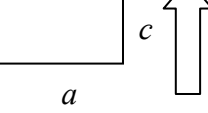
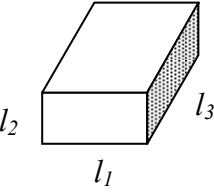
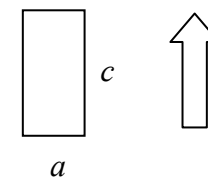
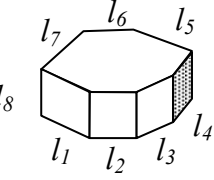
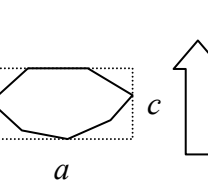
Shape of Particle	Volume of Particle (cm ³)	Dimensions of Particle (cm)								Symbol of Particle
		l_1								Cube
	1.0	1.0								C 1x1x1
	8.0	2.0								C 2x2x2
	27.0	3.0								C 3x3x3
	64.0	4.0								C 4x4x4
	125.0	5.0								C 5x5x5
		d								Sphere
	1.0	1.24								S 1
	8.0	2.48								S 2
	27.0	3.72								S 3
	64.0	4.96								S 4
	125.0	6.20								S 5
		l_1	l_2	l_3						Rect.Prism
	8.0	4.0	1.0	2.0						RP 4x1x2
	27.0	4.5	2.0	3.0						RP 4.5x2x3
	64.0	5.33	3.0	4.0						RP 5.33x3x4
	125.0	6.25	4.0	5.0						RP 6.25x4x5
		l_1	l_2	l_3						Rect.Prism
	8.0	2.0	1.0	4.0						RP 2x1x4
	27.0	3.0	2.0	4.5						RP 3x2x4.5
	64.0	4.0	3.0	5.33						RP 4x3x5.33
	125.0	5.0	4.0	6.25						RP 5x4x6.25
		l_1	l_2	l_3	l_4	l_5	l_6	l_7	l_8	Irregular
	8.0	1.49	1.70	1.46	1.43	1.15	1.91	1.78	1.0	Ir 4.37x1x2.63
	27.0	1.93	2.21	1.89	1.86	1.50	2.49	2.31	2.0	Ir 5.68x2x3.42
	64.0	2.43	2.77	2.38	2.34	1.88	3.14	2.91	3.0	Ir 7.14x3x4.3
	125.0	2.94	3.36	2.88	2.83	2.28	3.79	3.52	4.0	Ir 8.65x4x5.2

Table III-2: Defining lengths for particles used in the experiments.

Particle Shape	Top View and Flow Direction	\forall (cm ³)	a (cm)	b (cm)	c (cm)	L (cm)	SF	Particle Symbol
		1.0	1.0	1.0	1.0	1.41	1.000	C 1x1x1
		8.0	2.0	2.0	2.0	2.82	1.000	C 2x2x2
		27.0	3.0	3.0	3.0	4.24	1.000	C 3x3x3
		64.0	4.0	4.0	4.0	5.66	1.000	C 4x4x4
		125.0	5.0	5.0	5.0	7.07	1.000	C 5x5x5
		1.0	1.24	1.24	1.24	1.24	0.806	S 1
		8.0	2.48	2.48	2.48	2.48	0.806	S 2
		27.0	3.76	3.76	3.76	3.76	0.806	S 3
		64.0	4.92	4.92	4.92	4.92	0.806	S 4
		125.0	6.20	6.20	6.20	6.20	0.806	S 5
		8.0	4.0	1.0	2.0	4.12	1.250	RP 4x1x2
		27.0	4.5	2.0	3.0	4.92	1.083	RP 4.5x2x3
		64.0	5.33	3.0	4.0	6.12	1.042	RP 5.33x3x4
		125.0	6.25	4.0	5.0	7.42	1.025	RP 6.25x4x5
		8.0	2.0	1.0	4.0	2.24	0.375	RP 2x1x4
		27.0	3.0	2.0	4.5	3.61	0.556	RP 3x2x4.5
		64.0	4.0	3.0	5.33	5.00	0.656	RP 4x3x5.33
		125.0	5.0	4.0	6.25	6.40	0.720	RP 5x4x6.25
		8.0	4.37	1.0	2.63	4.48	0.905	Ir 4.37x1x2.63
		27.0	5.68	2.0	3.42	6.02	0.995	Ir 5.68x2x3.42
		64.0	7.14	3.0	4.3	7.74	1.044	Ir 7.14x3x4.3
		125.0	8.65	4.0	5.2	9.53	1.077	Ir 8.65x4x5.2

III.2. Experimental Procedure

Experiments were performed in two sets. In both sets the same experimental procedure is followed but the specific weights of particles are changed. In the first set, 22 particles with average specific weight of 1.96 g/cm^3 and in the second set again 22 particles having average specific weight of 2.36 g/cm^3 were used.

For each set, in a regular cycle of an experiment, first a fixed discharge is maintained. Then, the slope of the channel is altered in slow and small steps. In each step, considerable amount of time is consumed accounting for the development of uniform flow conditions. When the motion of the particle is observed i.e. particle's rolling over the obstructing element with a height 1.5/5 of the particle's, the slope of the channel was reduced to one step back in order to make sure that it was the critical condition. In each experiment when the critical condition was satisfied, the depth of flow in the tilting flume was measured with a point gage, vertical velocity profile over the flow depth in the mid-width of the channel was recorded with a total head tube, and the discharge was measured in the measuring channel with the suppressed sharp-crested rectangular weir. Vertical velocity profile in each experiment was established by recording velocity values at distances varying between half a centimeter and two centimeters, according to the rate of change of velocity, along the depth. At the end of each experiment three velocity values were recorded; the *average velocity in the vertical* over the depth in the mid-width of the channel, which is V_{vc} ; the *average bottom velocity* of the flow at the mid-height of the particle, which is V_{bc} ; and the *average cross-sectional velocity* of the flow, V_{cc} , which is calculated from the ratio of measured discharge to the area of the flow in the tilting flume (See Table B-1 in Appendix B). Critical shear stress, critical dimensionless shear stress, grain Reynolds number and other important and necessary parameters were also calculated. For each particle, at three different discharges, three different critical channel slopes each corresponding to the initiation of motion of particle were determined.

III.3. Analysis of Experimental Data, Comparison with Previous Study and Discussion of Results

Altogether more than 130 experiments with total duration of approximately 200 hours were performed. The results collected in the end were evaluated from various points of view. *In this chapter the results found for particles with a specific weight of 1.96 g/cm³ are given and they are compared with the results of study performed by Defne (2002) in order to find out the effect of obstacle height on incipient motion of particles.*

III.3.1. Relationship Between the Entrainment Function and the Grain Reynolds Number

Variation of entrainment function, τ^* , with the grain Reynolds number, Re^* , at condition of incipient motion, for different sizes of each particle shape is given in Figures III-4 through III-8.

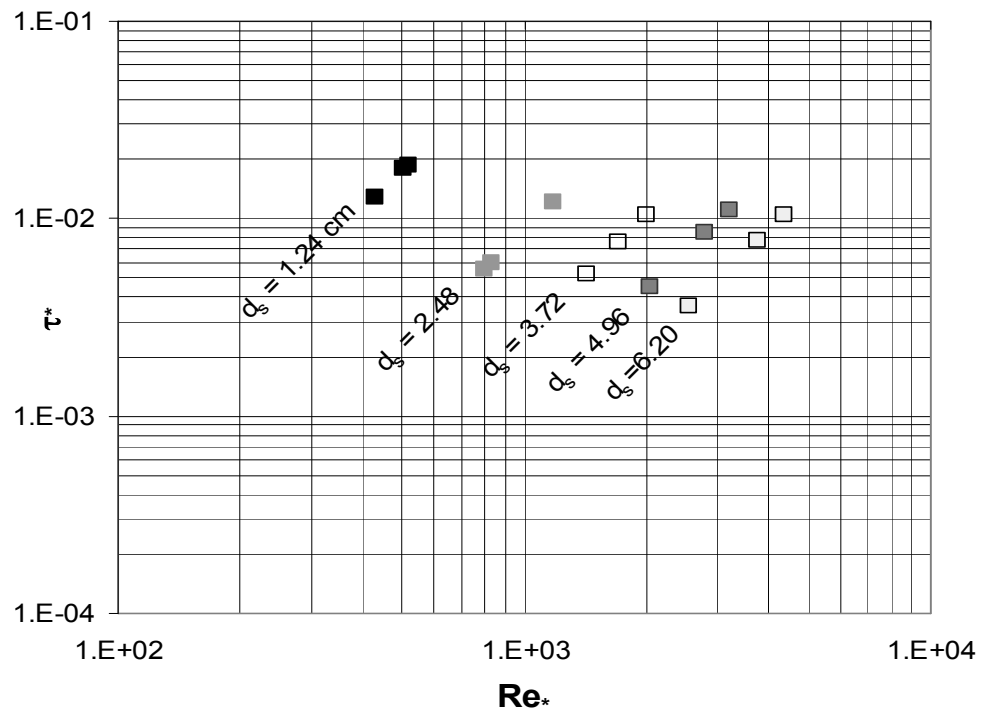


Figure III-4: τ^* vs. Re^* for cubic particles ($SF= 1.000$, $t/b=1.5/5$, $\gamma_s=1.96 \text{ g/cm}^3$)

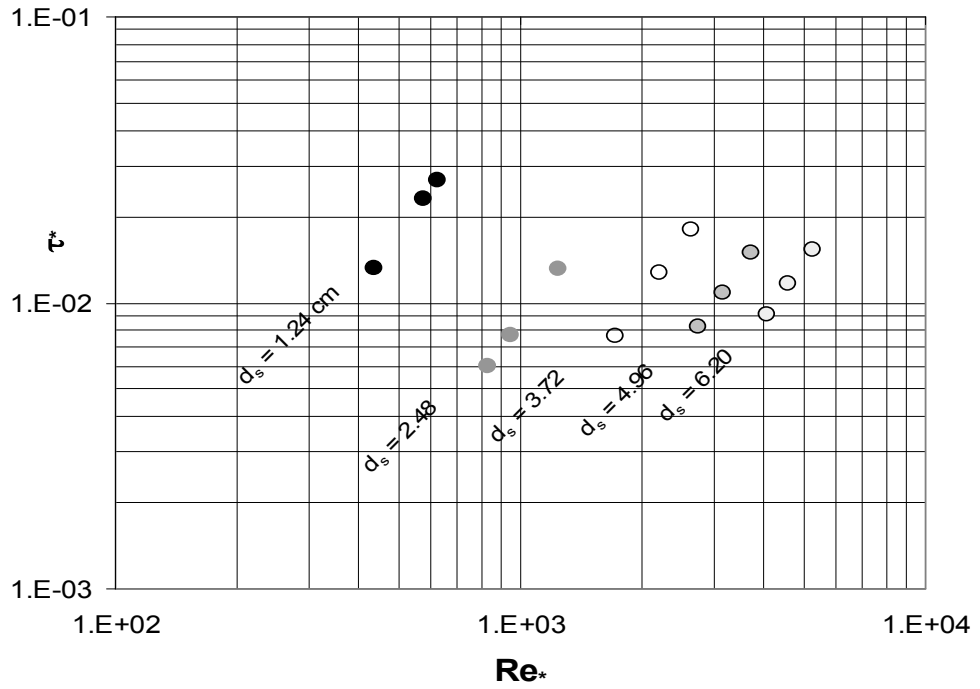


Figure III-5: τ_* vs. Re_* for spherical particles ($SF= 0.806$, $t/b=1.5/5$, $\gamma_s =1.96 \text{ g/cm}^3$)

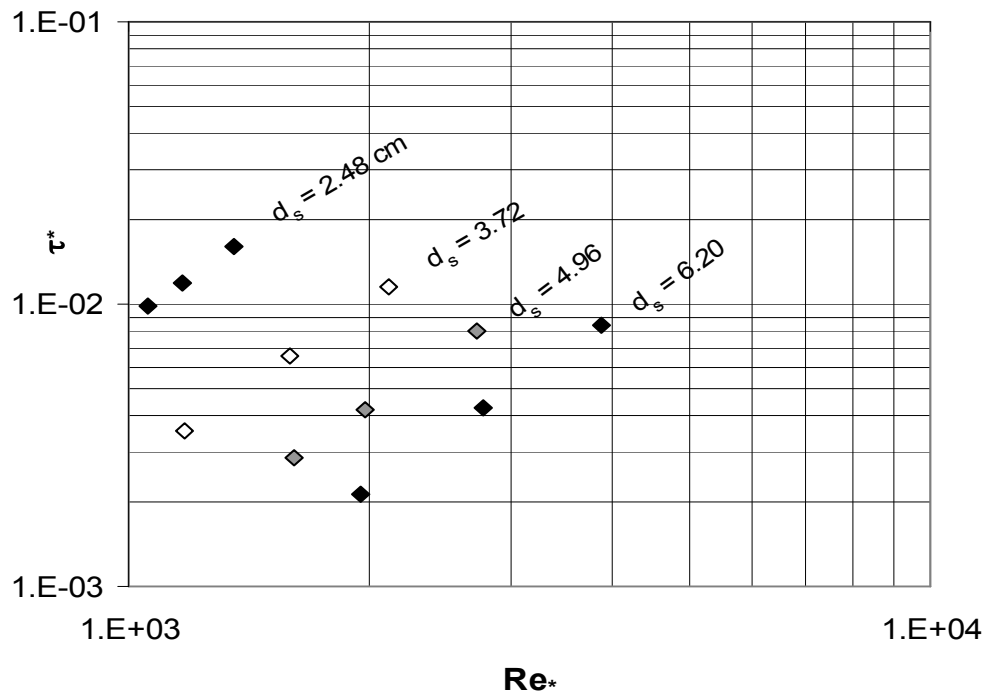


Figure III-6: τ_* vs. Re_* for rectangular prismatic particles ($SF= 1.025 \sim 1.250$, $t/b=1.5/5$, $\gamma_s =1.96 \text{ g/cm}^3$)

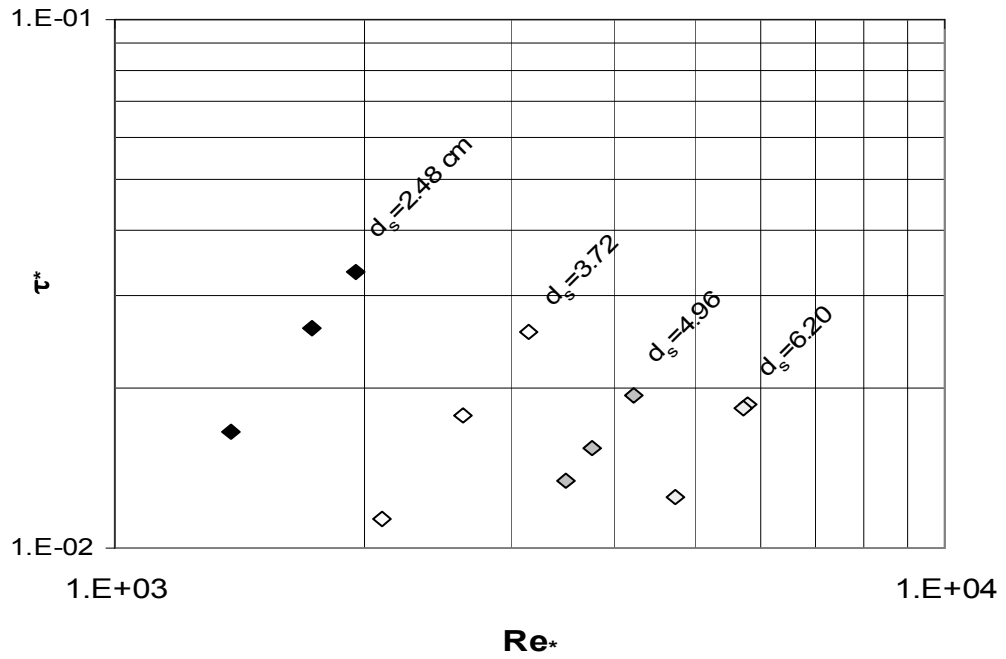


Figure III-7: τ^* vs. Re^* for rectangular prismatic particles ($SF = 0.375 \sim 0.720$, $t/b = 1.5/5$, $\gamma_s = 1.96 \text{ g/cm}^3$)

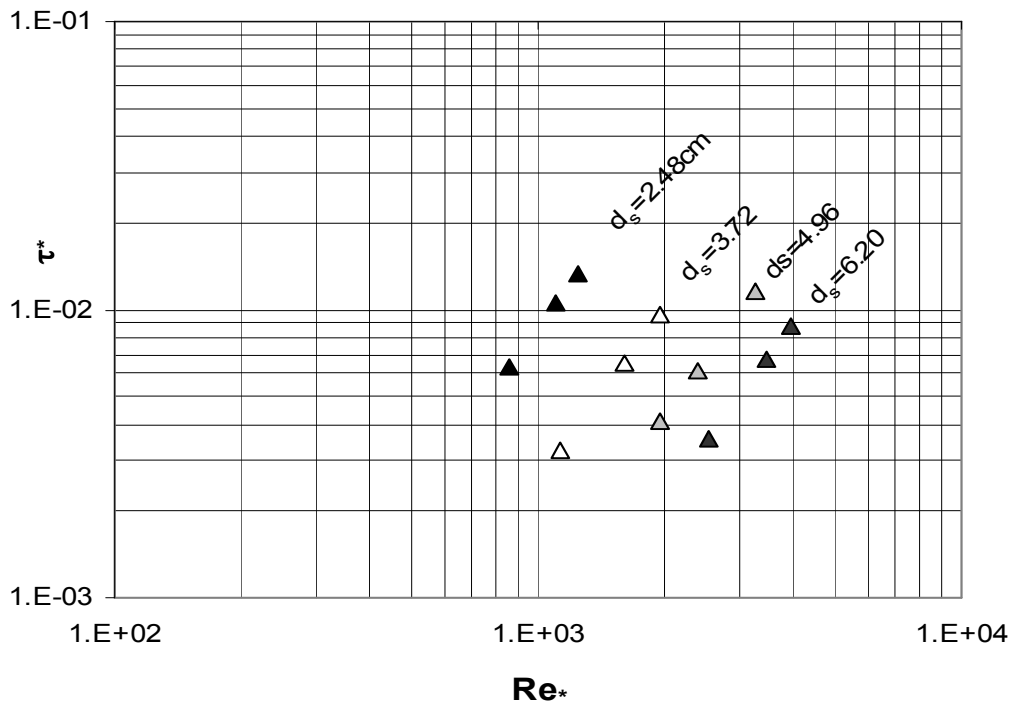


Figure III-8: τ^* vs. Re^* for irregular shaped particles ($SF = 0.905 \sim 1.077$, $t/b = 1.5/5$, $\gamma_s = 1.96 \text{ g/cm}^3$)

The grouping of data linearly at each sediment diameter value is due to the specific conditions of the experiments. In this part of experiments, the densities of all particles are the same and all particles of a given size group have the same volume. However, there is scatter between the data of particles having the same shape and size. This is an indication that besides the shape factor, there should be another parameter related to the phenomenon. This parameter is the relative depth, $\frac{d_s}{R_b}$, which has been derived and explained in the section where dimensional analysis of the problem was discussed. For each of the particles the experiments were repeated three times with distinct flow rates and slopes. As a result, it can be concluded that due to the changes in the hydraulic radius values of the flows, each experiment of the same particle results in different τ_* and Re_* . The effect of $\frac{d_s}{R_b}$ on the variation of experimental data for the particles of the same size but different shapes is clearly seen in Figure III-9.

In Figure III-10, collective results are given and the curve which was proposed by Shields, actually fit by Rouse (Buffington, 1999), is shown. As mentioned in the review of relevant literature, Shields had not considered the effect of relative depth explicitly and had obtained a band of critical condition. Later this band of critical condition was expressed by a curve that had been fit by Rouse. The study of Shields was based on the loose bed conditions, where the roughness of the river bottom was determined by the particles resting on the bed. This is completely different from the conditions of the present study, in which the experiments were conducted on a smooth fixed bed with solitary particles. The study of Shields was valid for a particle size range between 0.4 mm and 3.4 mm. In this study, coarse particles with sediment diameters between 1.24 cm and 6.20 cm were investigated. Nevertheless, the results are given comparatively for integrity with the overall studies.

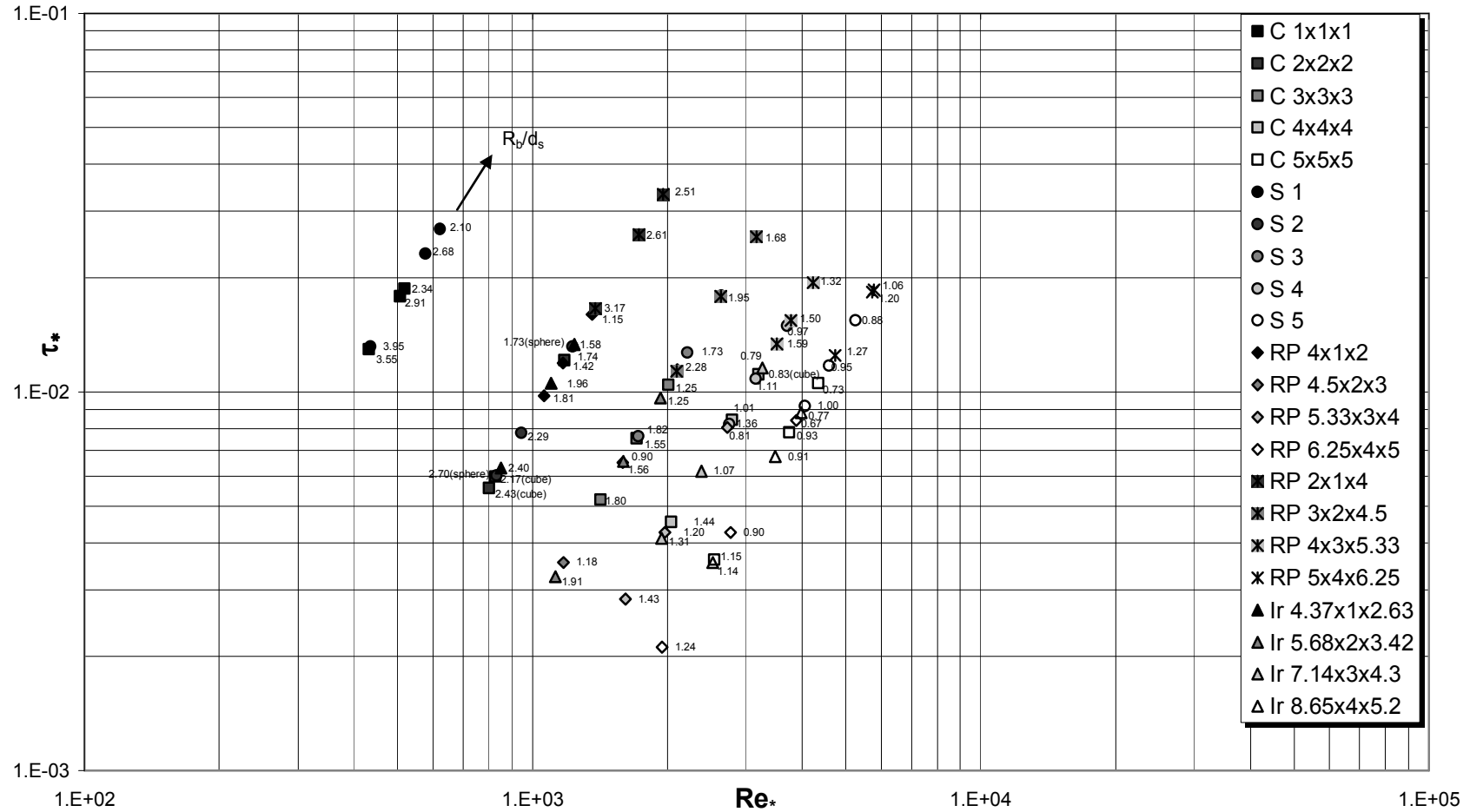


Figure III-9: R_b/d_s values on τ_* vs. Re_* plane for solitary particles ($SF=0.375\sim 1.250$, $t/b=1.5/5$, $\gamma_s=1.96\text{ g/cm}^3$)

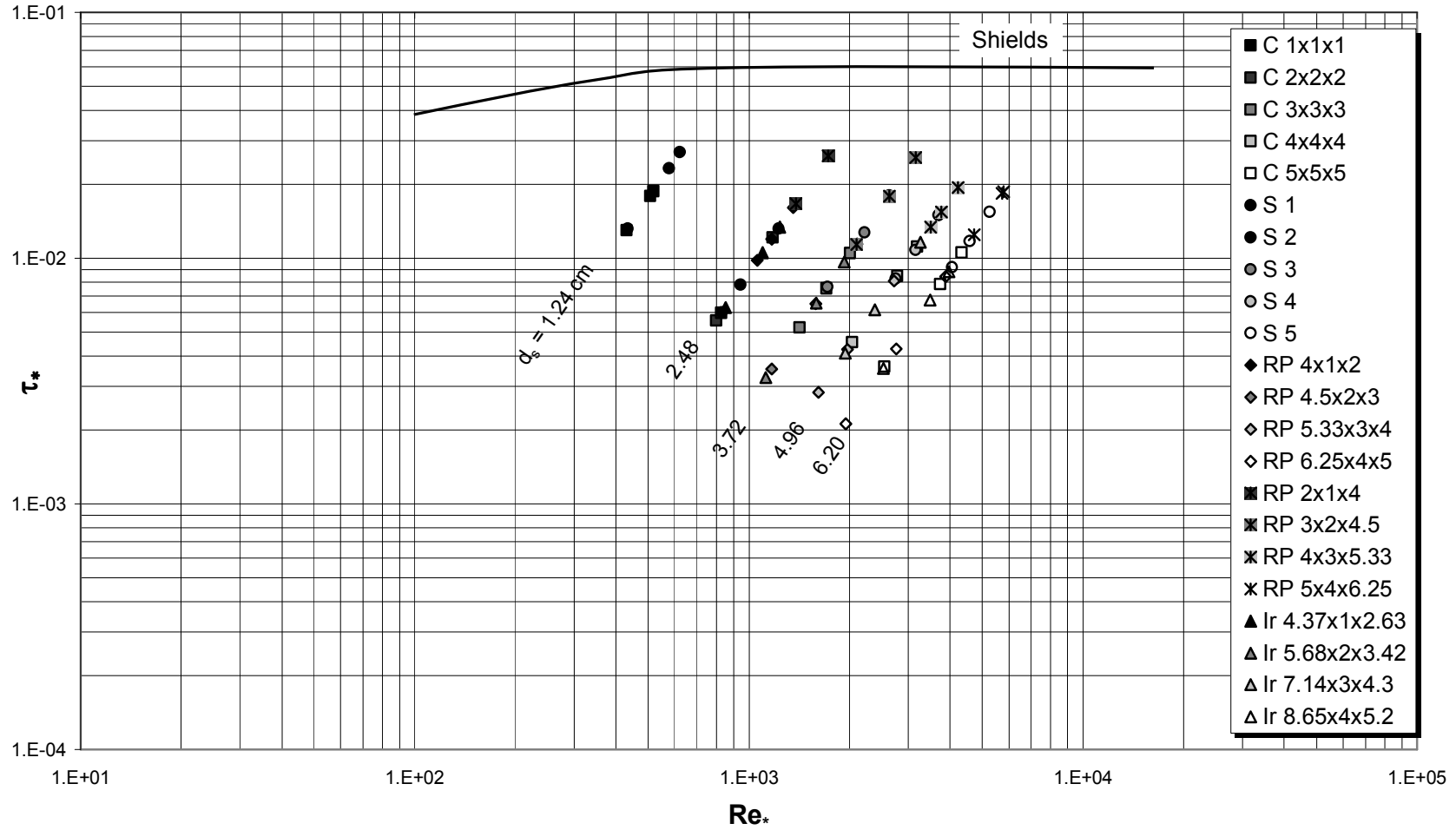


Figure III-10: τ_* vs. Re_* for solitary particles ($SF = 0.375 \sim 1.250$, $t/b = 1.5/5$, $\gamma_s = 1.96 \text{ g/cm}^3$)

In Figure III-11 the results of this study and Defne's study (2002) are presented to see the effect of obstacle height on the general trend of the data. This figure clearly prevails that the data of the present study and Defne's data fall on the same line for the same particle in such a way that in the present study the particles require higher τ^* values for incipient motion as expected.

Another graph indicating the relationship among Re^* , R_b/d_s and SF is given in Figure III-12 for particles of different shapes tested at $t/b=1/5$ by Defne (2002) and $t/b=1.5/5$ in this study. Best fit curves of the data for $t/b=1.5/5$ lie slightly above those of $t/b=1/5$ for the particles of the same shape factor as expected. Higher the roughness height behind the particle, larger the required Re^* for the particle motion. For a given particle size and shape, the critical value of the entrainment function increases with the decrease in the flow depth and consequently the relative depth, R_b/d_s . This was also stated by Shvidchenko and Pender (2000), and it has been explained within the relevant literature in details. For a particle to start motion, increasing slope requires less flow rate. Such an arrangement of decreased discharge and increased slope results in a reduced flow depth due to the nature of uniform flow conditions.

The relation between slope and critical entrainment function for each size group is given in Figures III-13 through III-17. As it is seen in these figures, variation of the critical dimensionless shear stress with slope is very similar to that presented in the study of Shvidchenko and Pender given in Figure I-6. On the other hand, the magnitudes of critical values differ. Shvidchenko and Pender studied under loose bed conditions with particle sizes between 1.5 mm and 12 mm to clarify the effect of relative depth on incipient motion. The results of present study are acquired for solitary coarse particles on smooth fixed beds in order to find out the effect of shape and size. Hence, the quantitative discrepancy between the results is conventional.

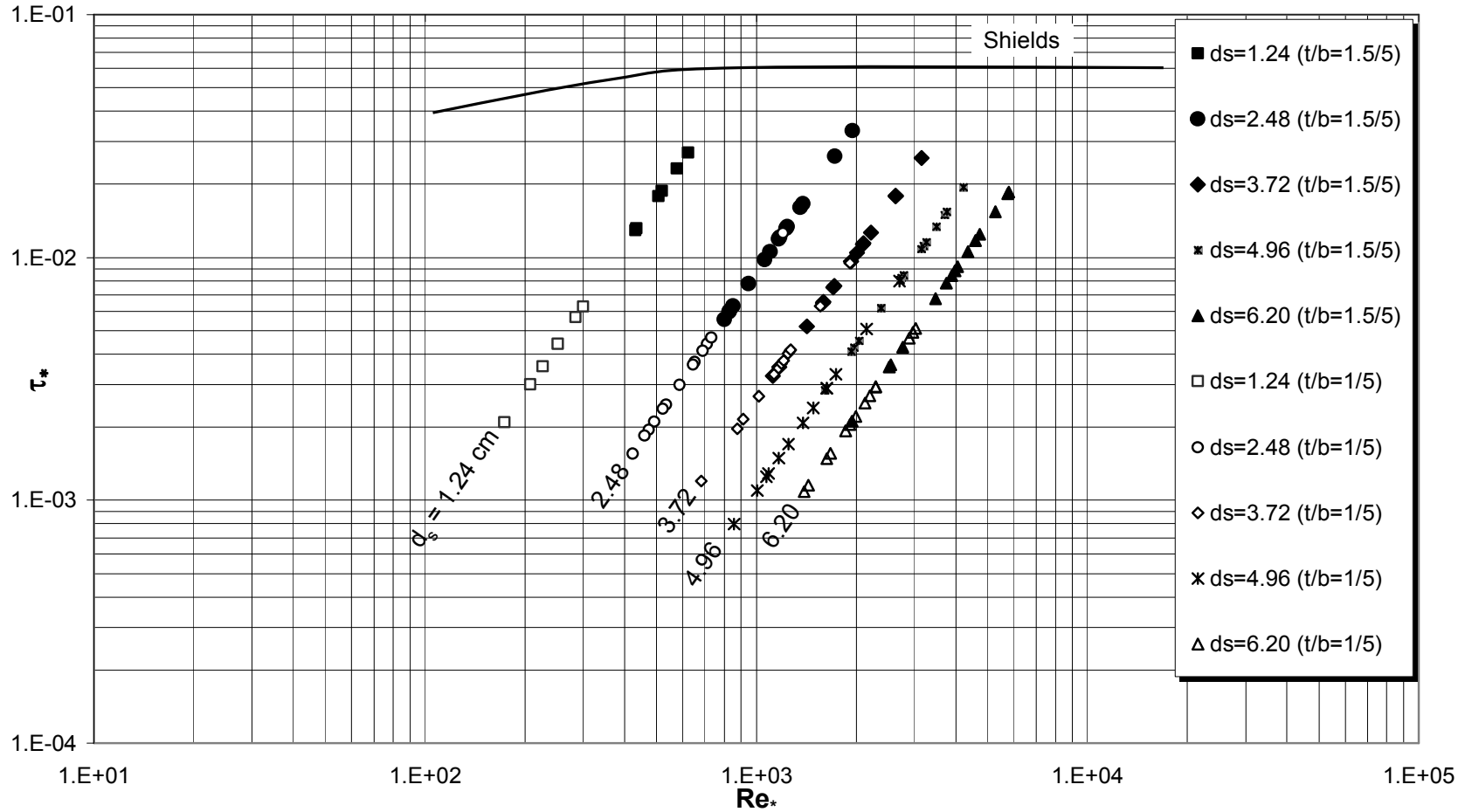


Figure III-11: Comparison of τ_* vs. Re_* of Defne's Study and Present Study ($SF=0.375 \sim 1.250$, $\gamma_s=1.96 \text{ g/cm}^3$)

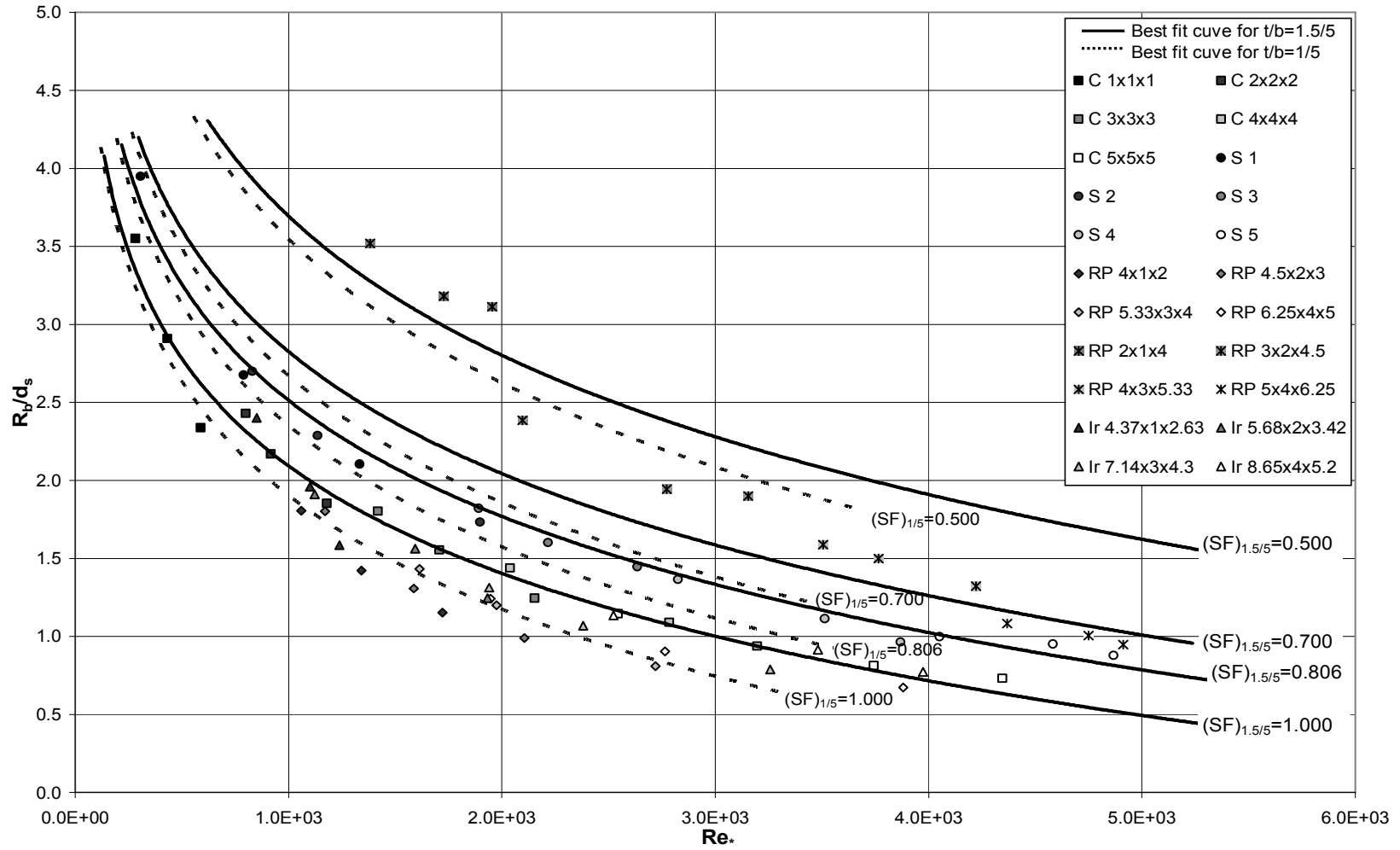


Figure III-12: R_b/d_s versus Re^* as a function of shape factor, SF ($\gamma_s=1.96 \text{ g/cm}^3$)

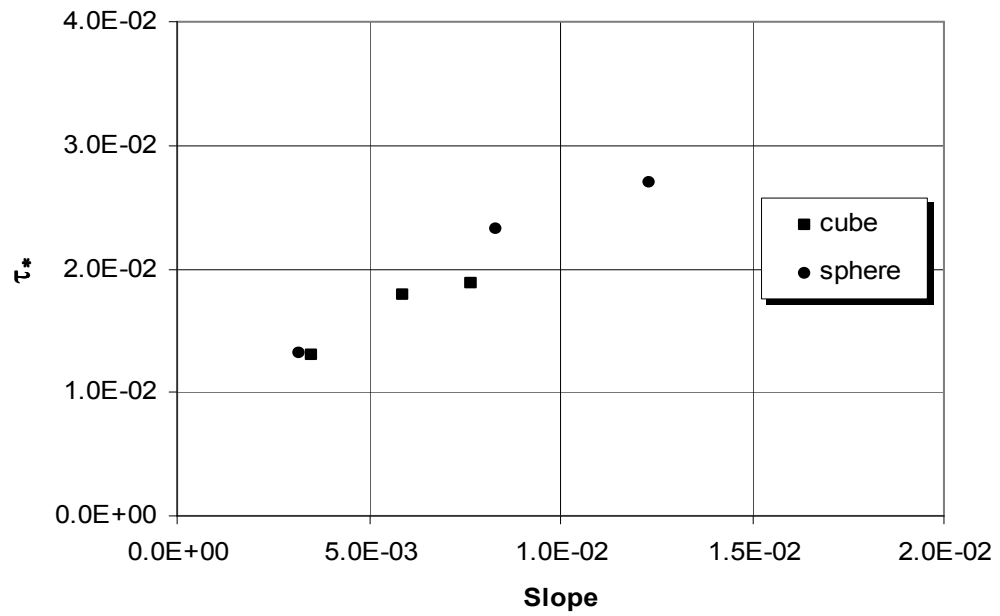


Figure III-13: τ_* vs. slope for solitary particles, size group 1 ($d_s = 1.24$ cm)

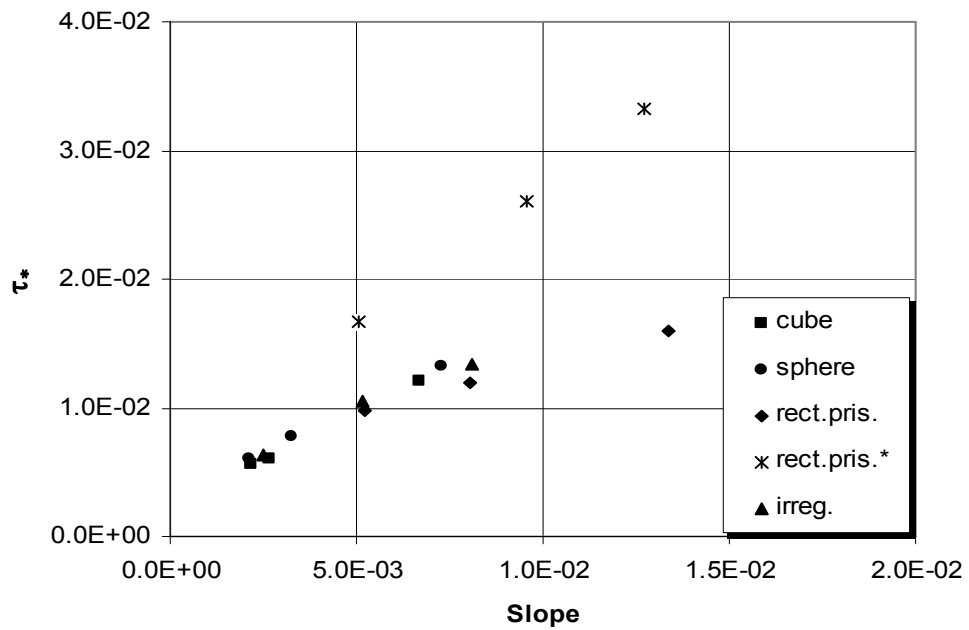


Figure III-14: τ_* vs. slope for solitary particles, size group 2 ($d_s = 2.48$ cm)

(*) Rectangular prisms placed in the most unfavorable orientation with the flow.

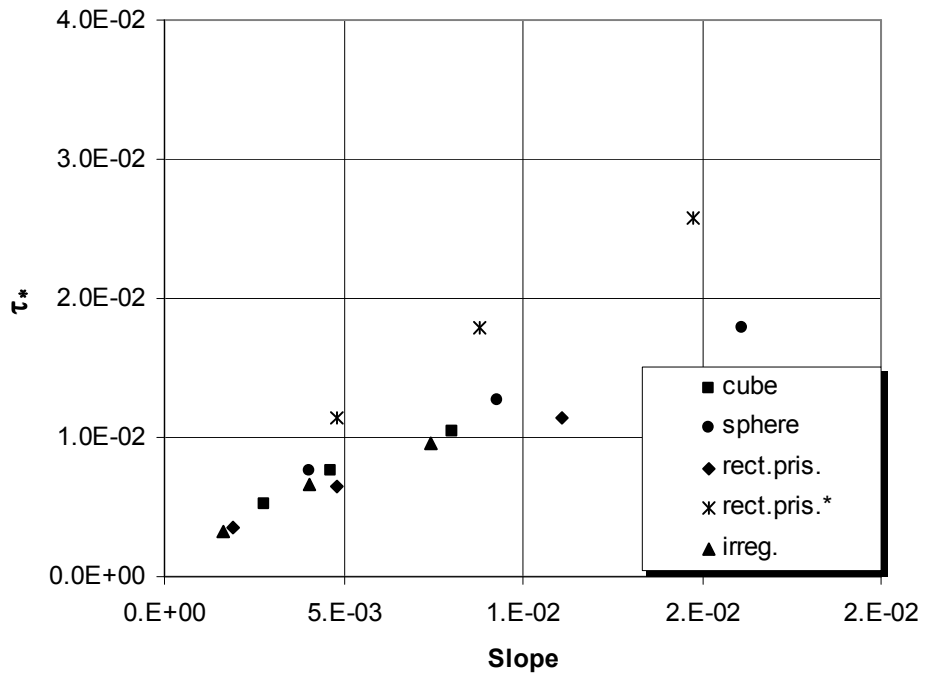


Figure III-15: τ^* vs. slope for solitary particles, size group 3 ($d_s = 3.72$ cm)

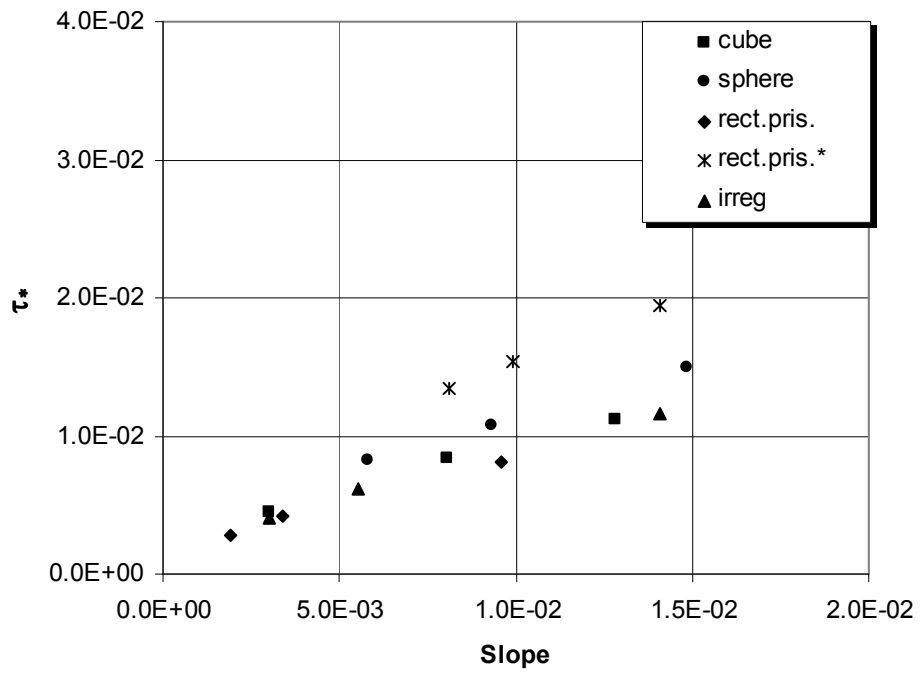


Figure III-16: τ^* vs. slope for solitary particles, size group 4 ($d_s = 4.96$ cm)

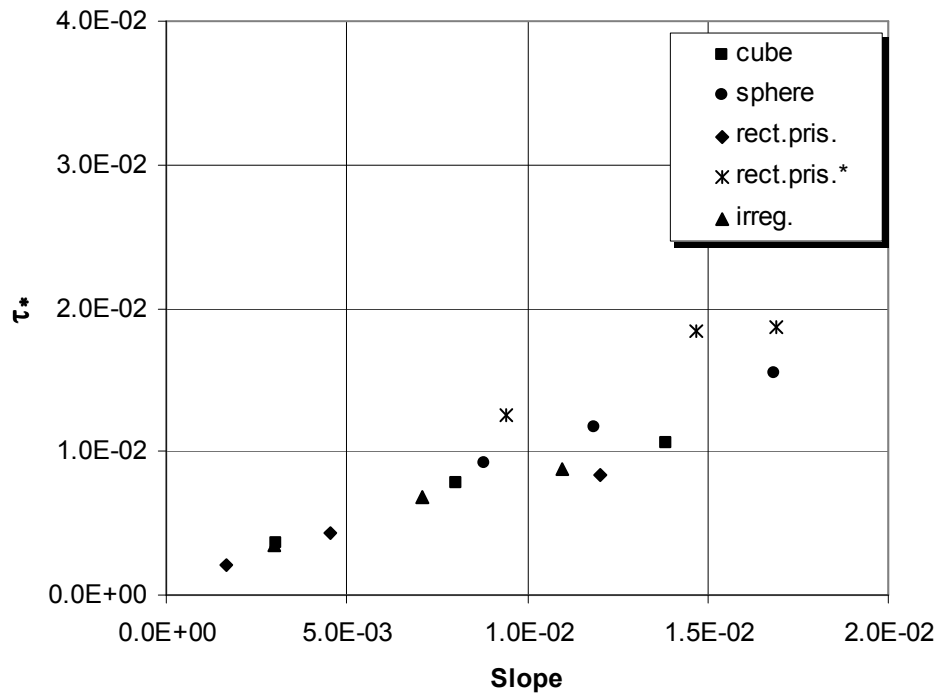


Figure III-17: τ^* vs. slope for solitary particles, size group 5 ($d_s = 6.20 \text{ cm}$)

The effect of particle shape on the data of these figures can be minimized with the application of the shape factor defined by Defne (2002) to the entrainment function on the vertical axis. Critical entrainment function values multiplied by the shape factors are presented in Figures III-18 through III-22 as a function of channel slope. This manipulation results in nearly concurrent critical values for particles having different shapes.

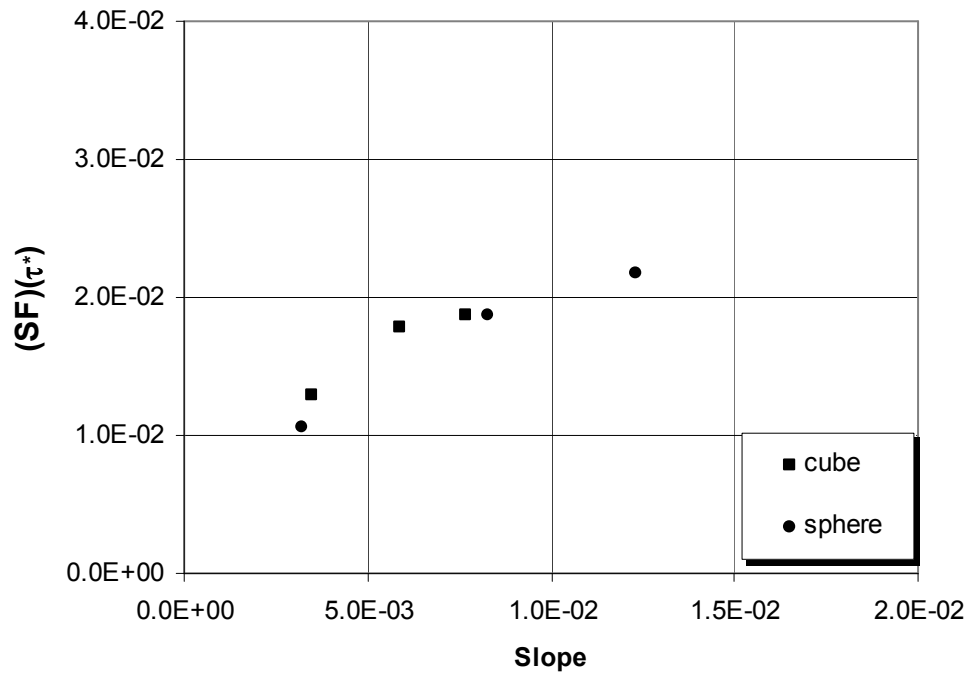


Figure III-18: Shape factor correction for τ^* vs. slope for $d_s = 1.24 \text{ cm}$

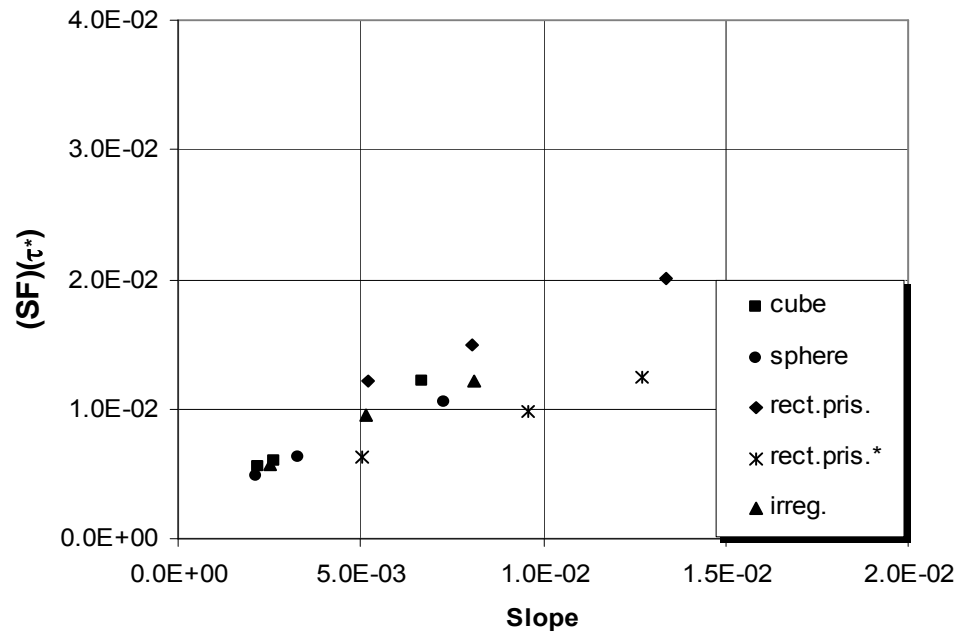


Figure III-19: Shape factor correction for τ^* vs. slope for $d_s = 2.48 \text{ cm}$

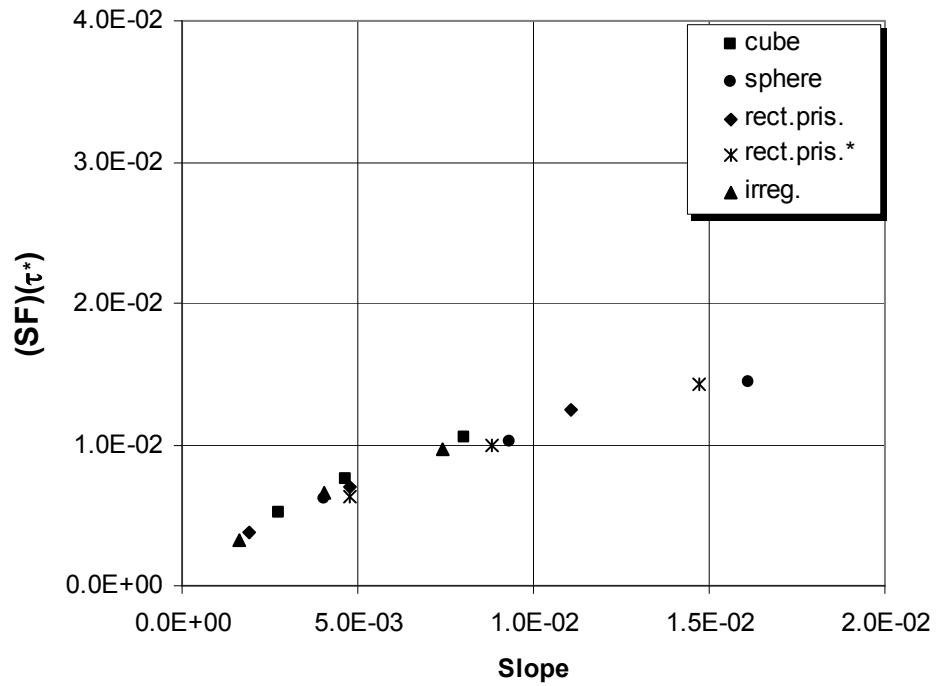


Figure III-20: Shape factor correction for τ^* vs. slope for $d_s = 3.72 \text{ cm}$

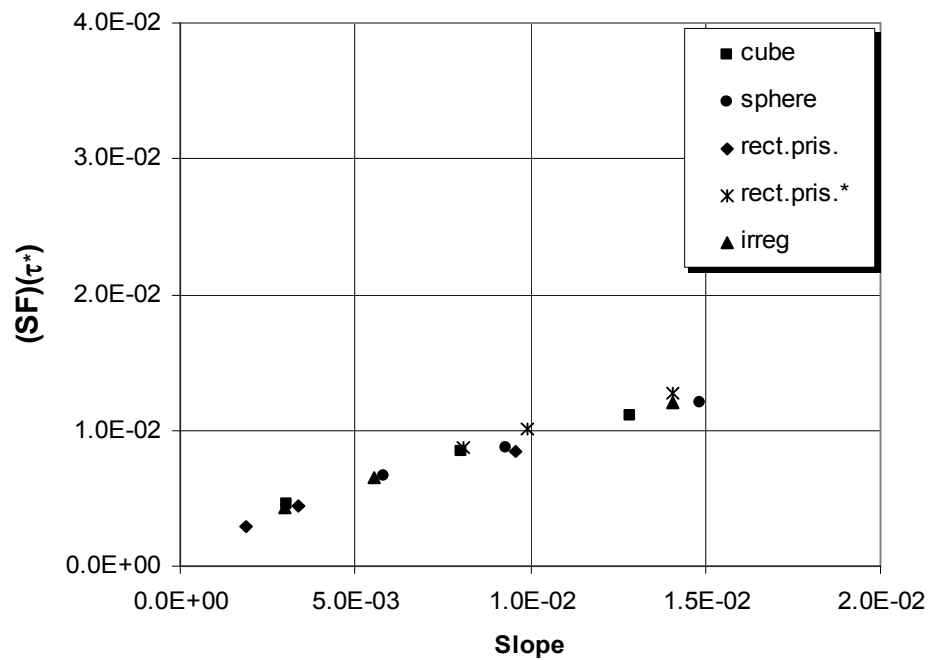


Figure III-21: Shape factor correction for τ^* vs. slope for $d_s = 4.96 \text{ cm}$

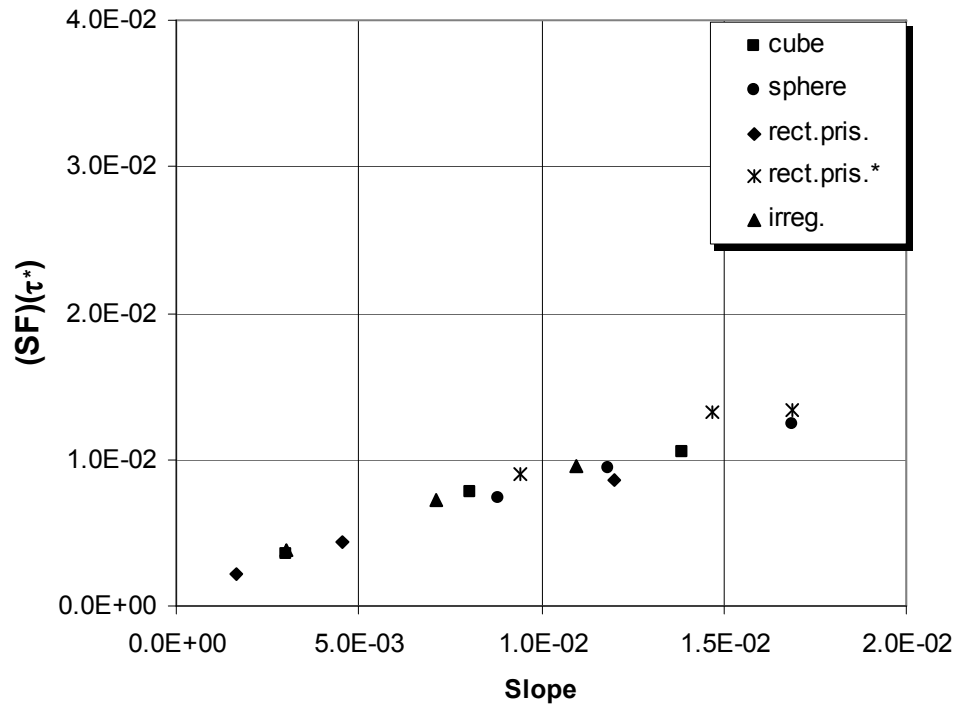


Figure III-22: Shape factor correction for τ^* vs. slope for $d_s = 6.20 \text{ cm}$

III.3.2. Relationship Between the Entrainment Function and the Dimensionless Grain Size

The relationship between the critical entrainment function and the dimensionless grain size, d^* is a modification of Shields relation, where entrainment function was related to the grain Reynolds number. Both relations are obtained through dimensional analysis of the problem with two different choices of repeating variables. In the case of dimensionless grain size the additional parameter relative depth, $\frac{R_b}{d_s}$, is eliminated from the relation. Theoretical background and deductions were given in details in Chapter II.

Figure III-23 represents the relation between the critical entrainment function and the dimensionless grain size in comparison with Shields relation. The reader should bear

in mind that ranges and experimental conditions of these two studies are very much different and that this comparison is given for the sake of identification of present study's position amongst the previous studies.

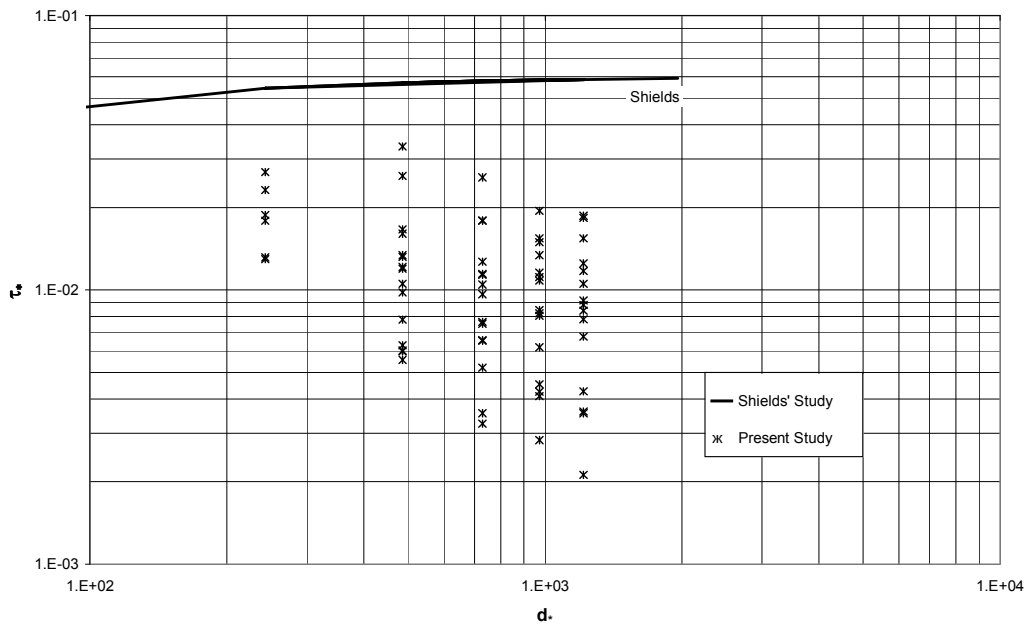


Figure III-23: τ_* vs. d_* for solitary particles

In Figure III-23, the experimental data are grouped into five vertical lines according to their particle sizes. This is a consequence of the theoretical derivation and characteristics of the experimental procedure. The particles used in the experiments are tested in water and they are made of the same material. Therefore, the only variable within d_* is the size of the particle. Working with particles of the same sizes allows clarifying the effect of their shapes on incipient motion more clearly.

A detailed presentation of variation of the critical entrainment function with the dimensionless grain size is supplied in Figure III-24 together with the corresponding bed slopes. The data tend to group according to the bed slopes though this tendency is not clear enough to construct trend lines. This is because there is still the effect of particle shape on the distribution of data.

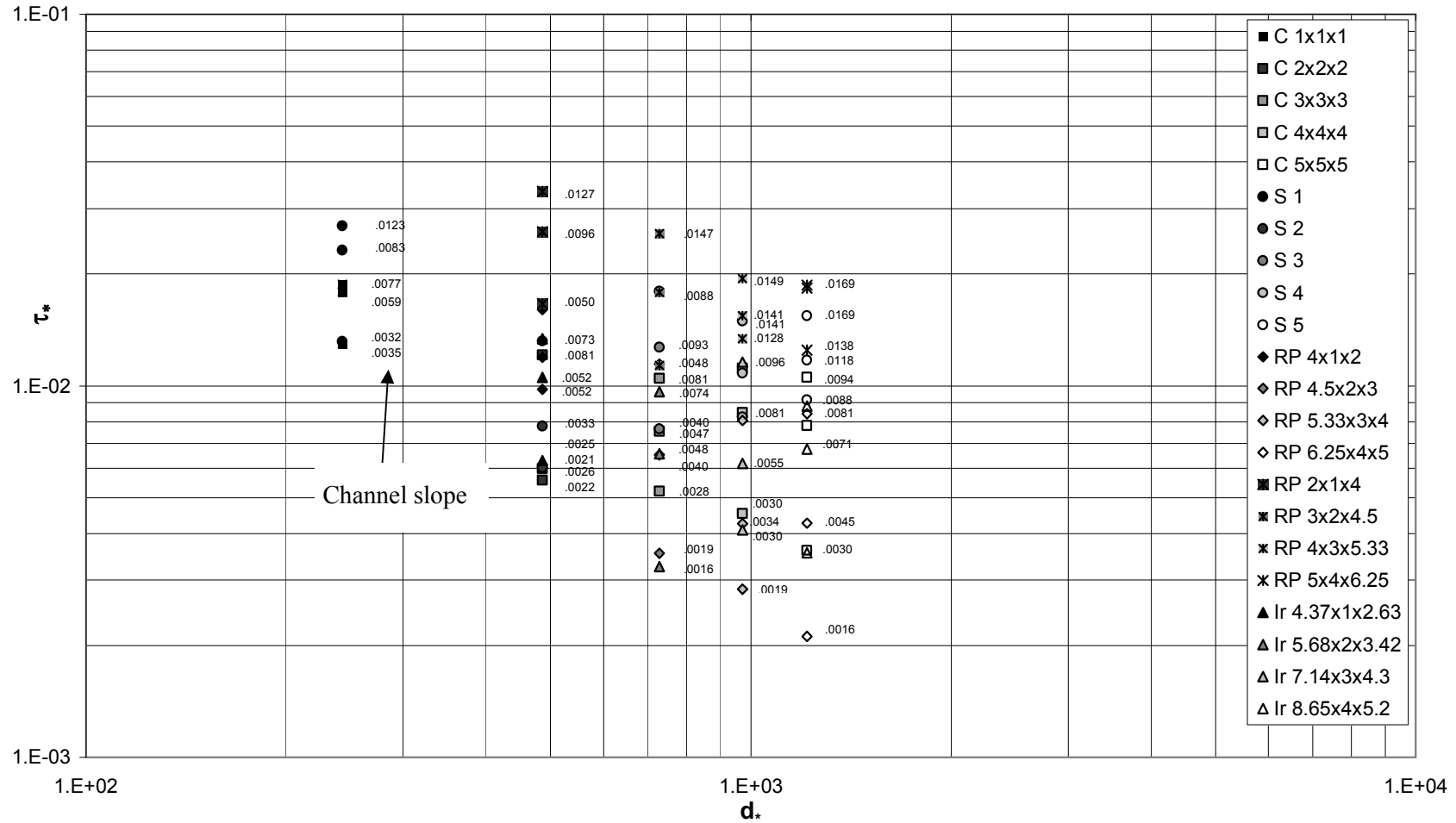


Figure III-24: Critical entrainment function τ_* vs. dimensionless grain size d_* for different slopes

In Figure III-25, effect of particle shape on the initiation of motion of the particle has been minimized by multiplying the critical entrainment function with the shape factor, SF . After this modification, sample trend lines are formed. The advantage of the graph in Figure III-25 is that the critical value of the entrainment function for a given particle shape and bed slope can be directly determined, since d^* can be calculated from known fluid and particle properties.

In Figure III-26, the results are given in comparison with the results of Shvidchenko and Pender (2000). The similarity of the two results is that the critical entrainment function is likely to decline with increasing dimensionless grain size. Shvidchenko and Pender had noted the downward trend both in this graph and in Shields graph. Their results were in contrast with the existing common expectation that entrainment function should be independent of the grain Reynolds number for rough turbulent flow. They suggested that more data with coarse particles at high Re^* values are necessary to clarify the situation. Although the conditions are different, results of the present study also supports the declining mood of the critical entrainment function. Note that for a given slope, larger particles start to move at smaller values of τ^* . However, this does not mean that larger particles start to motion easier than the smaller ones for a given slope and flow rate. Larger particles require larger flow rates.

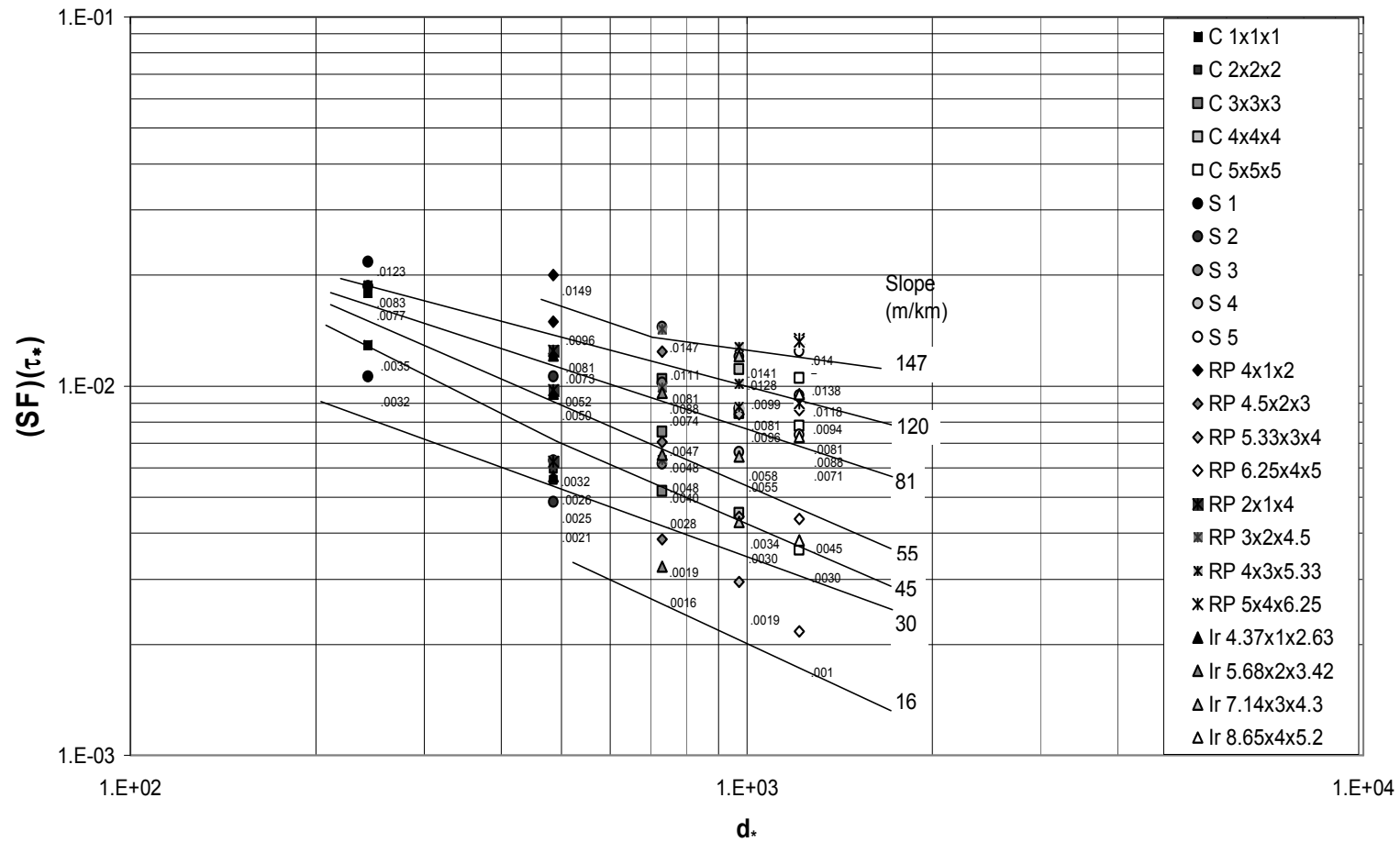


Figure III-25: Shape factor correction for τ_* vs. d_* for different slopes

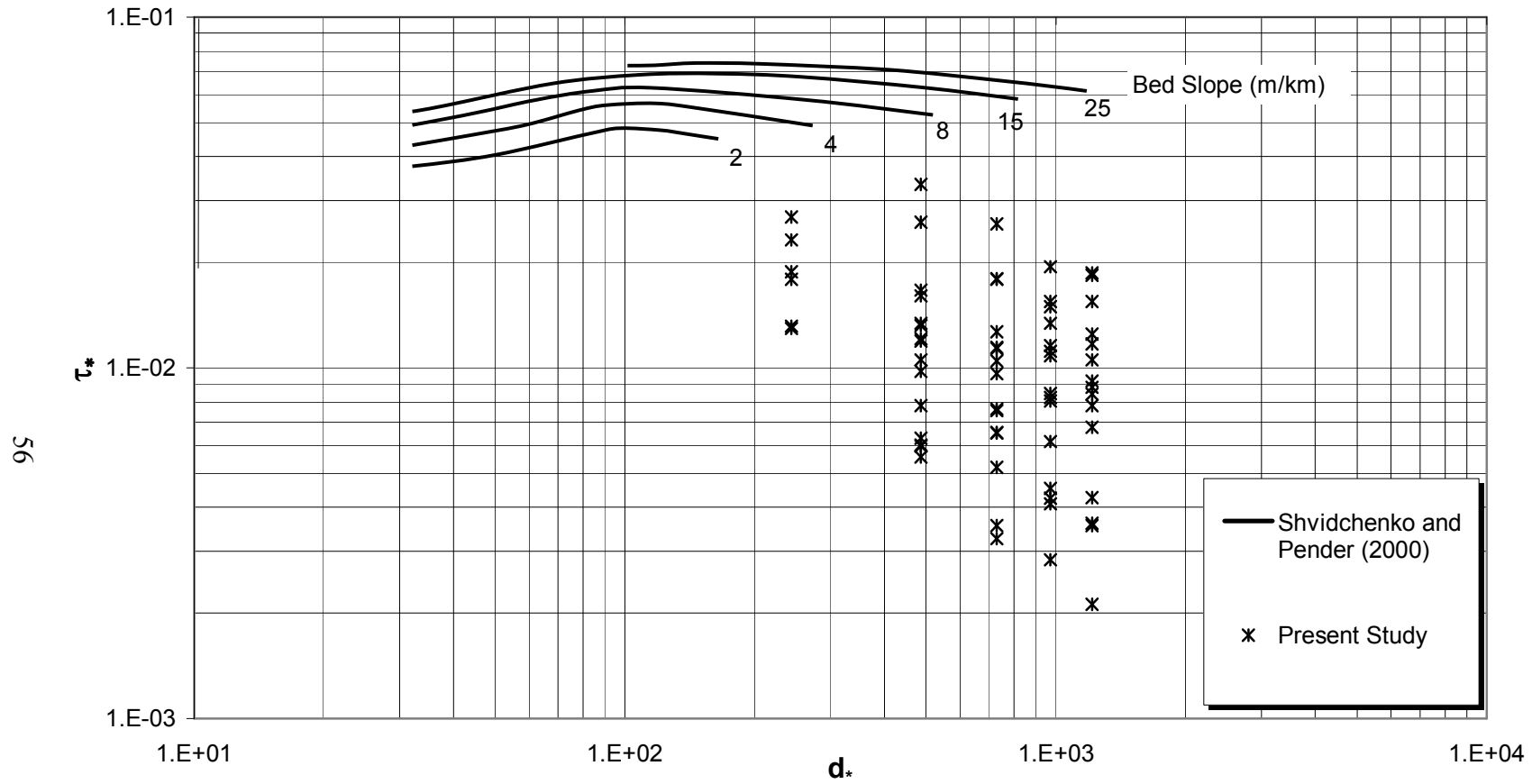


Figure III-26: Critical entrainment function τ_* vs. dimensionless grain size d_* together with results of Shvidchenko and Pender

III.3.3. Determination and Application of the Equivalent Sediment Diameter

Particle sizes were expressed in terms of equivalent sediment diameter instead of nominal diameter. Nominal diameter is solely based on the volumetric equality. Equivalent sediment diameter, $(d_s)_e$, is based on the conditions of initial motion and therefore it is a more powerful way of explaining the size and also the shape of a sediment grain. The values of $(d_s)_e$ computed through experiments are given in Figure III-27. It ranges from 0.85 cm to 9.28 cm.

Once the equivalent sediment diameters are determined, most of the expressions in terms of nominal diameter, d_s , can be given in terms of $(d_s)_e$. In Figure III-28, the relationship between the critical entrainment function and the grain Reynolds number is given in terms of $(d_s)_e$:

$$(\tau_*)_c = \frac{\tau_c}{(\gamma_s - \gamma) \cdot (d_s)_e} \quad (3.3)$$

$$Re_* = \frac{(u_*)_c \cdot (d_s)_e}{\nu} \quad (3.4)$$

In this figure, particles having the same nominal diameter, but different shapes lie on different lines, not like the case given in Figure III-10. However, there is still the effect of relative depth on the results. Unfortunately the amount and status of experimental results are not sufficient to obtain relative depth trend lines on the graph. Therefore referring to Figure III-28, it is not merely straightforward to determine whether there will be a motion or not for a particle of known equivalent sediment diameter without knowing R_b . Furthermore the results given are valid for the particles having the same material property with the ones used in the experiments and within the hydraulic ranges of the experiment (See Appendix B, Table B-1).

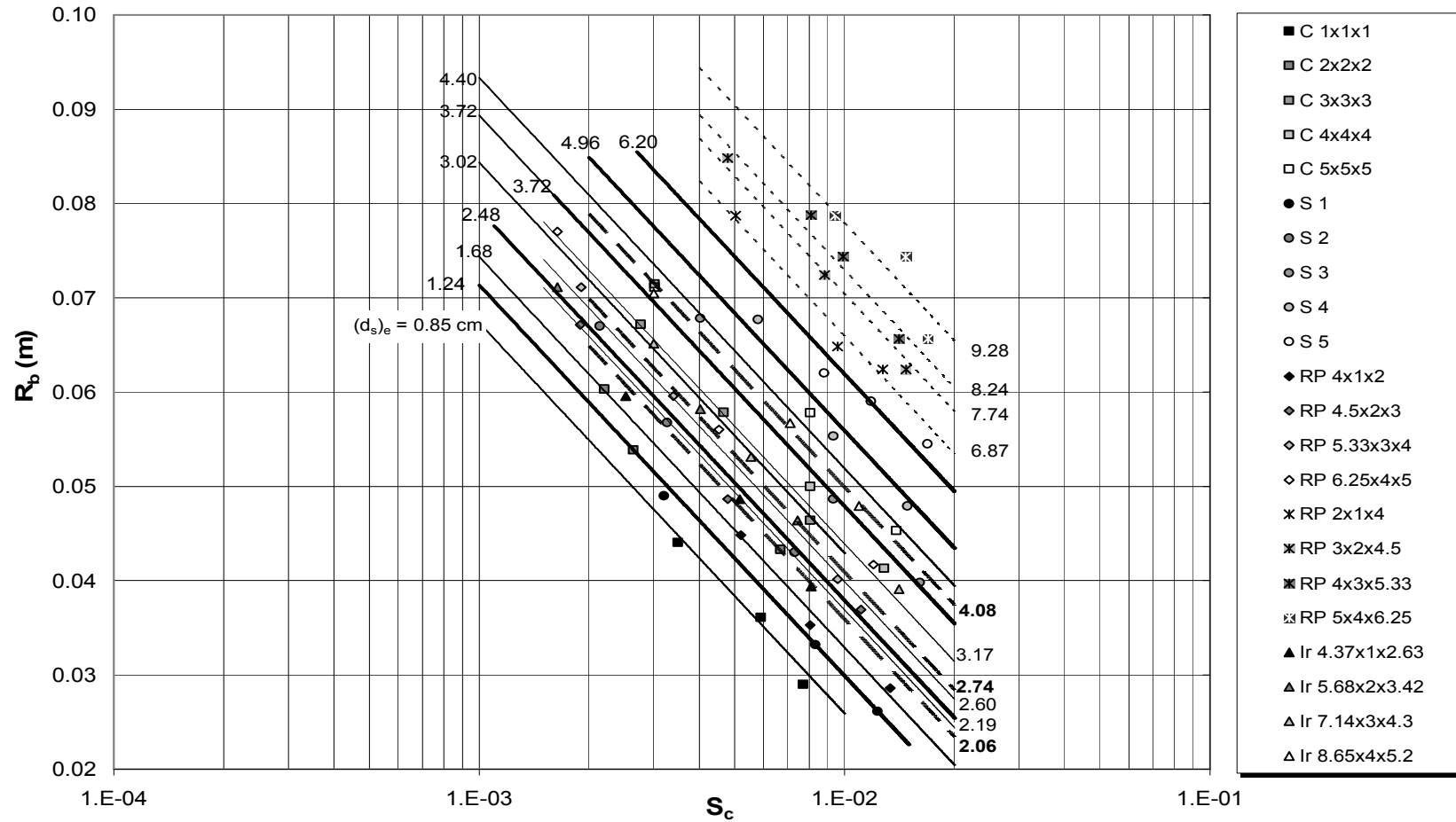


Figure III-27: Equivalent sediment diameters determined from the relationship of hydraulic radius and bed slope ($t/b=1.5/5$)

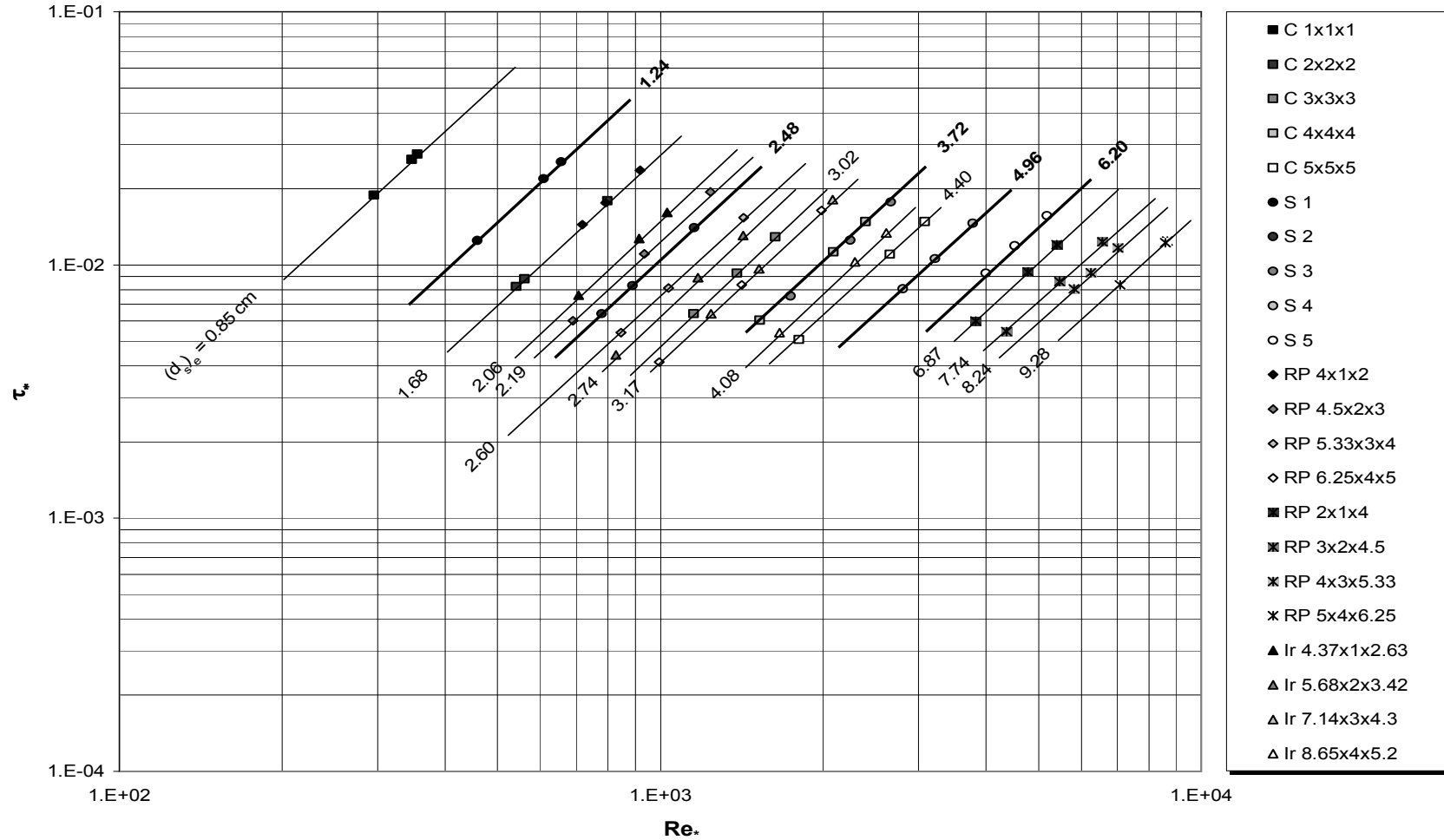


Figure III-28: τ_* versus Re_* in terms of $(d_s)_e$ ($t/b=1.5/5$)

The variation of relative depth $R_b / (d_s)_e$ with respect to the grain Reynolds number is given in Figure III-29. In this figure, different from Figure III-12, $(d_s)_e$ has been used for particle size instead of d_s . This eliminated the dependency of the relationship on the shape of particles. As a result, a single equation of best-fit curve has been given as

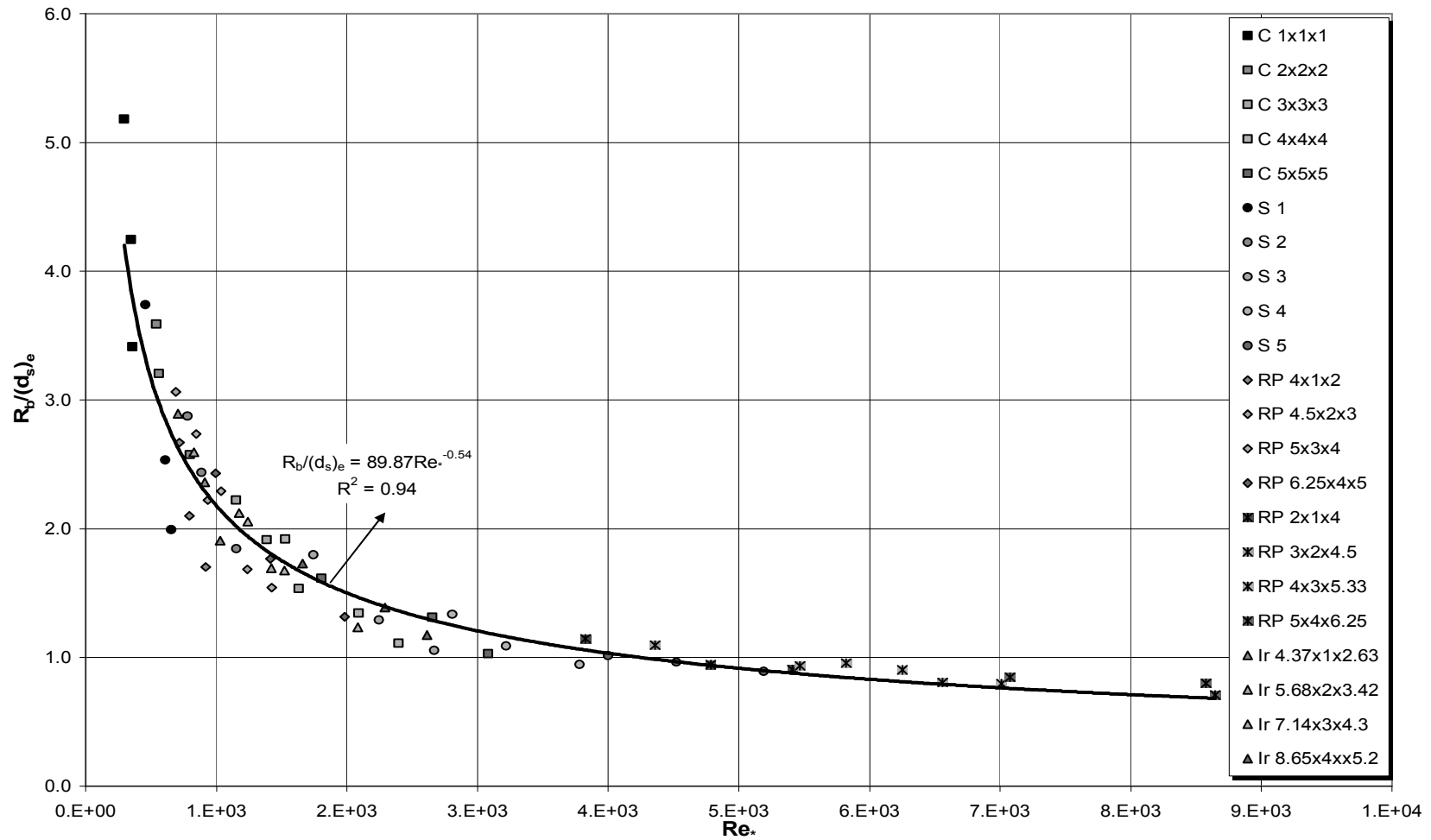
$$\frac{R_b}{(d_s)_e} = 89.87 \cdot Re_*^{-0.54} \quad (3.5)$$

with a correlation coefficient of $R^2=0.94$

where Re_* is also in terms of the equivalent sediment diameter $(d_s)_e$. This equation can be used in the determination of the equivalent sediment diameter for a particle as an alternative to Figure III-27 for known R_b or S values, or it can be used to determine either R_b or S for particles of known $(d_s)_e$.

In Figure III-30, the curve given in Figure III-29 which is valid for $t/b=1.5/5$ is compared with the one found in the previous study performed by Defne (2002) for $t/b=1/5$. The deviation between two curves is not so much even though the height of the obstruction element was increased 50%.

In the literature, usually sieve diameter and nominal diameter are used for particle size under consideration. Therefore, a transition from nominal diameter, d_s , to equivalent sediment diameter, $(d_s)_e$, is proposed in the following figures. In Figure III-31, variation of $(d_s)_e$ with d_s is given. Grouping of data according to the shape factors of the particles is presented in this graph. The trend lines of the data of cubic and spherical particles with their equations are presented in the figure. From the general trend of the data given in Figure III-31 it can be said that for a particle of known d_s , as the shape factor decreases, the value of $(d_s)_e$ increases.

Figure III-29: $R_b/(d_s)_e$ versus Re_* ($t/b=1.5/5$)

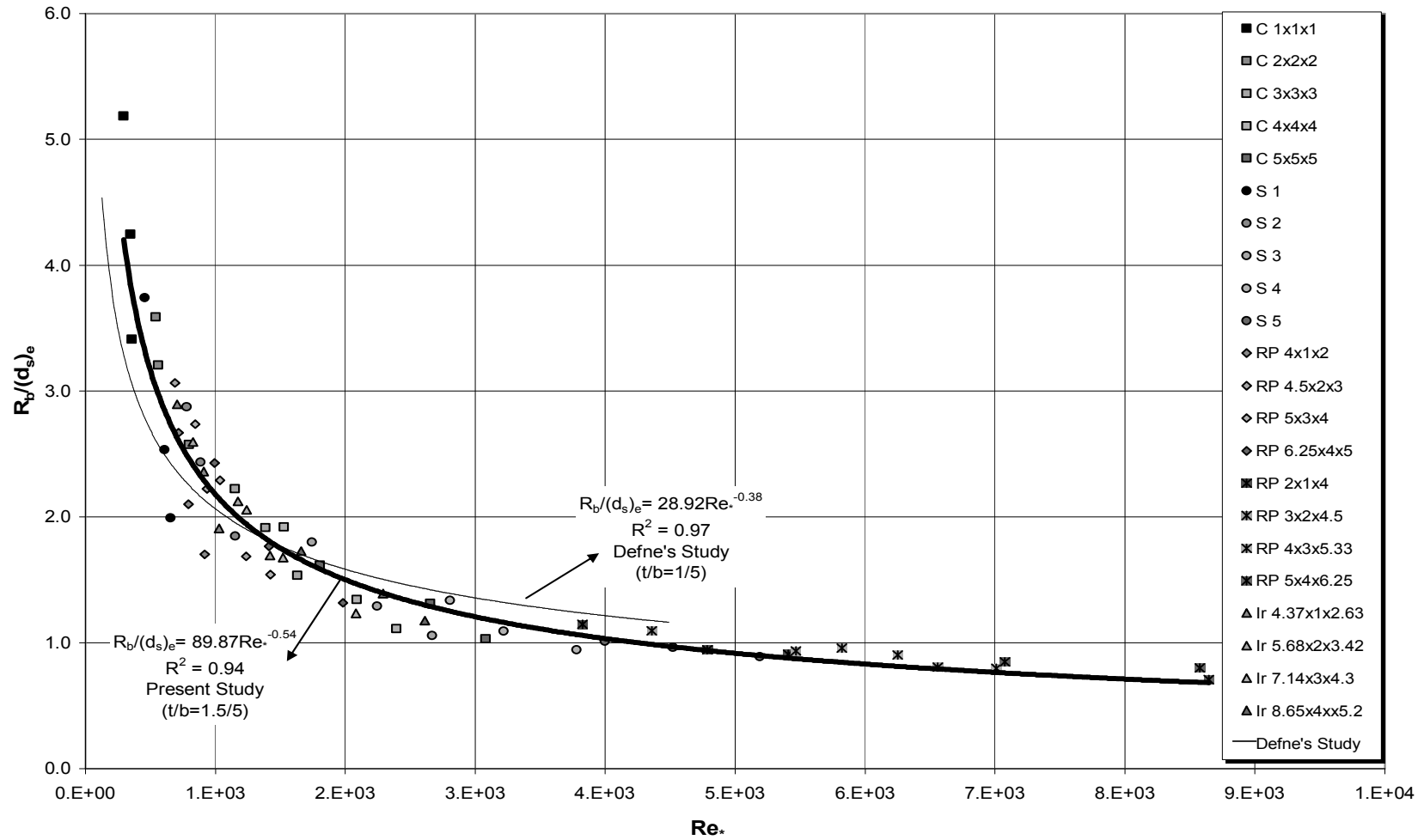


Figure III-30: Comparison of $R_b/(d_s)_e$ versus Re^* curves obtained in present study and Defne's Study

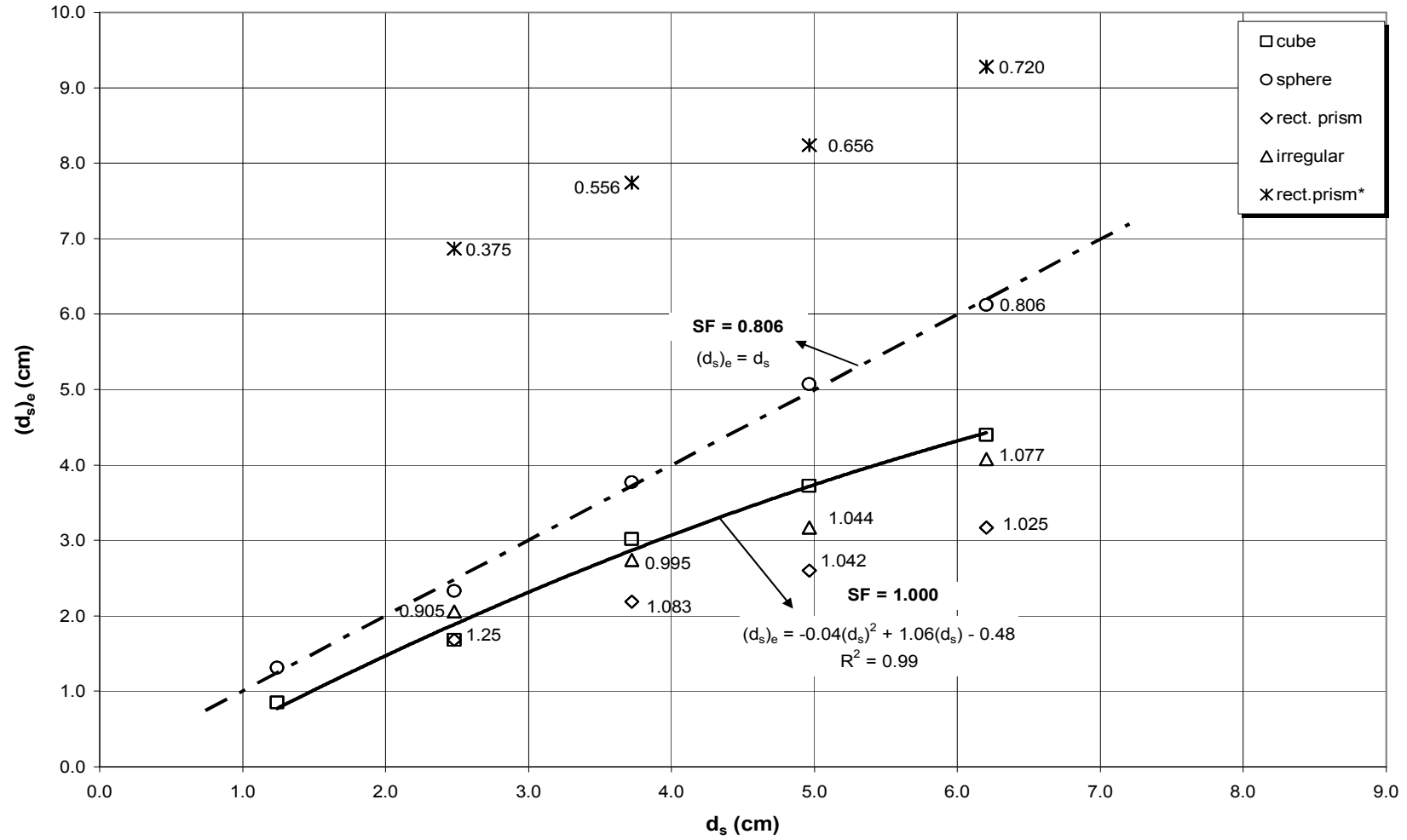


Figure III-31: $(d_s)_e$ versus d_s and shape factors ($t/b=1.5/5$)

The critical velocity at the condition of incipient motion can also be given as a function of the equivalent sediment diameter. Variation of the critical cross-sectional velocity, V_{cc} ; critical velocity in the vertical, V_{vc} ; and critical bottom velocity, V_{bc} , are given in Figure III-32, Figure III-33 and Figure III-34, respectively.

The critical velocities are determined with the equations

$$V_{cc} = 3.58 \cdot (d_s)_e^{0.54} \quad (3.6)$$

with a correlation coefficient of $R^2=0.90$

$$V_{vc} = 2.38 \cdot (d_s)_e^{0.42} \quad (3.7)$$

with a correlation coefficient of $R^2=0.92$

$$V_{bc} = 2.94 \cdot (d_s)_e^{0.50} \quad (3.8)$$

with a correlation coefficient of $R^2=0.91$

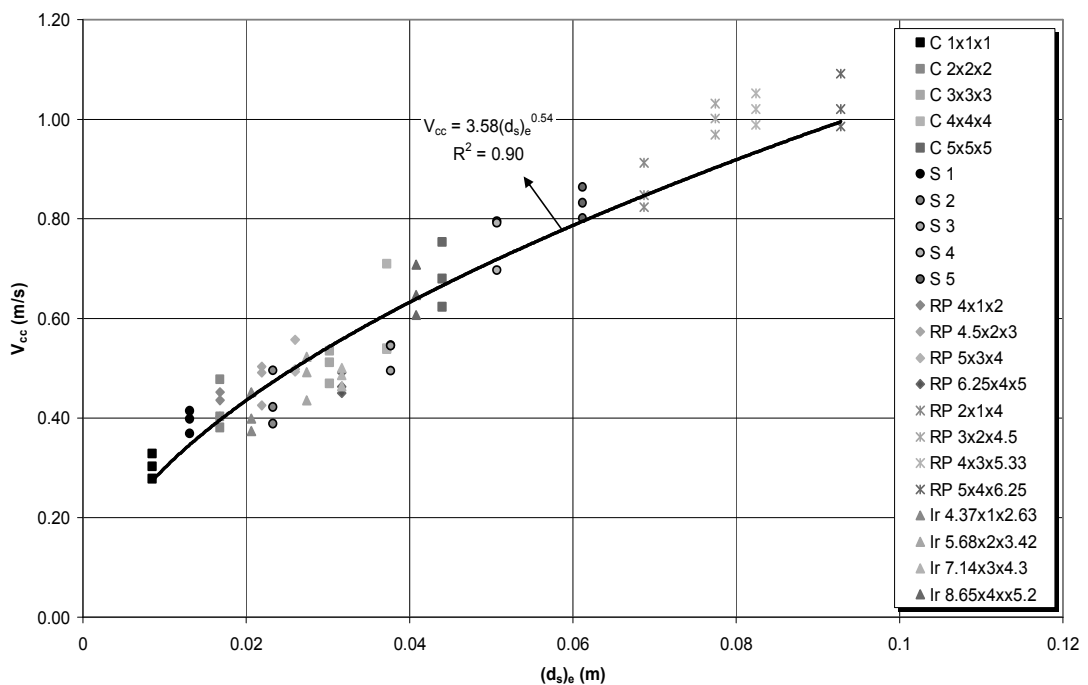


Figure III-32: Critical cross-sectional velocity, V_{cc} vs. $(d_s)_e$

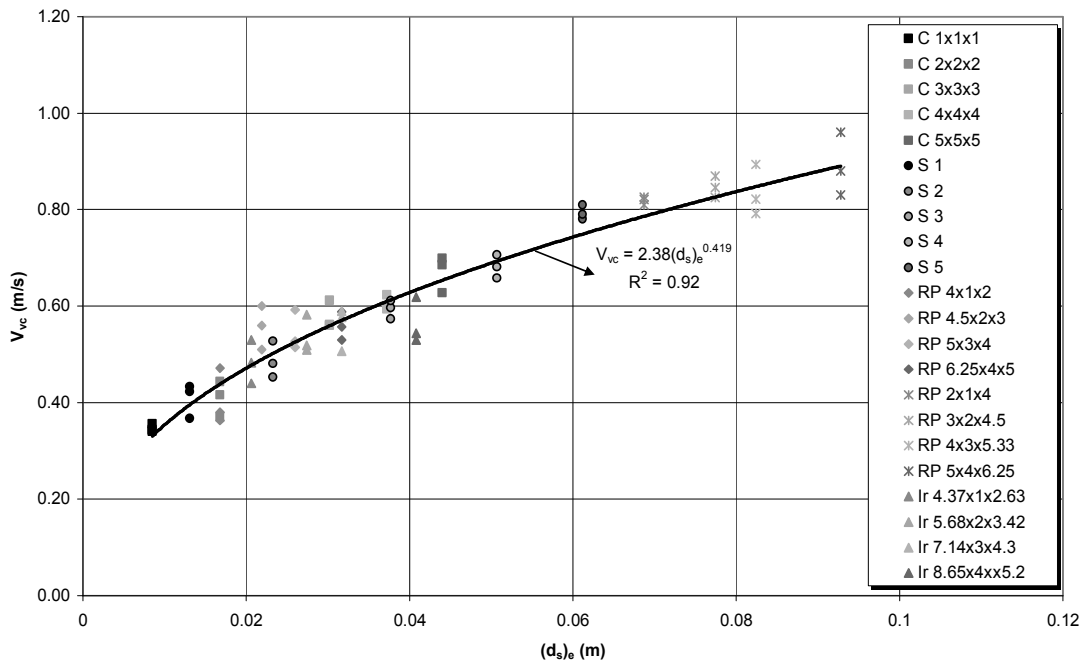


Figure III-33: Critical velocity in the vertical, V_{vc} vs. $(d_s)_e$

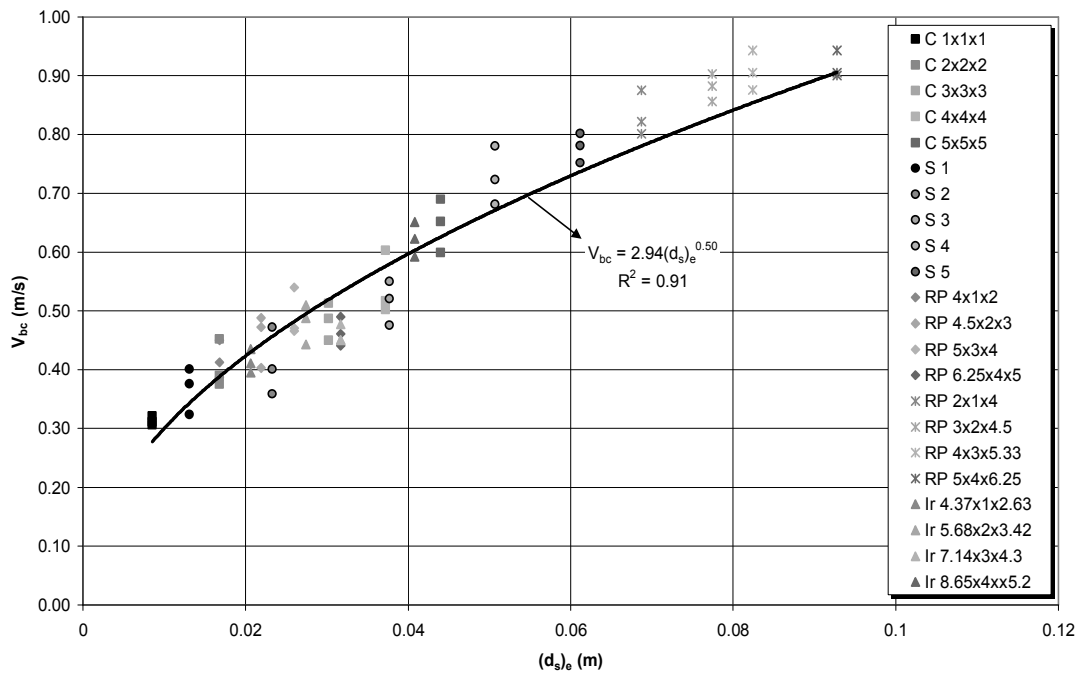


Figure III-34: Critical bottom velocity, V_{bc} vs. $(d_s)_e$

III.3.4. Re-analysis of Brahms Equation

The relations between the critical bottom velocities and the weights of particles having different shapes are given in Figure III-35. This figure indicates that separate trend lines can be obtained for different shape factors. For a particle of known shape factor and weight, the value of the critical bottom velocity, V_{bc} , can be determined straightforwardly from Figure III-35.

The empirical constant K in Brahms equation, Equation (2.22), is given as a function of the shape factor in Figure III-36. For a particle of known shape factor, K value can be directly computed with the equation

$$K = -0.62 \cdot \ln(SF) + 0.54 \quad (3.9)$$

with a correlation coefficient of $R^2=0.83$

In Figure III-37 the equations to find K in terms of the shape factor are given for both the present study ($t/b=1.5/5$) and Defne's study ($t/b=1/5$). It is obvious that as the height of the obstructing element increases, the critical bottom velocity required for particle motion will be higher, which requires higher K value as seen in Figure III-37. K values corresponding to $t/b=1/5$ and $t/b=1.5/5$ get closer to each other as the value of the shape factor increases and become the same for the shape factor of 1.00.

The results that are more precise are available when K is expressed as a function of SF and the relative depth, d_s/R_b as stated in Equation (2.23). This relationship is given in Figure III-38. For a particle of known shape factor if d_s/R_b is given, within the range of d_s/R_b tested in this study, and the corresponding critical bottom velocity is asked for the incipient motion of the particle, the K value needed for this computation can be obtained from the equation

$$K = -0.33 \cdot \ln\left(SF \cdot \frac{d_s}{R_b}\right) + 0.52 \quad (3.10)$$

with a correlation coefficient of $R^2=0.85$.

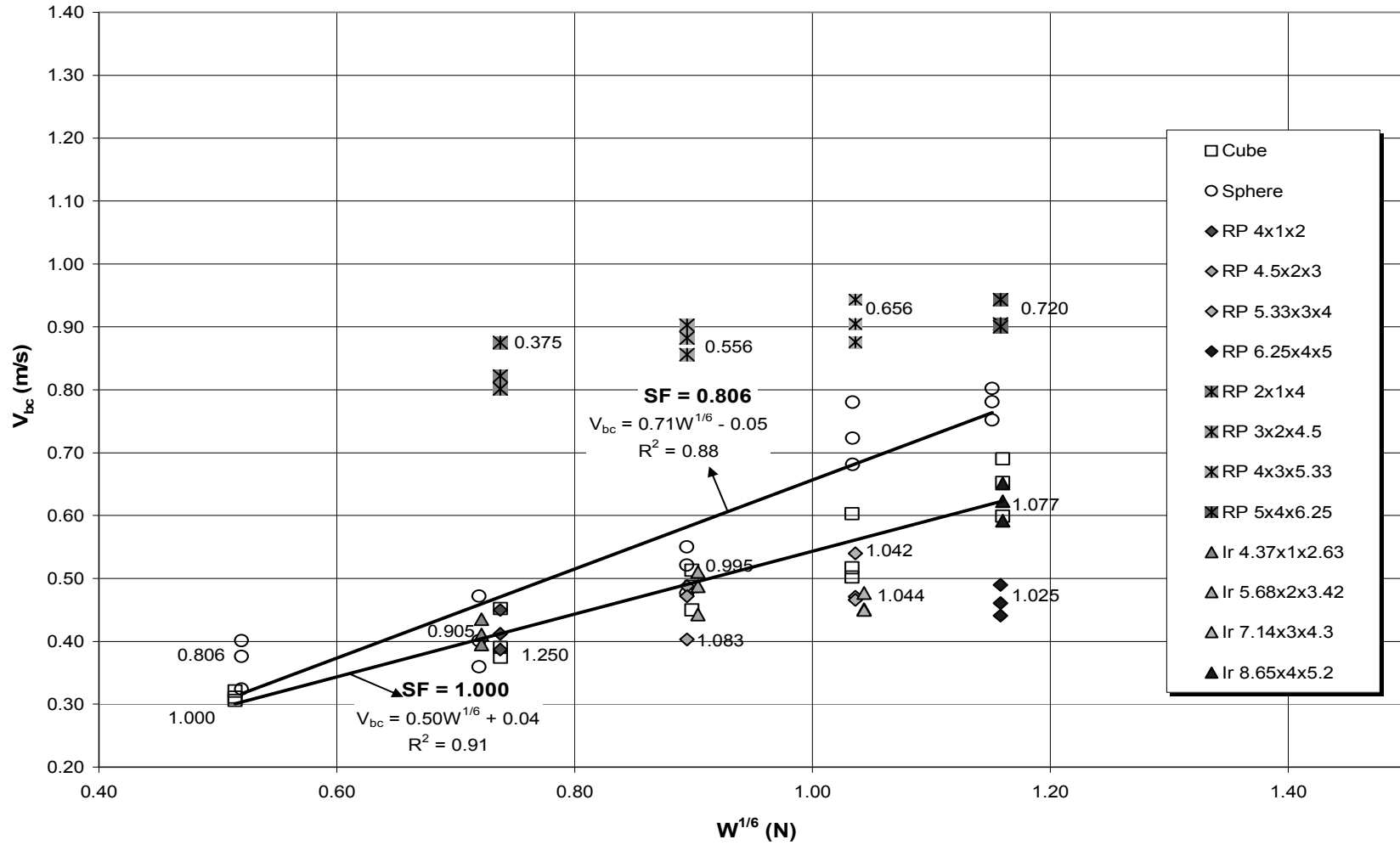


Figure III-35: V_{bc} versus $W^{1/6}$ for particles of different shape factors

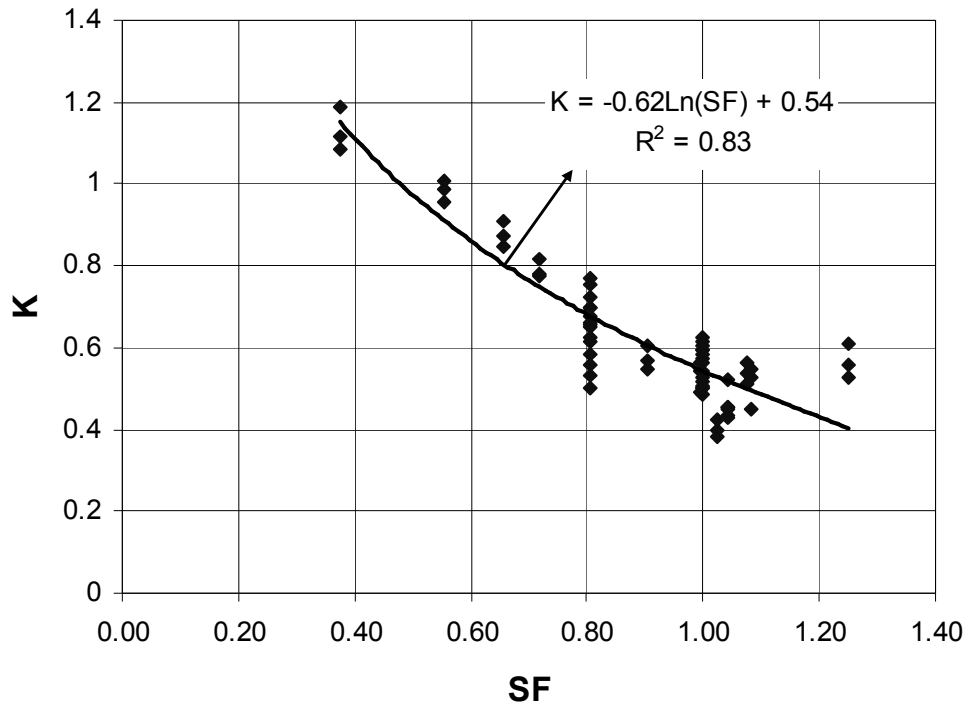


Figure III-36: Empirical constant, K , of Brahms equation versus shape factor, SF

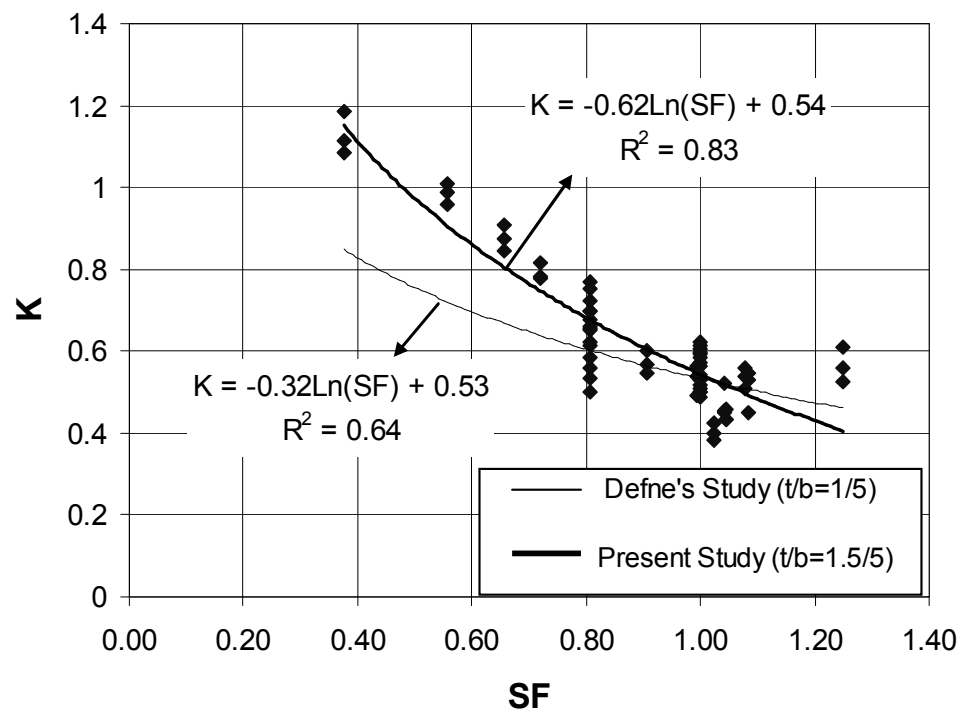


Figure III-37: Comparison of relation between K and shape factor, SF

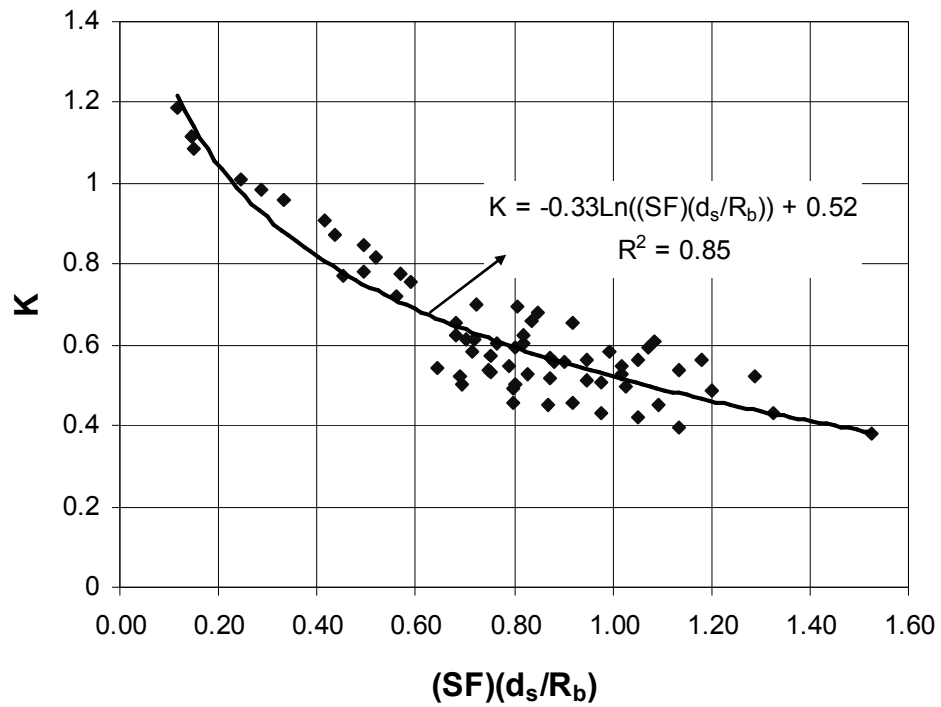


Figure III-38: K versus product of shape factor and relative depth

In Figure III-39 the equations to find K in terms of shape factor and relative depth are given for both the present study and Defne's study. As the value of $(SF)(d_s/R_b)$ gets larger, the K value of the two curves approach to each other and become almost the same at values of $(SF)(d_s/R_b)$ greater than about 1.00. This situation implies that at large values of $(SF)(d_s/R_b)$, the value of R_b required for particle motion becomes smaller for a known particle size and shape. The smaller R_b values are attained at steeper channel slopes at which having the t/b value as $1/5$ or $1.5/5$ does not influence the critical bottom velocity required for the motion of the particle.

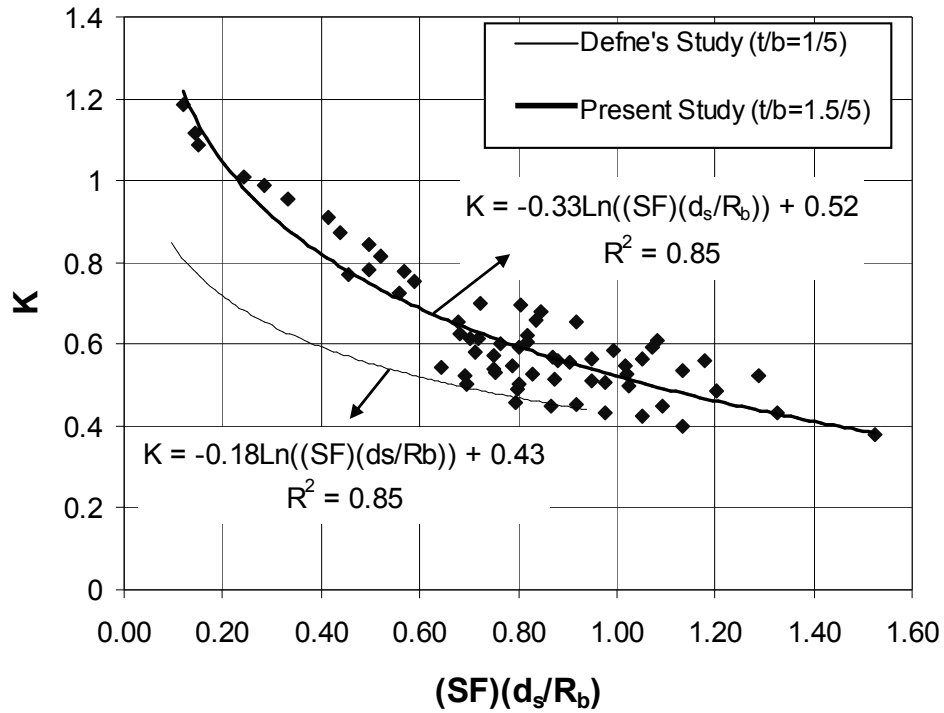


Figure III-39: Comparison of relation between K and product of shape factor and relative depth

III.3.5. Determination of the Critical Condition from the Height to Length Ratio of the Particle

In this section, determination of the critical condition from the height to length ratio, b/c , of the particle is proposed. Based on the derivation given in the theoretical part, the variation of $(Fr_v)_b / \sqrt{\cos \theta}$ with b/c is presented in Figure III-40. The equation of the best fitting curve to the data presented in Figure III-40 is given by

$$\frac{(Fr_v)_b}{\sqrt{\cos \theta}} = 4.10 \cdot \left(\frac{b}{c}\right)^2 - 7.52 \cdot \left(\frac{b}{c}\right) + 4.40 \quad (3.11)$$

with a correlation coefficient of $R^2=0.72$.

Where $(Fr_v)_b$ is the critical densimetric Froude number in terms of average velocity; therefore, the critical velocity can be calculated directly from the above relationship.

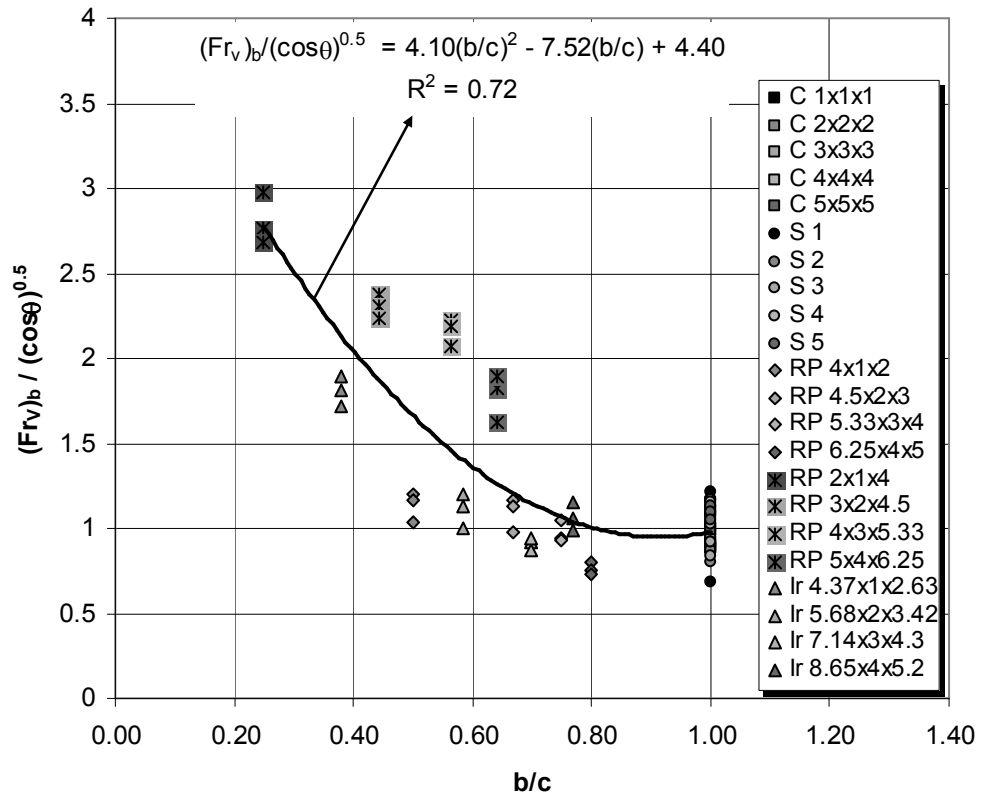


Figure III-40: $(Fr_v)_b / \sqrt{\cos \theta}$ versus b/c

The rehabilitation to Equation (3.11) is suggested with the introduction of the shape factor. The relationship between $(Fr_v)_b$ and product of $(SF)(b/c)$, given in Figure III-41, is generalized with the expression

$$\frac{(Fr_v)_b}{\sqrt{\cos \theta}} = 2.81 \cdot \left(SF \cdot \frac{b}{c} \right)^2 - 5.26 \cdot \left(SF \cdot \frac{b}{c} \right) + 3.40 \quad (3.12)$$

with a correlation coefficient of $R^2=0.92$.

The use of this expression in the determination of the critical condition terms yields results that are more accurate than the previous equation.

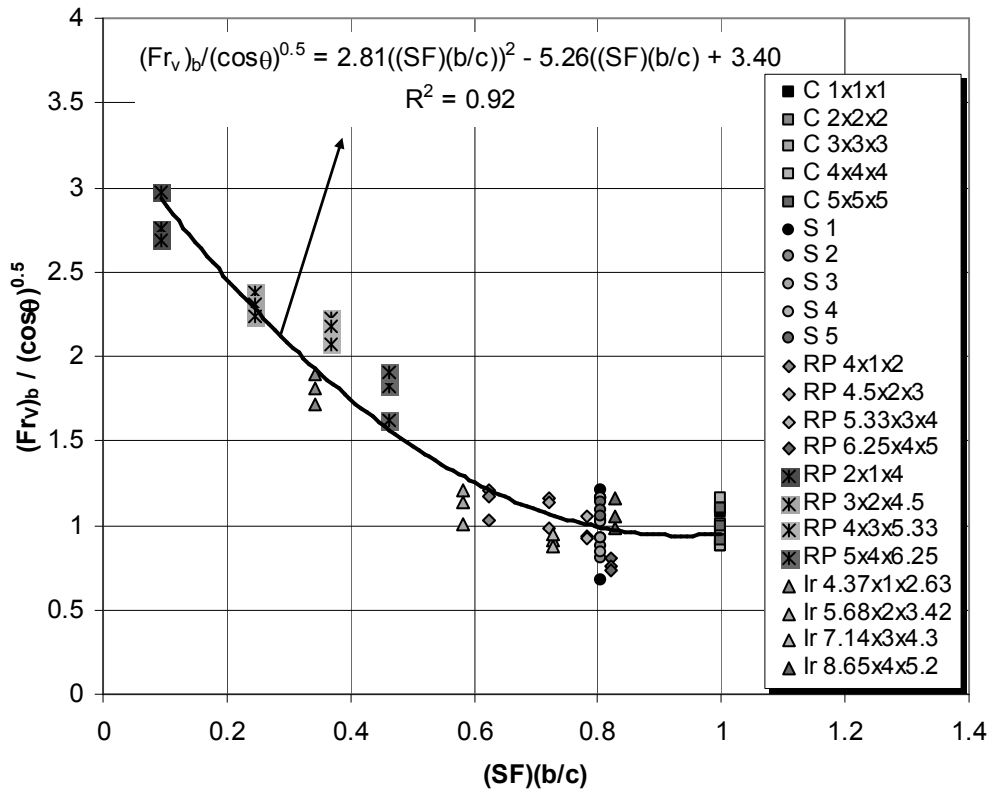


Figure III-41: $(Fr_v)_b / \sqrt{\cos\theta}$ versus $(SF)(b/c)$

The relationship given by Equation (3.12) and the corresponding one obtained by Defne are presented in Figure III-42 together to show the effect of t/b on the experimental results. At values of $(SF)(b/c)$ greater than about 0.6, the two curves almost coincide with each other whereas deviation between two curves increase as $(SF)(b/c)$ gets smaller than 0.6.

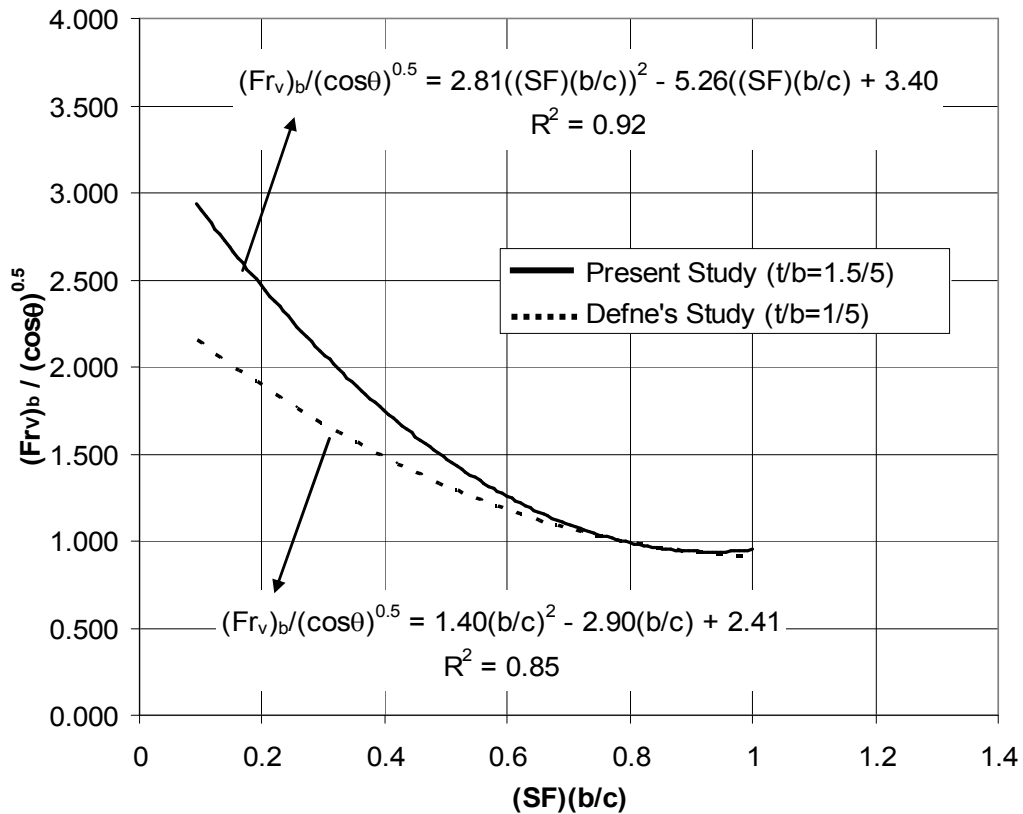


Figure III-42: Comparison of $(Fr_v)_b / \sqrt{\cos \theta}$ versus $(SF)(b/c)$

III.3.6. Evaluation of the Relationship Between the Critical Velocity and the Grain Size

Stelczer (1981) gave a collection of numerous studies on the relationship between the critical velocity and the grain size related to the incipient motion. The results of present study are given below in graphical terms together with the previous studies.

In terms of the critical cross-sectional velocity, Stelczer's summary of the relevant literature in graphical form is presented in Figure III-43. Besides, experimental findings of the present study are indicated in the same figure. From this figure, it is clearly seen that the data of the present study follow very similar trend to those given in the figure.

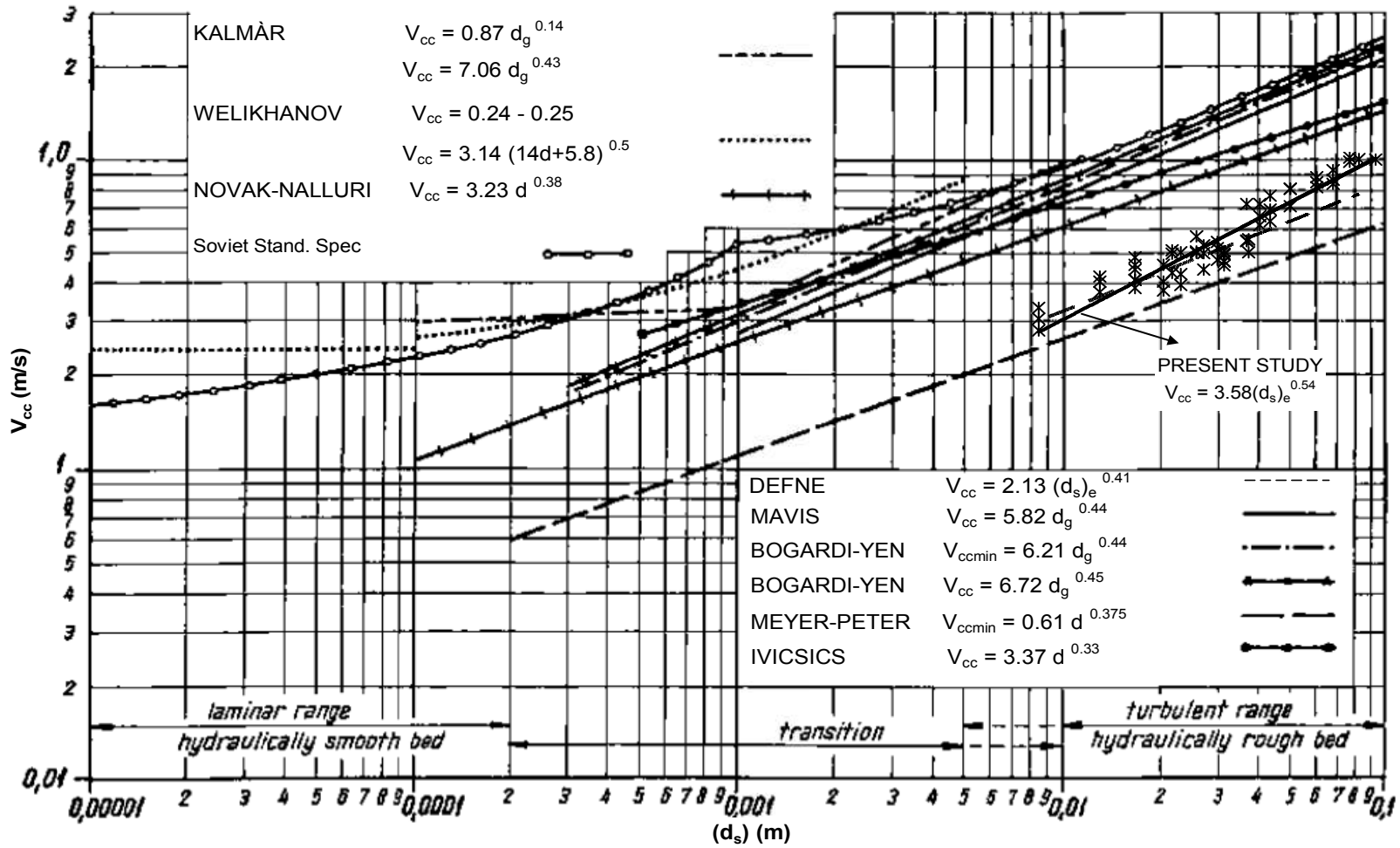


Figure III-43: Critical cross-sectional velocity versus grain size

Even though the range of the experiments have been extended up to grain diameters equal to 10.0 cm in the above figure, actual ranges do not cover that much large sizes. Amongst the researchers mentioned above, only Kalmár studied with particles with median particle diameters up to 1.0 cm. The range of Meyer-Peter's equation is not given (Stelczer, 1981).

The term d_g in the equations given in the figure stands for granulometric median size of sediment grains. This term is used where the group of particles studied consists of mixed size grains. The term d , without any subscription, indicates the sieve diameter of a particle.

In the present study, coarse, single particles made of same material were examined on a smooth fixed bed. An obstructing element was placed immediately downstream of the particles with particle height to obstructing element height ratio of 3.33 (5/1.5). Particle size was defined either by nominal diameter or by equivalent sediment diameter. The range of particle size was within 1.0 cm and 10.0 cm.

The relationship between the critical velocity in the vertical, V_{vc} and the grain size is given in Figure III-44. Gontsharov's equation is valid for uniform particle sizes, for different values of flow depth. For smaller water depths, the trend lines approach to the trend line given in the present study.

The relationship between the critical bottom velocity, V_{bc} , and the particle diameter is presented in Figure III-45. Particle sizes examined in the given studies do not exceed 1.0 cm.

In spite of the specific conditions of the present study, throughout the figures it is seen that the results are parallel to the existing studies on the subject matter. At the end, expressions in the form of power function are suggested to define the relationship between the critical velocity and the grain size.

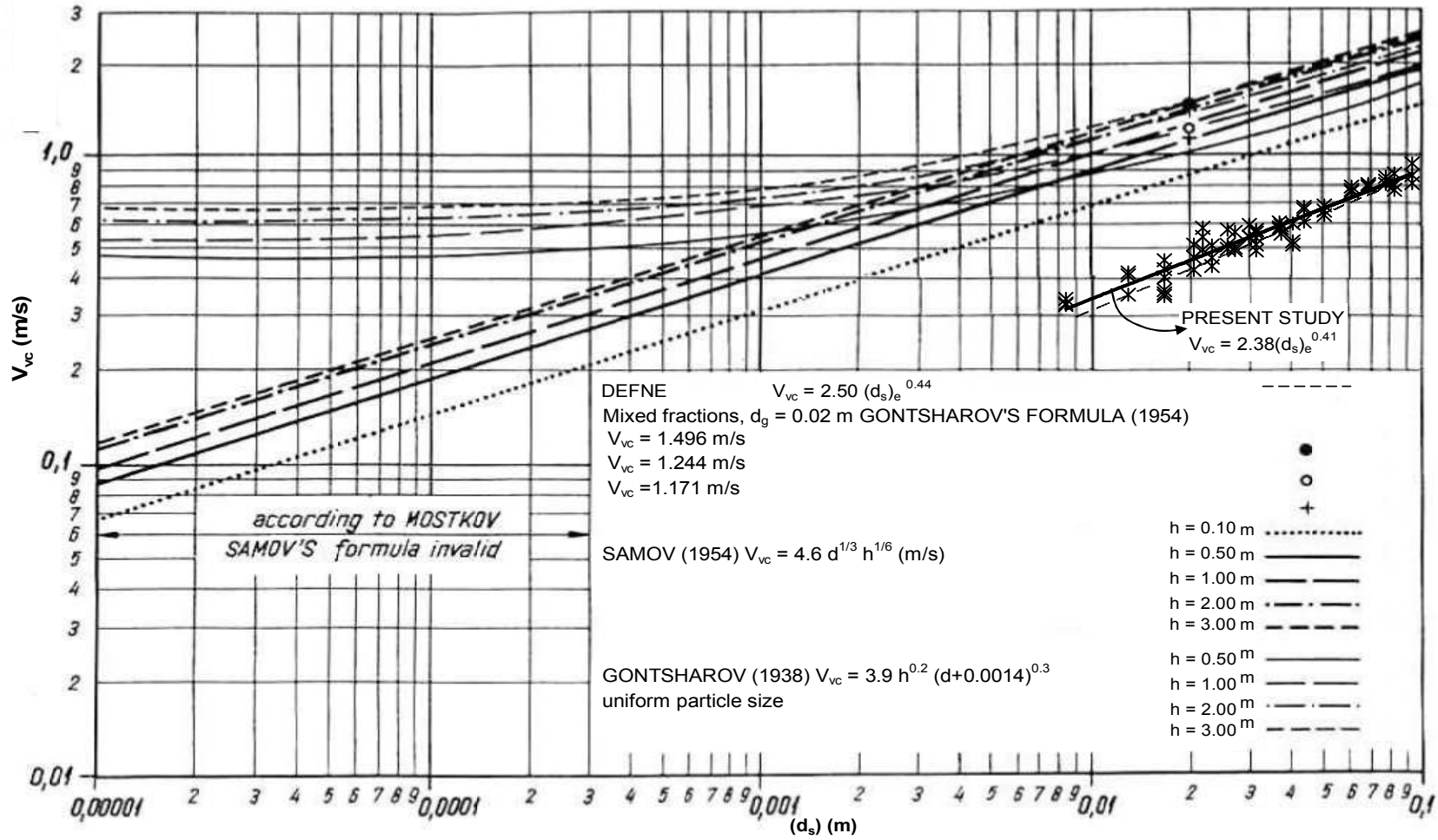


Figure III-44: Critical velocity in the vertical versus grain size

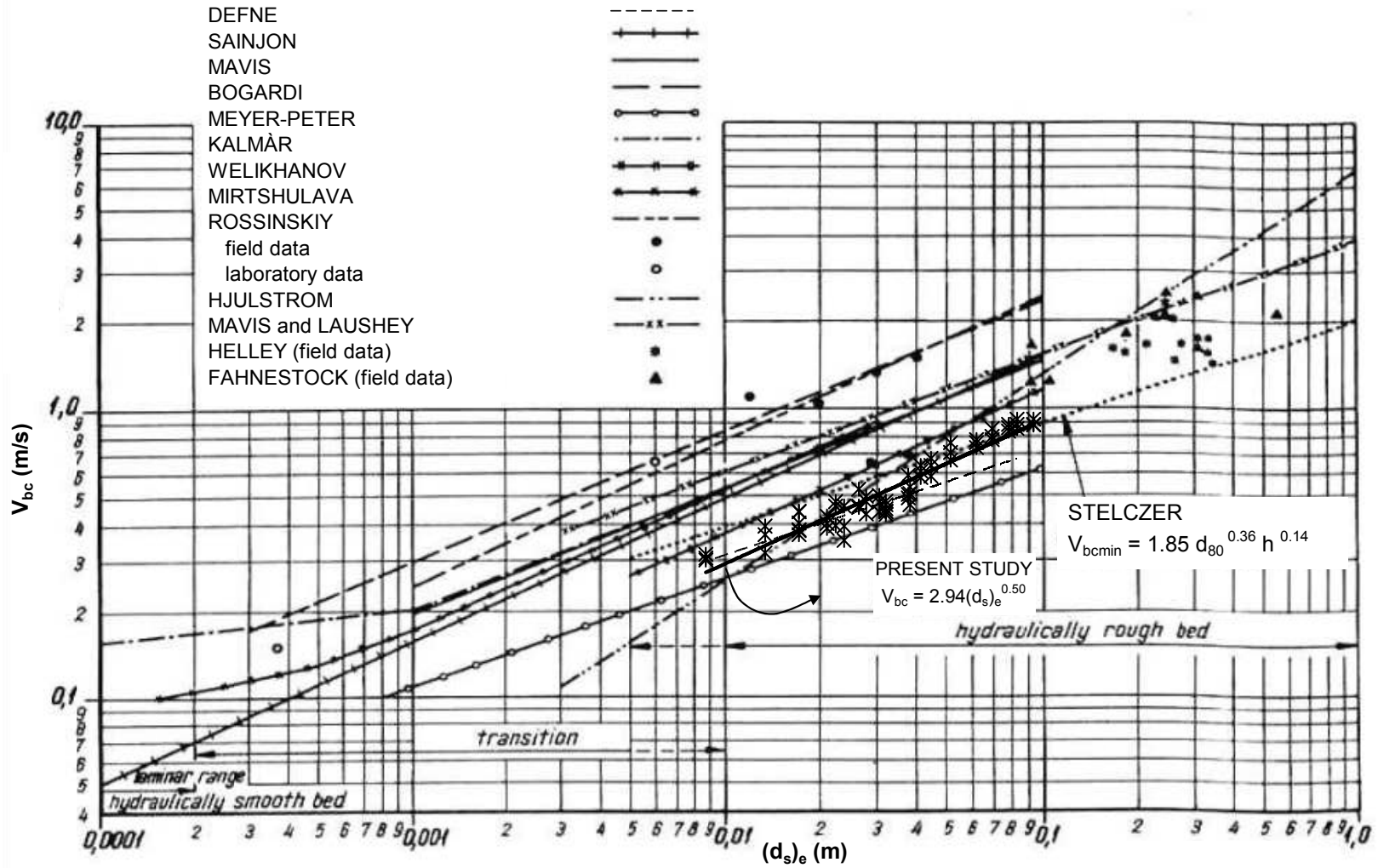


Figure III-45: Critical bottom velocity versus grain size

III.3.7. Comparison of Present Study with the Study of Novak and Nalluri

The relationship between the densimetric Froude number and the relative depth was investigated in details by Novak and Nalluri (1984) as mentioned within the relevant literature. They had studied with single particles on smooth fixed beds and rough fixed beds. A comparative presentation of their results and present results are given in Figure III-46. In their study they had concluded that as the relative roughness, d_s/k , increases a similar behavior to loose bed can be observed. This trend is shown in the figure with dotted lines. The experiments of the present study were performed on smooth fixed bed and they fit well within a region bounded by smooth boundary conditions as seen in the figure. However, due to the obstructing element the results diverge from smooth boundary conditions towards rough boundary conditions.

The variation of the critical shear stress with respect to the grain size is given in Figure III-47 in comparison with the trend line suggested by Novak and Nalluri (1984). Here, $(d_s)_e$ is used for the grain sizes of experimental data. The present data give somewhat higher τ_c values for a given grain size than those proposed by Novak and Nalluri.

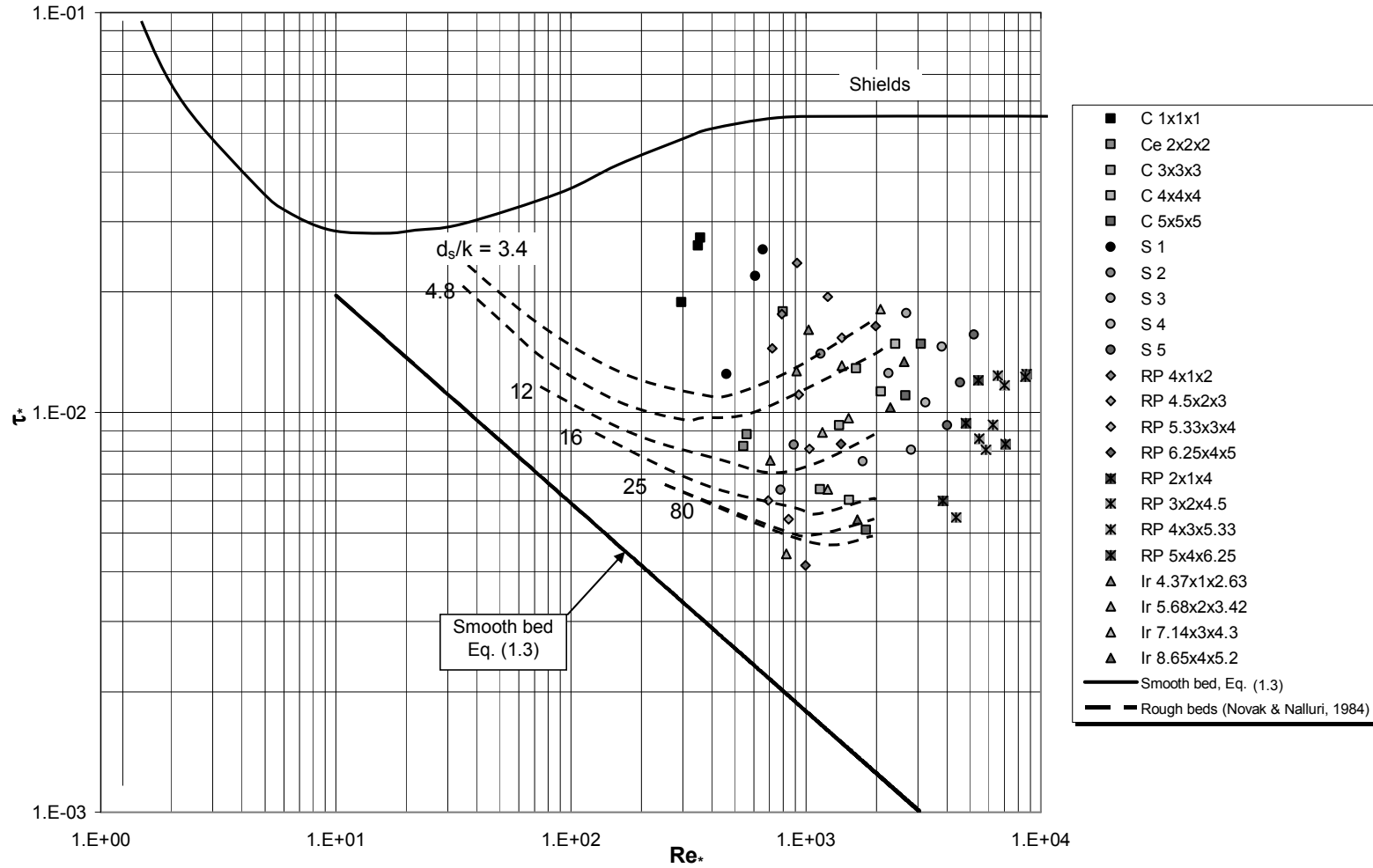


Figure III-46: Variation of τ^* and Re^* based on $(d_s)_e$ as a function of d_s/k

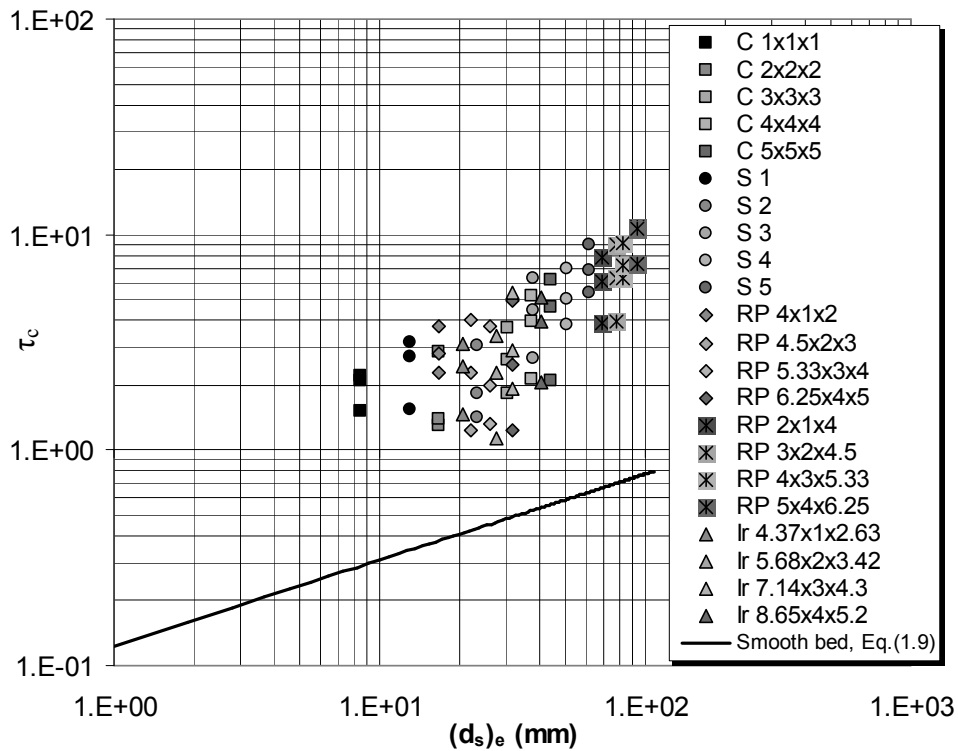


Figure III-47: τ_c versus grain size

The relationship between the relative depth, d_s/R_b , and the densimetric Froude number in terms of cross sectional velocity and particle diameter, $(Fr_v)_d$, is demonstrated in Figure III-48. In this figure the results obtained by Novak and Nalluri are also given. In their study, in the case of rough fixed bed, the relationship between two parameters was gathered for a relative roughness ratio of about 10.0. Throughout this part of the present study, ratio of b/t was kept constant at 3.33 (5/1.5), consequently the results have higher densimetric Froude number values. Moreover, grouping of the particles according to their shape factors is also applicable to this relationship. This is also shown in Figure III-49.

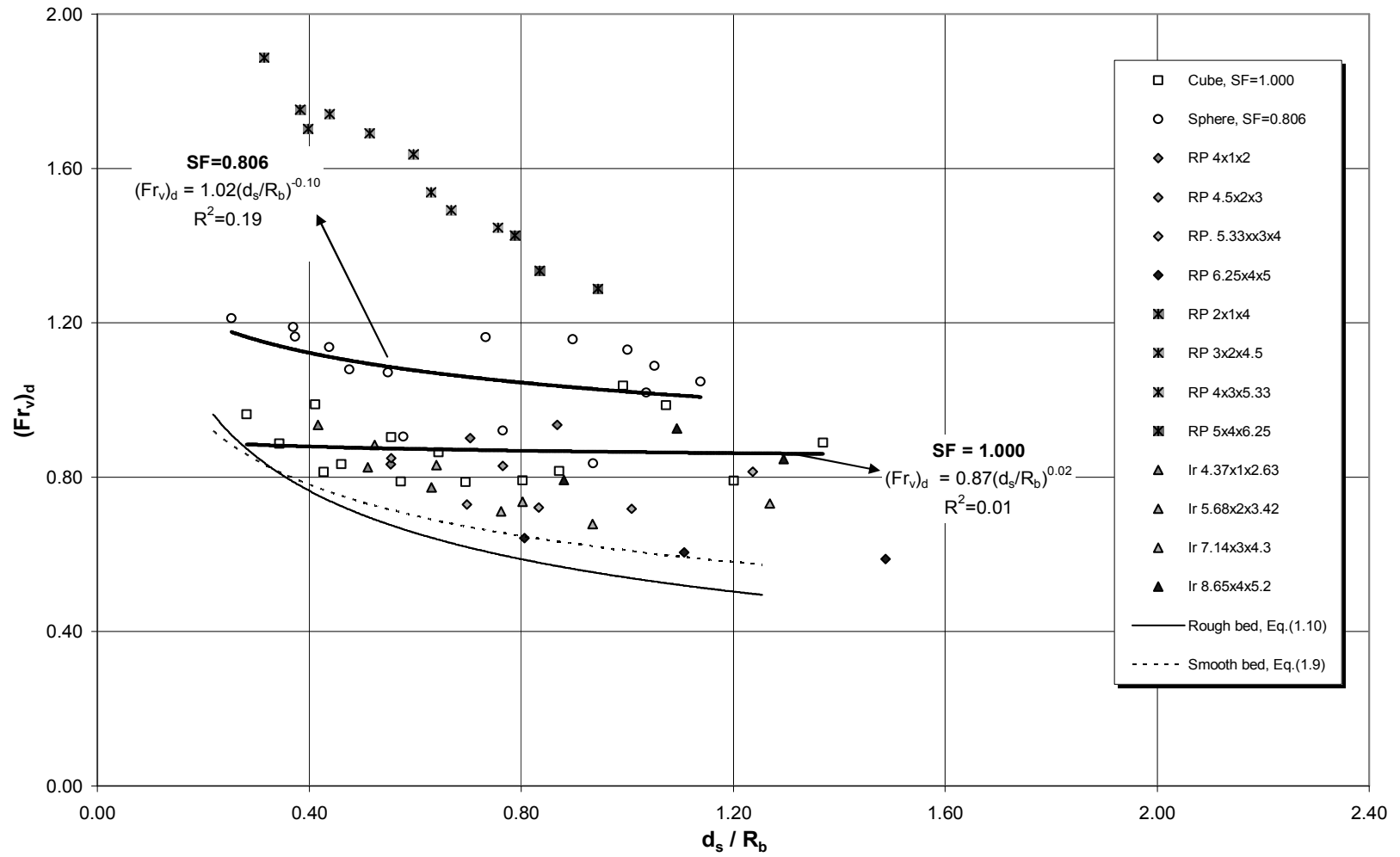


Figure III-48: Densimetric Froude number in terms of cross-sectional velocity versus relative depth

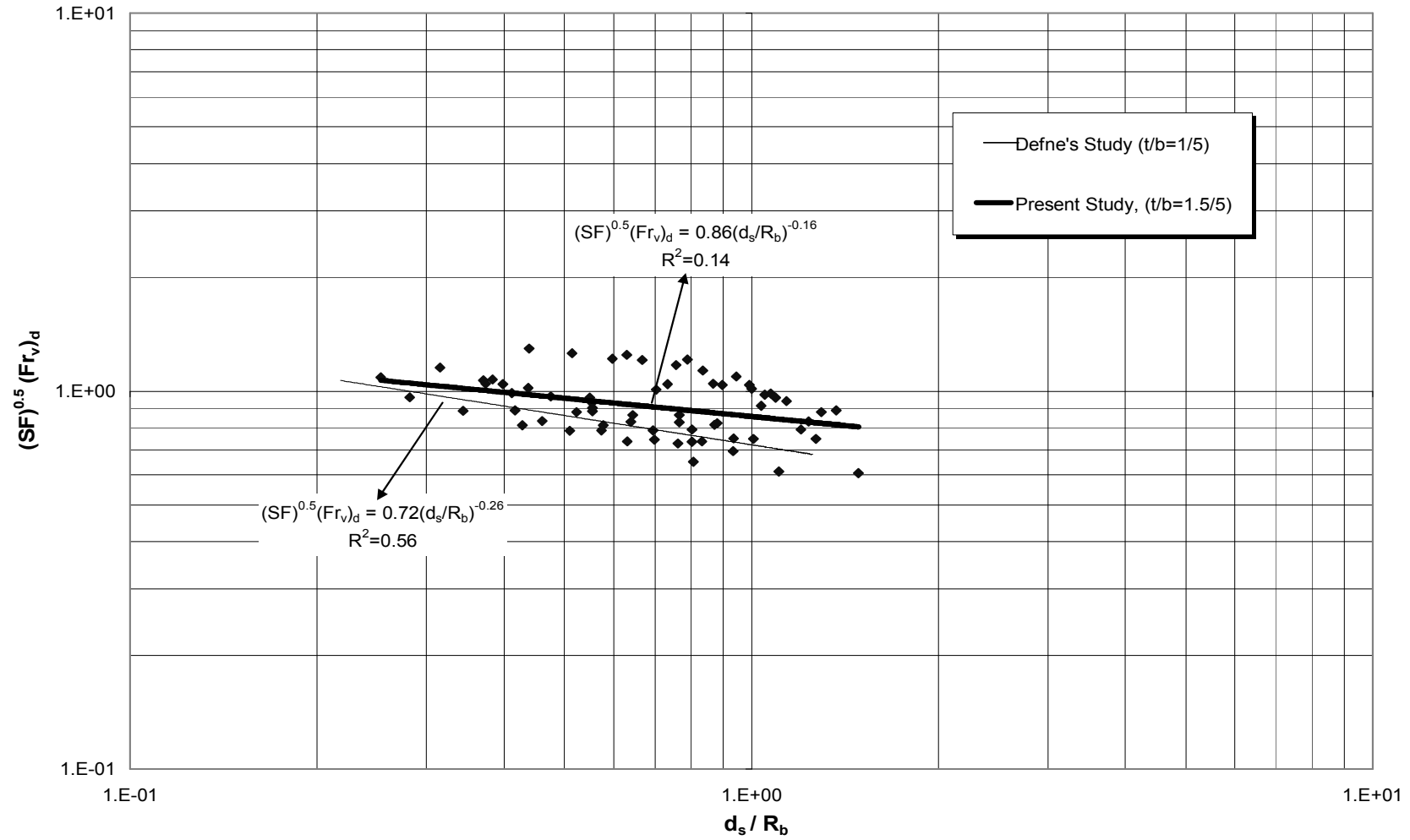


Figure III-49: The relationship between $(SF)^{0.5} (Fr_v)_d$ and d_s/R_b

The effect of particle shape on the relationship can be minimized by multiplying the densimetric Froude number by the square root of the shape factor (See Figure III-49). The equation of the best fitting curve of the data presented in Figure III-49 is given by

$$(SF)^{0.5} \cdot (Fr_v)_d = 0.86 \cdot \left(\frac{d_s}{R_b} \right)^{-0.16} \quad (3.13)$$

with a correlation coefficient of $R^2=0.14$.

In this figure the best fitting curve for the study performed for the same particles with $t/b=1/5$ (Defne,2002) is also plotted. The above equation follows almost the same trend as those given by Defne (2002) and Novak-Nalluri (1984).

CHAPTER IV

THE EXPERIMENTAL INVESTIGATIONS WITH THE SECOND GROUP OF PARTICLES

In this chapter the experimental results of particles having specific weight of 2.36 g/cm³ are compared with those of particles of 1.96 g/cm³ specific weight in order to find out the effect of specific weight of particles on incipient motion. The obstacle height to particle height ratio was kept constant as 1.5/5 at all of the experiments.

IV.1. Relationship Between the Entrainment Function and the Grain Reynolds Number

The relationship between the entrainment function, τ^* , and the grain Reynolds number, Re^* had been explained in section III.3.1 for particles of 1.96 g/cm³ specific weight. In Figure IV-1 the variation of entrainment function, τ^* , with the grain Reynolds number, Re^* , at the condition of incipient motion, for particles having specific weight of 1.96 g/cm³ and 2.36 g/cm³ is given together. As seen in this figure, the data of particles of $\gamma_s = 2.36 \text{ g/cm}^3$ follow almost the same trend as those of $\gamma_s = 1.96 \text{ g/cm}^3$.

Another graph indicating the relationship among Re^* , R_b/d_s and SF is given in Figure IV-2 for both sets of the particles tested. This figure prevails that for the particles of $SF=1.00$ the data set of both particle groups almost coincide with each other. As the SF decreases, a certain amount of deviation between aforementioned curves is observed especially as the value of Re^* decreases.

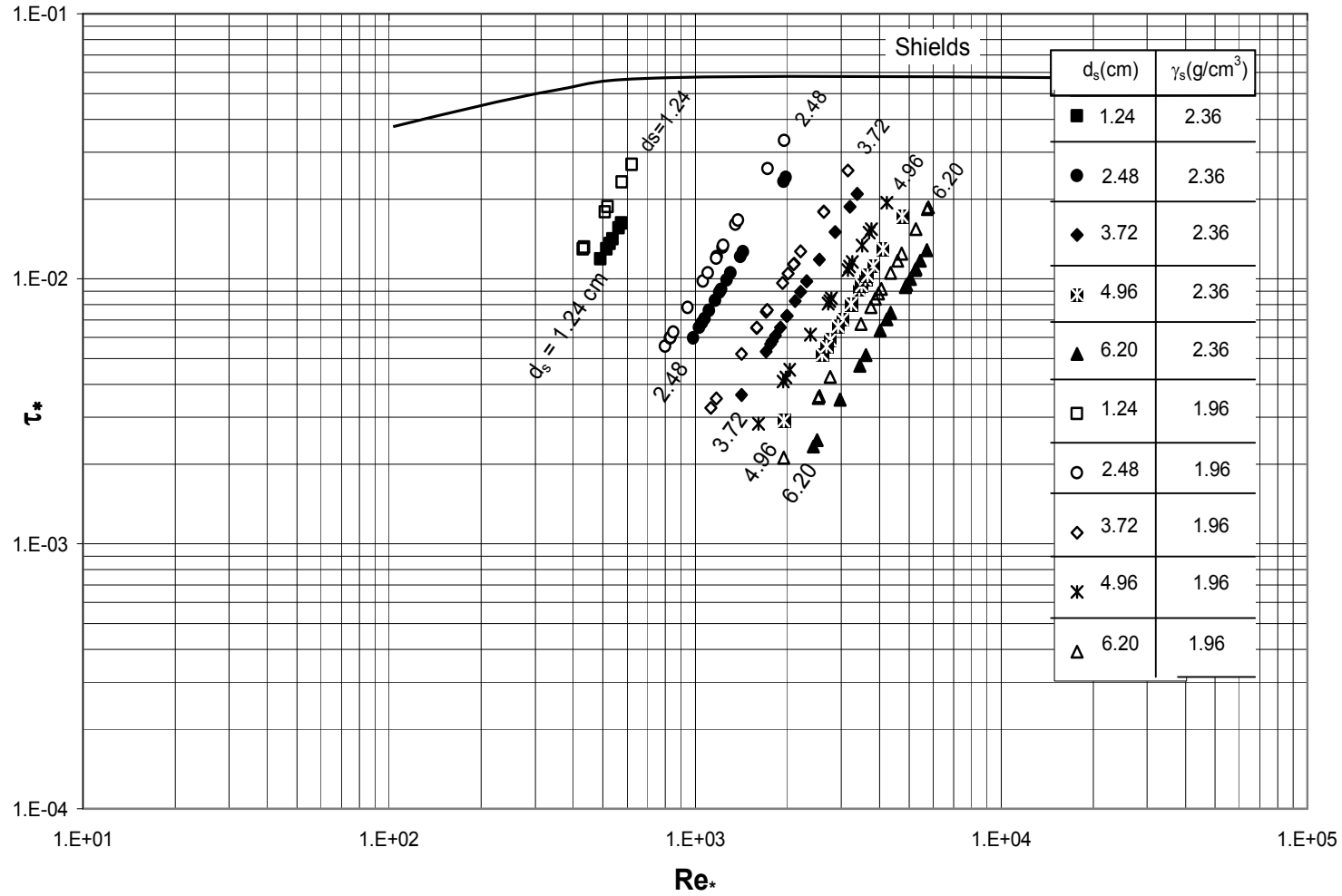


Figure IV-1: Comparison of τ^* vs. Re^* for particles with $\gamma_s = 1.96 \text{ g/cm}^3$ and $\gamma_s = 2.36 \text{ g/cm}^3$

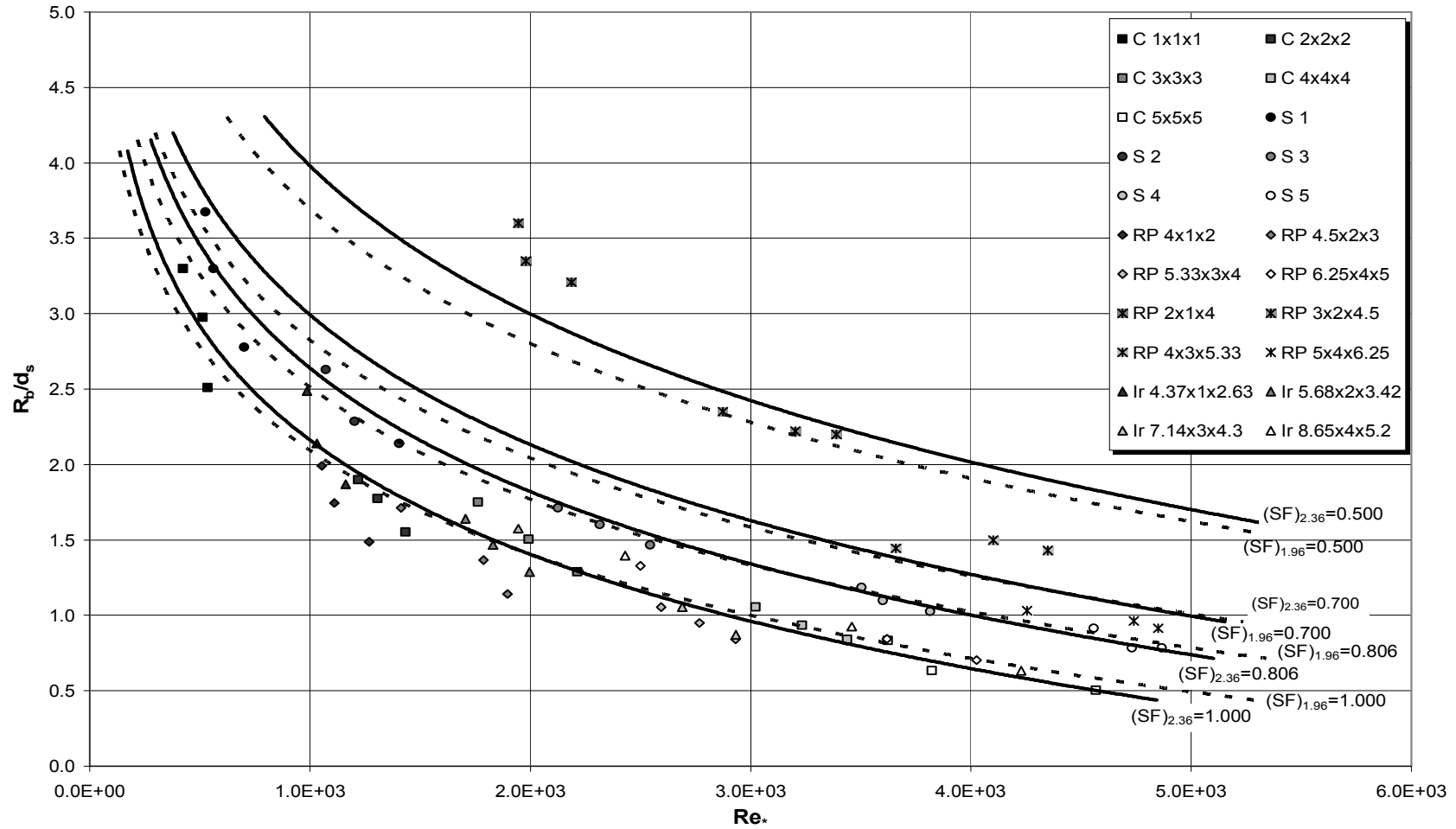


Figure IV-2: Comparison of R_b/d_s versus Re_* as a function of shape factor, SF for particles with $\gamma_s=1.96 \text{ g/cm}^3$ and $\gamma_s=2.36 \text{ g/cm}^3$

IV.2. Relationship Between the Entrainment Function and the Dimensionless Grain Size

In section III.3.2 the relationship between the entrainment function and the dimensionless grain size has been investigated and the related figures have been given for the particles of $\gamma_s = 1.96 \text{ g/cm}^3$. Figure IV-3 covers the relationship stated above for the particles of $\gamma_s = 1.96 \text{ g/cm}^3$ and also that of new particles of $\gamma_s = 2.36 \text{ g/cm}^3$. The general trends of the data sets of particles of $\gamma_s = 1.96 \text{ g/cm}^3$ and $\gamma_s = 2.36 \text{ g/cm}^3$ are very similar to each other for the particles having the same shape factor. The main difference between them is that the new particles require higher channel bottom slopes for the initiation of motion than the previous particles.

IV.3. Determination of the Equivalent Sediment Diameter

As explained in section III.3.3, in this study particle sizes were expressed in terms of equivalent sediment diameters instead of nominal diameters. The values of $(d_s)_e$ for the particles of $\gamma_s = 2.36 \text{ g/cm}^3$ computed through experiments range between 0.97 cm and 8.24 cm and are given in Figure IV-4.

In Figure IV.5 data and corresponding best fit curve $R_b/(d_s)_e$ versus Re_* are given for particles of $\gamma_s = 2.36 \text{ g/cm}^3$. This figure also includes the best fit curve of particles of $\gamma_s = 1.96 \text{ g/cm}^3$ for the reason of comparison.

$$\frac{R_b}{(d_s)_e} = 89.87 \cdot Re_*^{-0.54}, \text{ for } \gamma_s = 1.96 \text{ g/cm}^3 \quad (3.5)$$

with a correlation coefficient of $R^2 = 0.94$.

and

$$\frac{R_b}{(d_s)_e} = 168.73 \cdot Re_*^{-0.61}, \text{ for } \gamma_s = 2.36 \text{ g/cm}^3 \quad (4.1)$$

with a correlation coefficient of $R^2 = 0.96$.

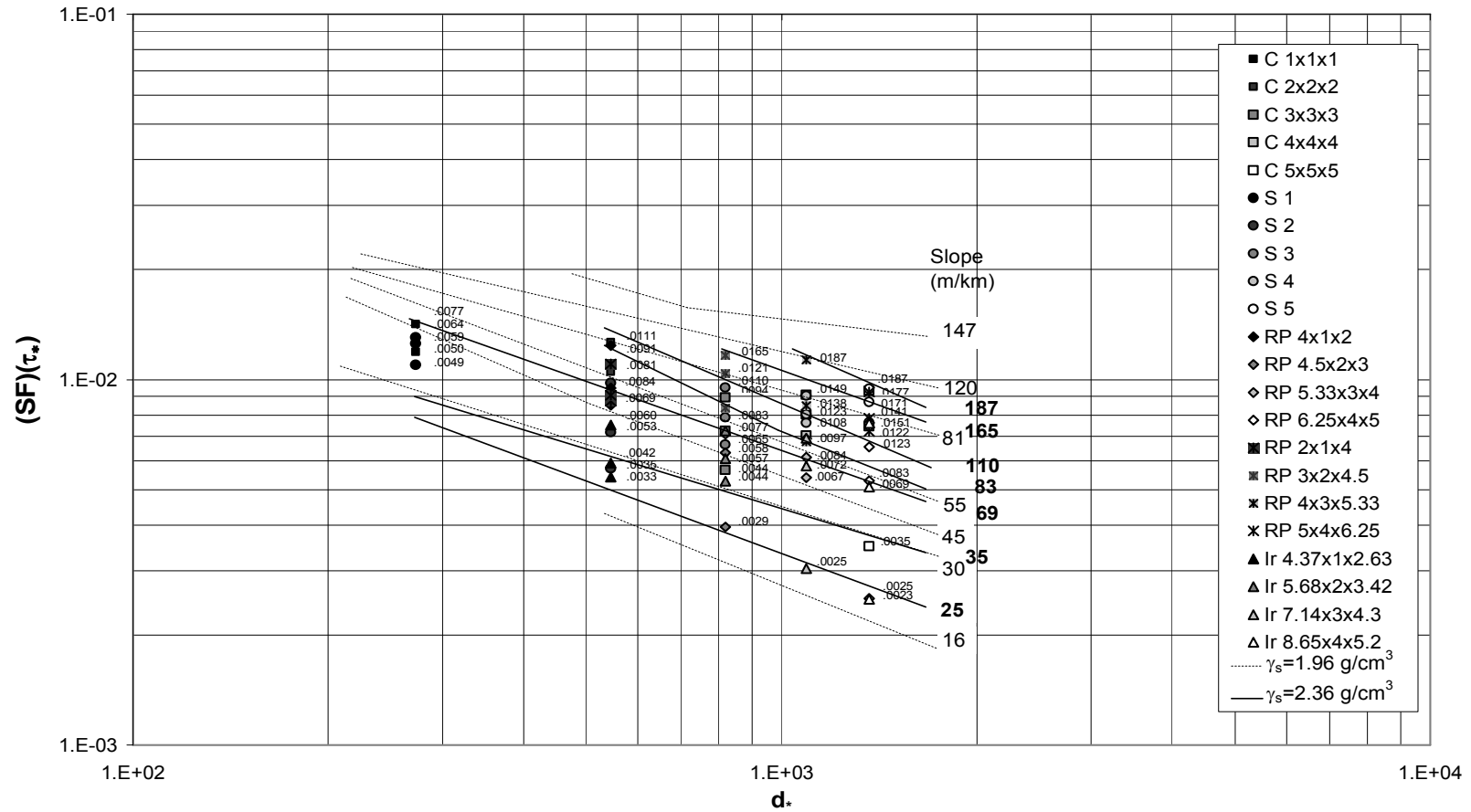


Figure IV-3: Comparison of trend lines for particles with $\gamma_s=1.96 \text{ g/cm}^3$ and $\gamma_s=2.36 \text{ g/cm}^3$

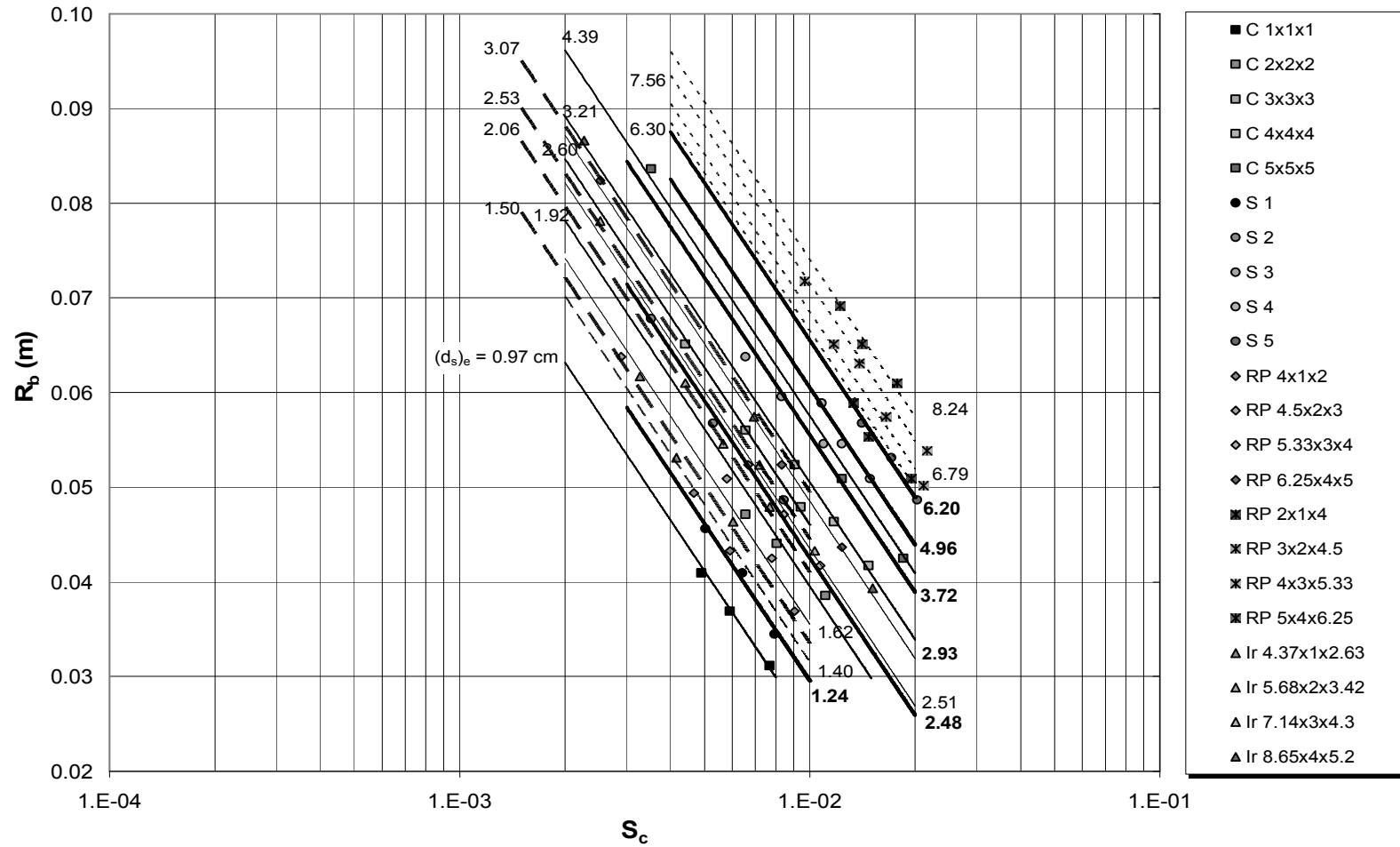


Figure IV-4: Equivalent sediment diameters determined from the relationship of hydraulic radius and bed slope

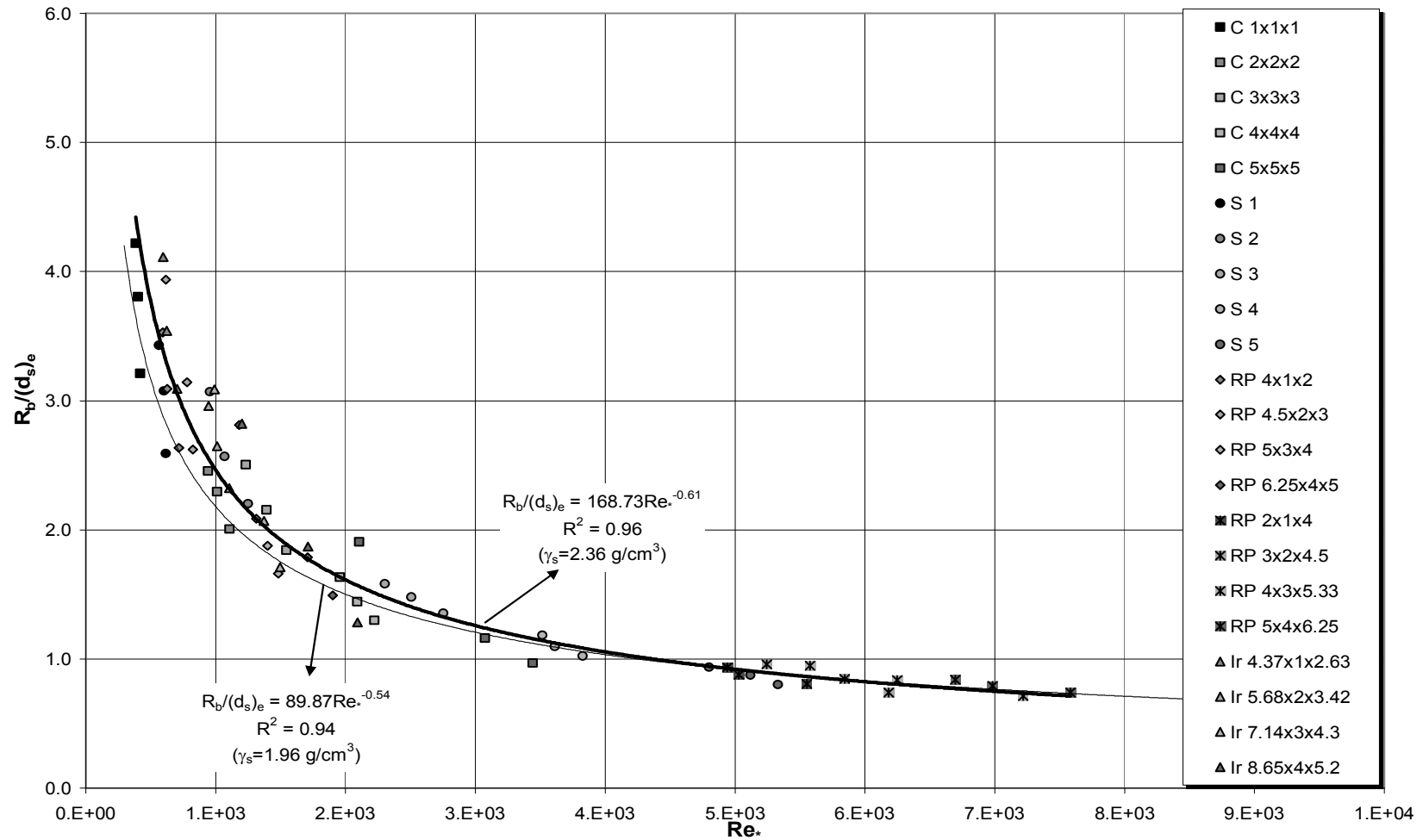


Figure IV-5: Comparison of $R_b/(d_s)_e$ versus Re_* curves obtained for both sediment groups having different specific weights

As it is seen from this figure, the two curves coincide with each other for the values of Re^* greater than about 4×10^3 . As Re^* gets smaller than this value, the deviation between these curves increases.

In Figure IV-6 the variation of $(d_s)_e$ with d_s is given for the particles of both specific weight groups. Due to the definition of the equivalent sediment diameter, the data of the spherical particles having different specific weights fall on the same trend line. For the cubic particles having different specific weights the maximum deviation on the value of $(d_s)_e$ for a given d_s varies around 10 %.

The critical velocity at the condition of incipient motion can also be given as a function of the equivalent sediment diameter. The variation of the critical cross-sectional velocity, V_{cc} ; the critical velocity in the vertical, V_{vc} ; and the critical bottom velocity, V_{bc} , are presented in Figure IV-7, Figure IV-8 and Figure IV-9, respectively as a function of $(d_s)_e$. In all these figures the data and the best fit lines of the data for particles of $\gamma_s = 2.36 \text{ g/cm}^3$ and only best fit lines of particles of $\gamma_s = 1.96 \text{ g/cm}^3$ are given. These figures clearly show that the required velocity values for the motion of particles of $\gamma_s = 2.36 \text{ g/cm}^3$ are always higher than those of particles of $\gamma_s = 1.96 \text{ g/cm}^3$.

The equations for the critical velocities presented in Figures IV-7 – IV-9 are

$$V_{cc} = 3.58 \cdot (d_s)_e^{0.54}, \gamma_s = 1.96 \text{ g/cm}^3, R^2 = 0.90 \quad (3.6)$$

$$V_{cc} = 7.63 \cdot (d_s)_e^{0.69}, \gamma_s = 2.36 \text{ g/cm}^3, R^2 = 0.97 \quad (4.2)$$

$$V_{vc} = 2.38 \cdot (d_s)_e^{0.41}, \gamma_s = 1.96 \text{ g/cm}^3, R^2 = 0.92 \quad (3.7)$$

$$V_{vc} = 3.80 \cdot (d_s)_e^{0.43}, \gamma_s = 2.36 \text{ g/cm}^3, R^2 = 0.91 \quad (4.3)$$

$$V_{bc} = 2.94 \cdot (d_s)_e^{0.50}, \gamma_s = 1.96 \text{ g/cm}^3, R^2 = 0.91 \quad (3.8)$$

$$V_{bc} = 2.10 \cdot (d_s)_e^{0.30}, \gamma_s = 2.36 \text{ g/cm}^3, R^2 = 0.92 \quad (4.4)$$

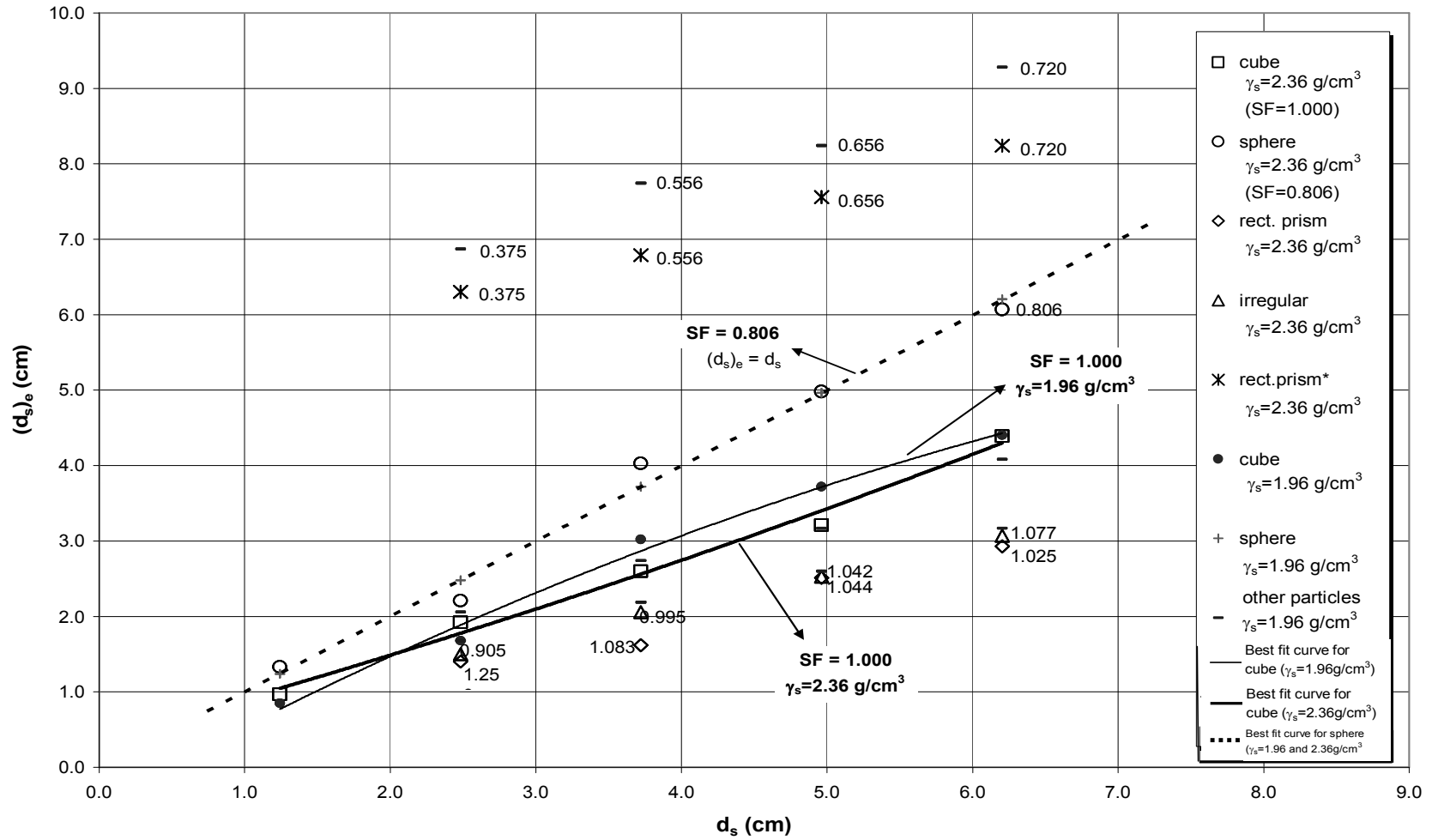


Figure IV-6: Variation of $(d_s)_e$ with d_s

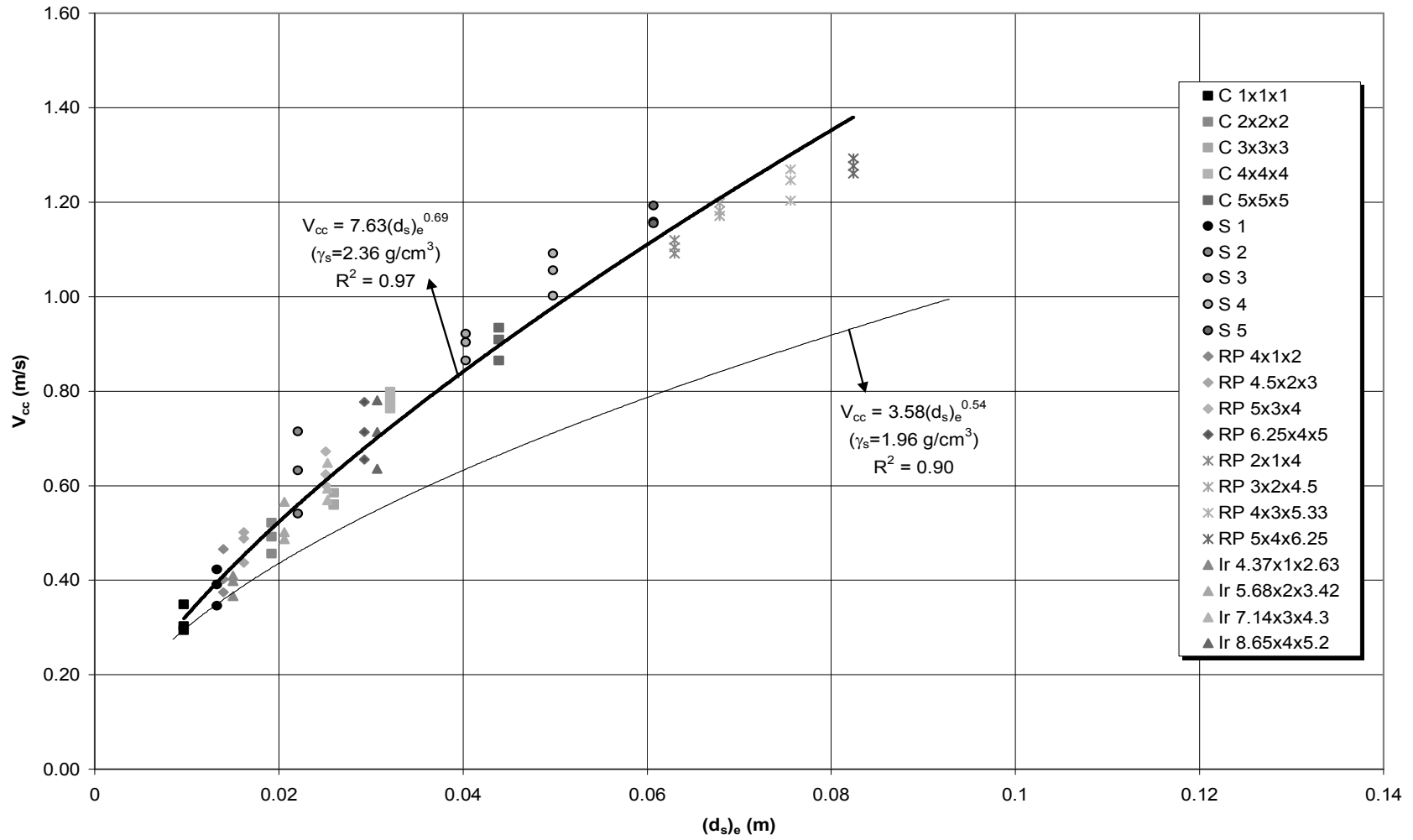


Figure IV-7: Critical cross-sectional velocity, V_{cc} vs. $(d_s)_e$

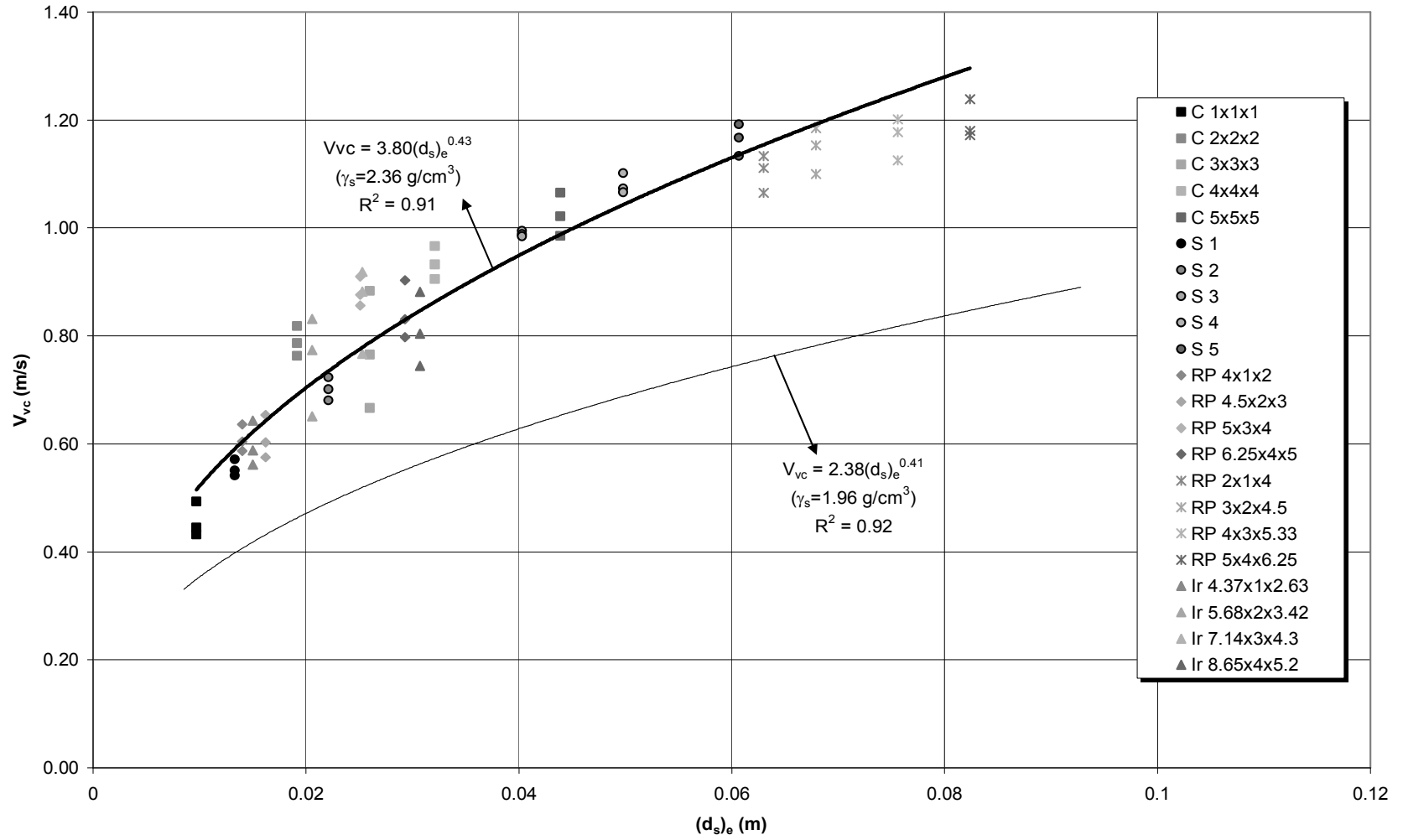


Figure IV-8: Critical velocity in the vertical, V_{vc} vs. $(d_s)_e$

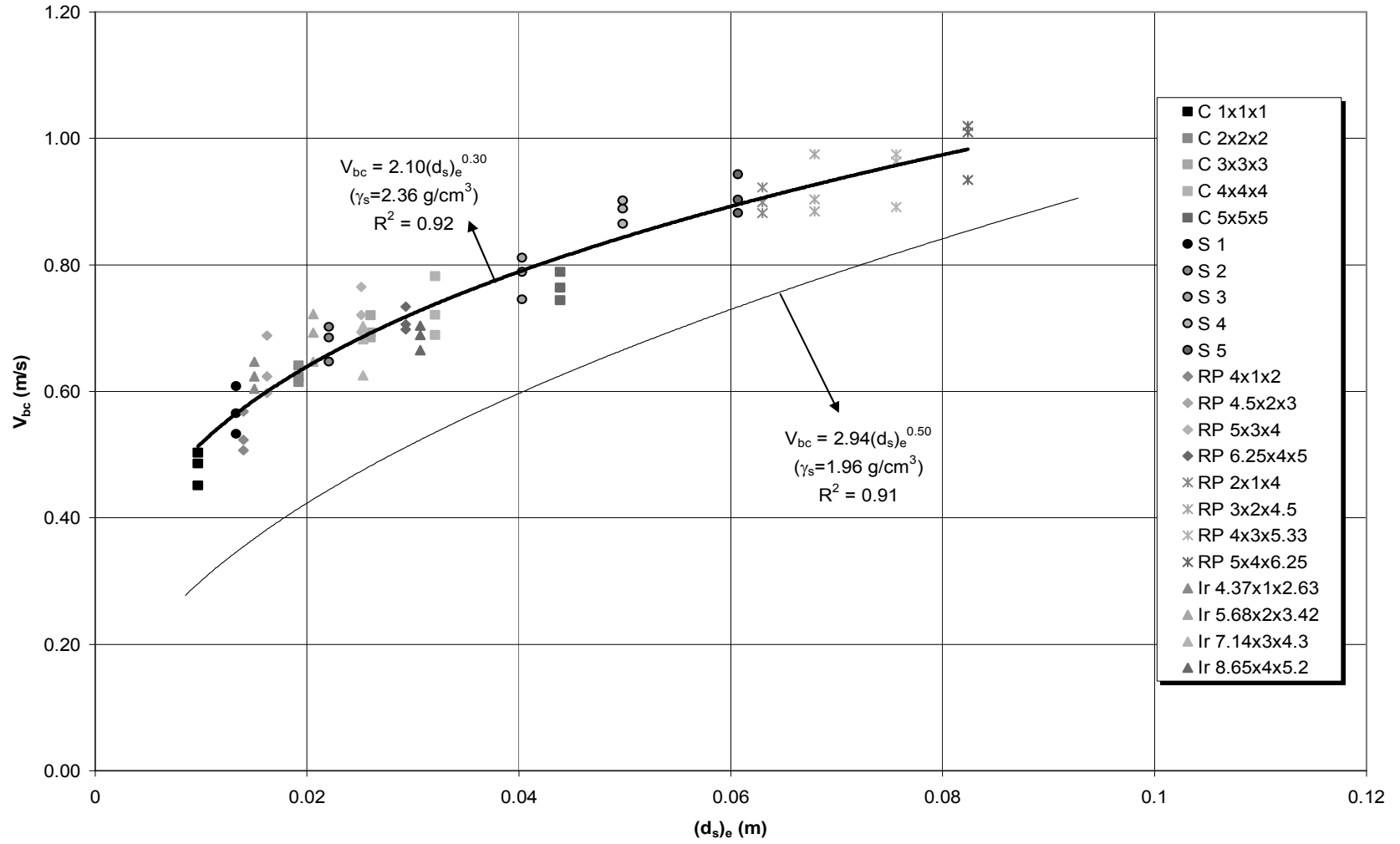


Figure IV-9: Critical bottom velocity, V_{bc} vs. $(d_s)_e$

IV.4. Re-analysis of Brahm's Equation

The relation between the critical bottom velocity and the weight of particles having different shapes is given in Figure IV-10. In this figure separate trend lines are obtained for different shape factors as those presented in Figure III-35 for the particles of $\gamma_s=1.96 \text{ g/cm}^3$. If one compares Figure III-35 and Figure IV-10 it is clearly seen that larger V_{bc} values are required to move the particles of $\gamma_s=2.36 \text{ g/cm}^3$ than those of $\gamma_s=1.96 \text{ g/cm}^3$ when the particles have the same shape and size given in Figure III-35 and Figure IV-10. To show this situation the best fit curves for spherical and cubic particles are represented in Figure IV-11.

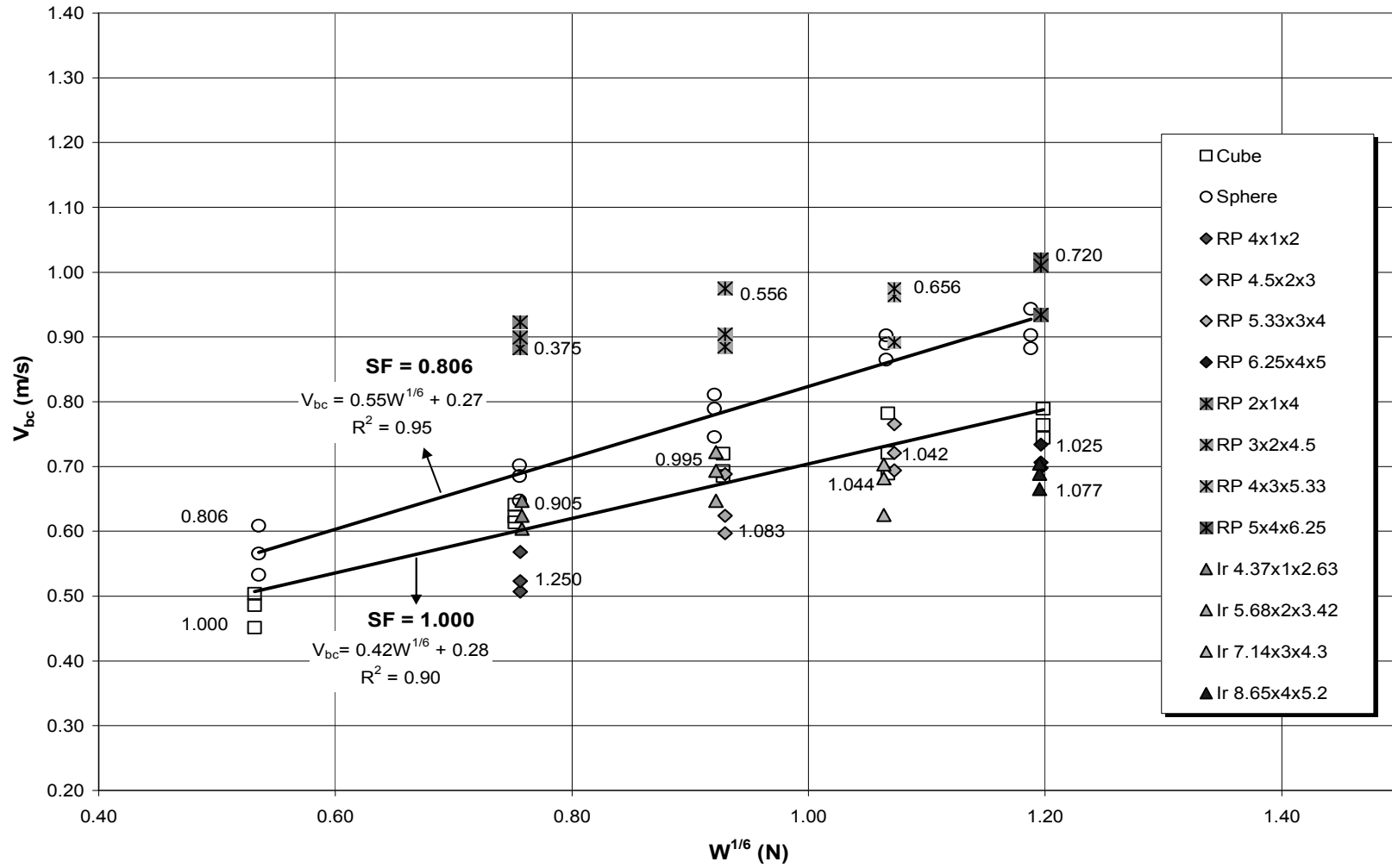


Figure IV-10: V_{bc} versus $W^{1/6}$ for particles of different shape factors

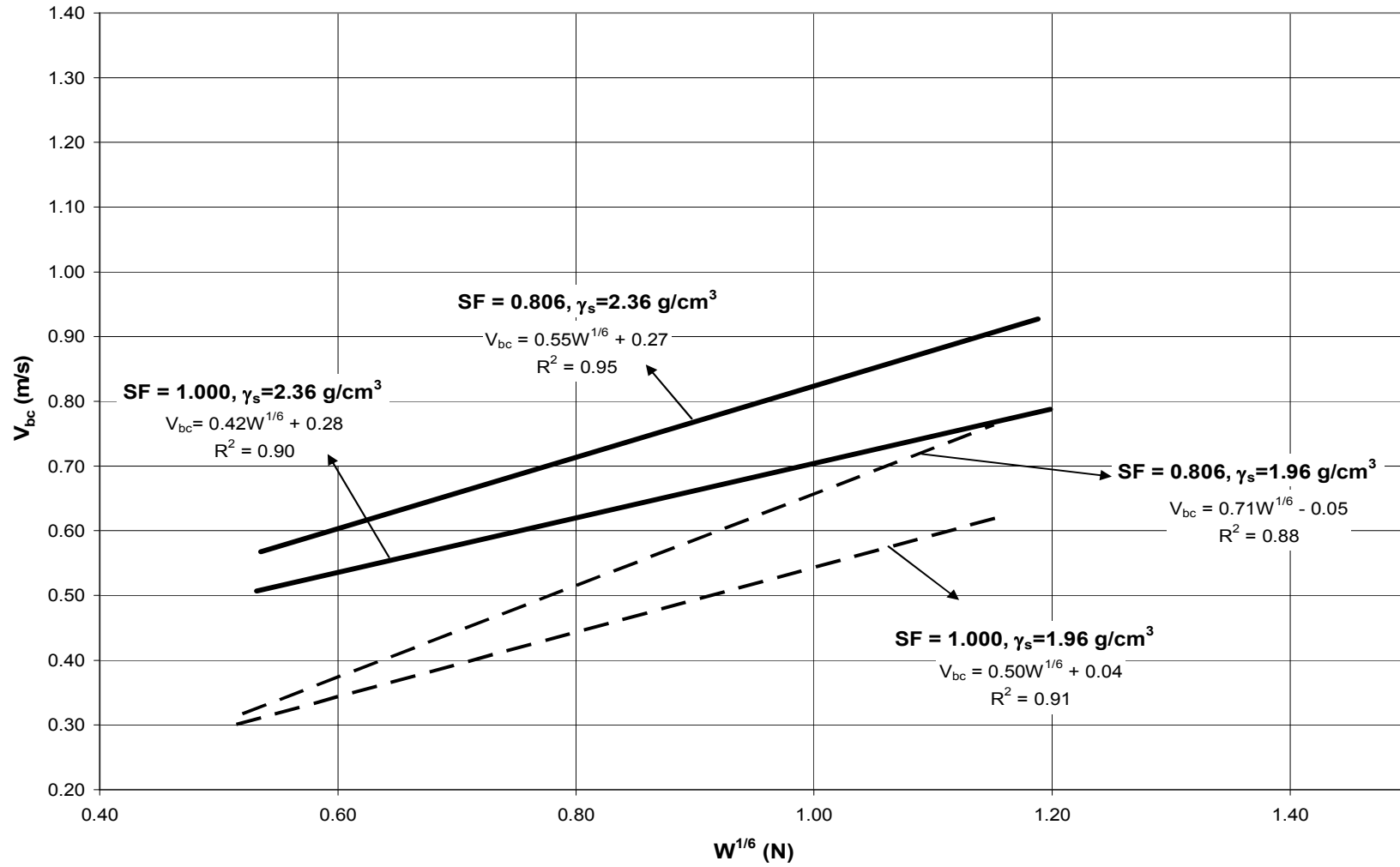


Figure IV-11: V_{bc} versus $W^{1/6}$ for cubic and spherical particles of $\gamma_s=1.96 \text{ g/cm}^3$ and $\gamma_s=2.36 \text{ g/cm}^3$

In Figure IV-12 the variation of K with SF is given for the particles of $\gamma_s=2.36 \text{ g/cm}^3$ along with the best fitting curve of the data of particles with $\gamma_s=1.96 \text{ g/cm}^3$. For a given particle with a certain shape factor, K value is directly computed with the following equation:

$$K = -0.45 \cdot \ln(SF) + 0.74, \gamma_s=2.36 \text{ g/cm}^3, R^2=0.66 \quad (4.5)$$

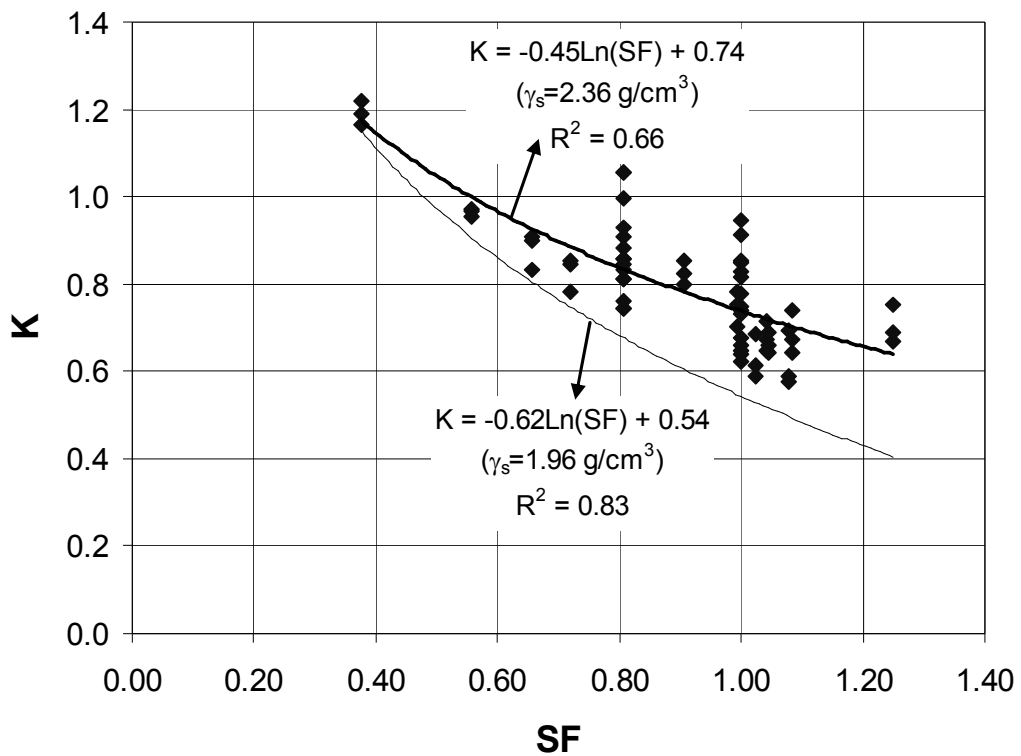


Figure IV-12: Comparison of K vs SF values of particles with $\gamma_s=1.96 \text{ g/cm}^3$ and $\gamma_s=2.36 \text{ g/cm}^3$

The results that are more precise are available when K is expressed as a function of SF and the relative depth, d_s/R_b . This relationship is given in Figure IV-13 again for both particle classes. If two particles have the same shape factor and d_s but different specific weights ($\gamma_s=1.96 \text{ g/cm}^3$ and $\gamma_s=2.36 \text{ g/cm}^3$), the lighter particle will have larger $(SF)(d_s/R_b)$ value than the heavier one. Therefore, K value of the particle of $\gamma_s=2.36 \text{ g/cm}^3$ is always larger than that of $\gamma_s=1.96 \text{ g/cm}^3$ as seen in Figure IV-13.

The difference between these two K values gets smaller as the values of $(SF)(d_s/R_b)$ decrease. The equation of the best fitting curve of the related data for the particle group of $\gamma_s=2.36 \text{ g/cm}^3$ is

$$K = -0.24 \cdot \ln\left(SF \cdot \frac{d_s}{R_b}\right) + 0.68, \gamma_s=2.36 \text{ g/cm}^3, R^2=0.78 \quad (4.6)$$

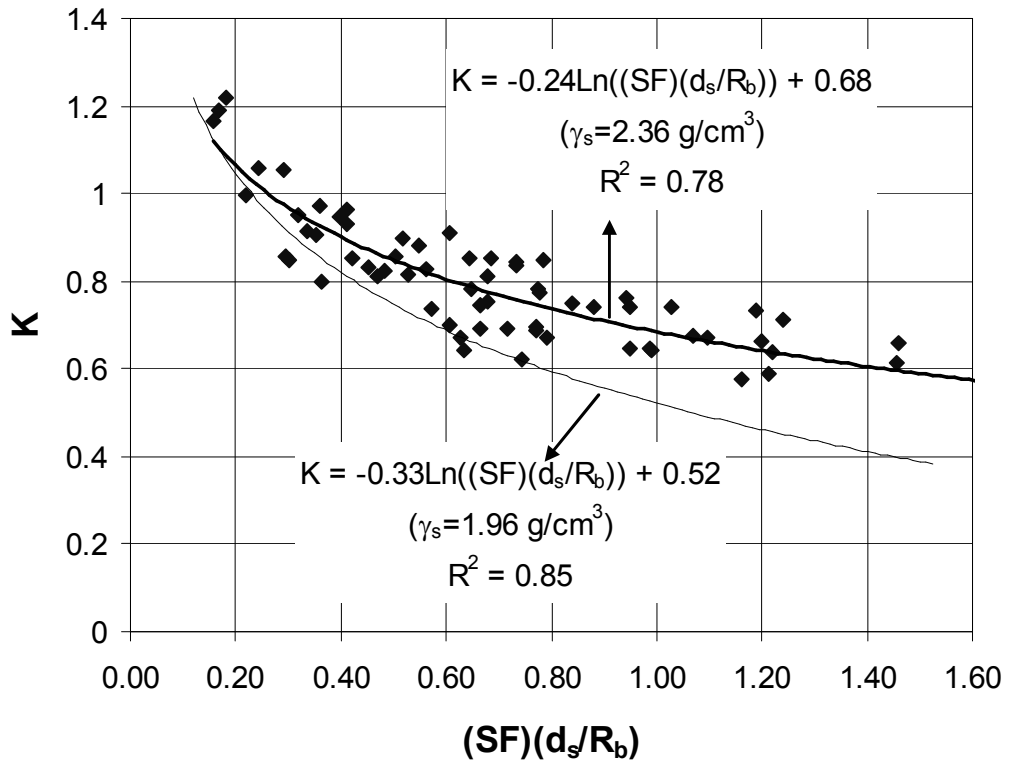


Figure IV-13: Comparison of K vs $(SF)(d_s/R_b)$ values of particles with $\gamma_s=1.96 \text{ g/cm}^3$ and $\gamma_s=2.36 \text{ g/cm}^3$

IV.5. Determination of the Critical Condition from the Height to Length Ratio of the Particle

The variation of $(Fr_v)_b / \sqrt{\cos\theta}$ with first b/c and then $(SF)(b/c)$ for the second group of particles with $\gamma_s=2.36 \text{ g/cm}^3$ is presented in Figure IV-14 and Figure IV-15, respectively, along with the best fit curves of Figures III-40 and III-41 for particles of

$\gamma_s=1.96 \text{ g/cm}^3$. The equations of the best fitting curves of the new data presented in the aforementioned figures are as follows.

$$\frac{(Fr_v)_b}{\sqrt{\cos\theta}} = 5.17 \cdot \left(\frac{b}{c}\right)^2 - 8.94 \cdot \left(\frac{b}{c}\right) + 4.84, \gamma_s=2.36 \text{ g/cm}^3, R^2=0.71 \quad (4.7)$$

$$\frac{(Fr_v)_b}{\sqrt{\cos\theta}} = 3.04 \cdot \left(SF \cdot \frac{b}{c}\right)^2 - 5.55 \cdot \left(SF \cdot \frac{b}{c}\right) + 3.52, \gamma_s=2.36 \text{ g/cm}^3, R^2=0.90 \quad (4.8)$$

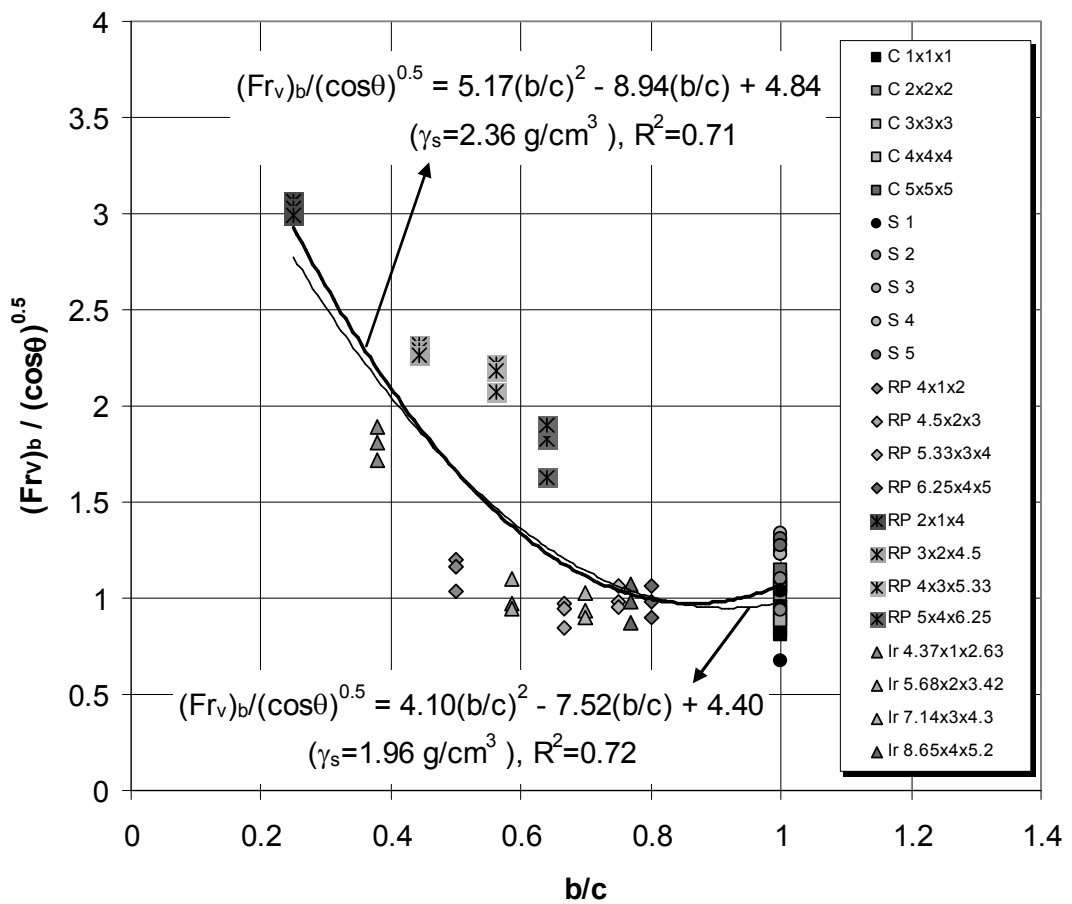


Figure IV-14: Comparison of b/c vs $(Fr_v)_b / \sqrt{\cos\theta}$ values of particles with $\gamma_s=1.96 \text{ g/cm}^3$ and $\gamma_s=2.36 \text{ g/cm}^3$

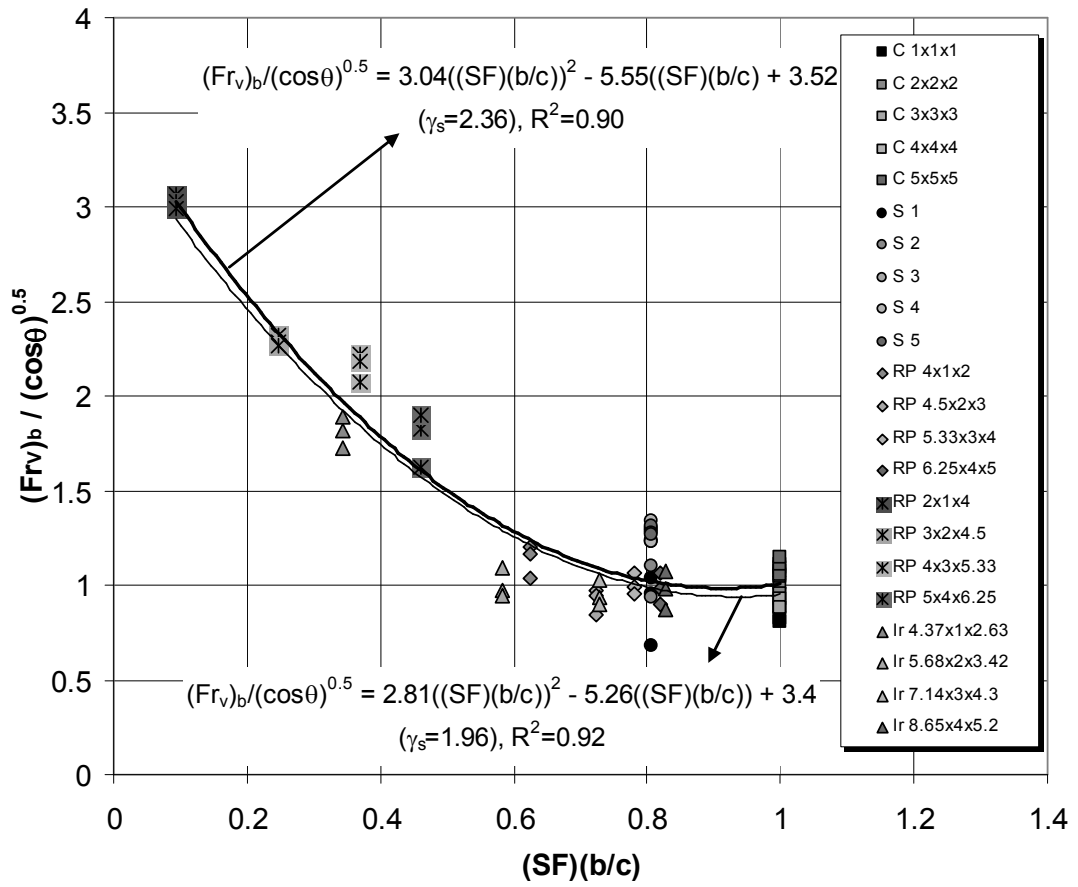


Figure IV-15: Comparison of $(SF)(b/c)$ vs $(Fr_v)_b / \sqrt{\cos\theta}$ values of particles with $\gamma_s=1.96 \text{ g/cm}^3$ and $\gamma_s=2.36 \text{ g/cm}^3$

The best fitting curves presented in Figure IV-15 for the particles of $\gamma_s=1.96 \text{ g/cm}^3$ and $\gamma_s=2.36 \text{ g/cm}^3$ are almost the same.

CHAPTER V

CONCLUSIONS AND THE FURTHER RECOMMENDATIONS

In this study, the effect of obstacle height and specific weight on incipient motion of coarse solitary particles was investigated. The hydraulic parameters are given in Appendix B in a tabular form.

From the analysis of the experimental results the following conclusions can be drawn:

For a particle of known shape and size, there is not a unique relationship between τ^* and Re^* ; R_b/d_s is also an important parameter on which they depend (Figure III-9).

Higher the obstacle height behind the particle, larger the required Re^* for the particle motion (Figure III-12).

The critical entrainment function is also function of the particle shape. By introducing the shape factor defined by Defne (2002) for large solitary particles, a good relationship can be obtained between the critical entrainment function and the critical channel slope for the particles of the same size and weight but different shapes with high correlation coefficients.

The critical entrainment function declines with increasing dimensionless grain size for a given critical channel slope as stated by Shvidchenko and Pender (2000) (Figure III-25). This means that the entrainment function is not independent of the grain Reynolds number for rough turbulent flows.

The introduction of the equivalent sediment diameter into the analysis of the experimental data reduces the parameter of the shape factor among the parameters involved. Using the relationship given between $R_b/(d_s)_e$ and Re^* one can determine at which R_b a particle of known shape and size will have initial motion at a given channel slope.

The variation of t/b from $1/5$ to $1.5/5$ does not significantly affect the relationship between $R_b/(d_s)_e$ and Re^* within the ranges of Re^* tested (Figure III-30).

The critical velocities required for the incipient motion of particles; V_{cc} , V_{vc} and V_{bc} can be expressed as a function of only $(d_s)_e$ with high correlation coefficients.

As t/b value increases for a particle of given shape and size, the required K value of Brahms gets larger for the incipient motion of the particle.

When the specific weight of the particle increases, the required channel slope must be increased for a given R_b value, or for a given channel slope R_b value must be increased to have the incipient motion.

The variation of the particle specific weight does not influence the relationship between $R_b/(d_s)_e$ and Re^* significantly (Figure IV-5).

An increase in the specific weight of the particle significantly increases the required values of the critical velocities; V_{cc} , V_{vc} and V_{bc} as well as the K value of Brahms equation for the incipient motion of the particle.

The variation of the particle specific weight does not affect the relationship between the densimetric Froude number in terms of the average velocity and b/c within the range of b/c investigated in this study.

Recommendations for future studies are as follows:

Experiments similar to those conducted in this study should be repeated not only with smooth channel bed but also with rough channel beds, using coarse solitary particles of different shapes and specific weights.

REFERENCES

Addison, H. (1954). "A Treatise on Applied Hydraulics", New York, John Willey & Sons Inc.

Bathurst, J. C., Cao, H. H., and Graf, W. H. (1984). "Hydraulics and Sediment Transport in a Steep Flume: Data from the EPFL Study Report", Inst. of Hydrol., Wallingford, Oxon, England.

Buffington, J. M. (1999). "The Legend of A. F. Shields", J. Hydr. Eng., ASCE, 125, 376-387.

Chow, V. T. (1959). "Open-Channel Hydraulics", McGraw-Hill, New York.

Defne, Z. (2002). "Effect of Particle Shape and Size on Incipient Motion of Solid Particles", Thesis Submitted in Partial Fulfillment of the Requirements for the Degree of Master of Science in the Department of Civil Engineering", The Middle East Technical University, Ankara, Turkey.

Gogus, M. (1980). "Flow Characteristics Below Floating Covers with Application to Ice Jams", Thesis Submitted in Partial Fulfillment of the Requirements for the Degree of Doctor of Philosophy in Mechanics and Hydraulics", The Graduate College of the University of Iowa, Iowa, USA.

Gogus, M., and Defne, Z. (2005). "Effect of Shape on Incipient Motion of Large Solitary Particles", J. Hydr. Eng., ASCE, 131(1), 38-45.

Gogus, M., Ipekci, O. N., Kokpinar, M. A. (2001). "Effect of Particle Shape on Fall Velocity of Angular Particles", *J. Hydr. Eng., ASCE*, 127, 860-869.

Graf, W. H., and Suszka, L. (1987). "Sediment Transport in Steep Channels", *J. Hydrosoci. Hydraul. Eng. Jpn. Soc. Civ. Eng.*, 5(1), 11-26.

Henderson, F. M. (1966). "Open Channel Flow", New York, Macmillan Publishing Co. Inc.

King, H. W. (1954). "Handbook of Hydraulics", New York, McGraw Hill Book Co. Inc.

Novak, P., and Nalluri, C. (1975). "Sediment Transport in Smooth Fixed Bed Channels", *J. Hydraul. Div., Am. Soc. Civ. Eng.*, 101(9), 1139-1154.

Novak, P., and Nalluri, C. (1984). "Incipient Motion of Sediment Particles over Fixed Beds", *J. Hydraul. Res.*, 22(3), 181-197.

Raudkivi, A. J. (1967). "Loose Boundary Hydraulics", Pergamon, New York.

Shvidchenko, A. B., and Pender, G. (2000). "Flume Study of the Effect of Relative Depth on the Incipient Motion of Coarse Uniform Sediments", *Water Resour. Res.*, 36(2), 619-628.

Simons, D. B., and Senturk, F. (1992). "Sediment Transport Technology", Littleton, Colo.: Water Resources Publications.

Stelczer, K. (1981). "Bed-Load Transport: Theory and Practice", Littleton, Colo.: Water Resources Publications.

Uzuner, M. S. (1977). "Stability Analysis of Floating and Submerged Ice Floes", Journal of the Hydraulics Division, ASCE, Vol. 103, No. HY7, 713-722.

Yalin, M. S. (1977). "Mechanics of Sediment Transport", Oxford, New York, Pergamon Press.

APPENDIX A

SIDE-WALL CORRECTION PROCEDURE

Side-wall correction procedure used in the present study is based on the procedure proposed by Shvidchenko and Pender (2000).

This method is based on the Manning roughness coefficient of the bed, n_b , and Manning roughness coefficient of the walls, n_w . The principal assumption is that cross-sectional water area can be divided into bed area and wall area having the same energy gradient, which is equal to the bed slope, and having mean flow velocity V of the total section. Applying the Manning formula $V = \frac{I}{n} \cdot R^{2/3} \cdot \sqrt{S}$ to each part of the

water area one can obtain $n_{eq} = \frac{(P_b \cdot n_b^{3/2} + P_w \cdot n_w^{3/2})^{2/3}}{P^{2/3}}$. Then the calculation of

the bed hydraulic radius is straightforward using the relationship $R_b = R \left(\frac{n_b}{n} \right)^{3/2}$. In

these equations R is the hydraulic radius of the total area, n_{eq} is the equivalent Manning roughness coefficient, P is the wetted perimeter of the complete section, P_b and P_w are the wetted perimeters associated with the bed and walls, respectively. This method was shown to give comparable results with the commonly used Vanoni and Brooks method (Shvidchenko and Pender, 2000).

In the present study Manning roughness for the finished concrete bed and the glass walls were taken as 0.013 and 0.010, respectively.

APPENDIX B

EXPERIMENTAL RESULTS

Table B-1: Experimental data.

	V (cm^3)	d_s (cm)	γ_s (g/cm^3)	a (cm)	b (cm)	c (cm)	L (cm)	SF $f(a,b,c)$	t/b	h (m)	R (m)	S	V_{vc} (m/s)	V_{cc} (m/s)	V_{bc} (m/s)	R_b (m)
CUBIC PARTICLES	1	1.241	1.960	1.00	1.00	1.00	1.41	1.000	1.5/5	0.050	0.0417	0.0035	0.34	0.33	0.26	0.0441
	1	1.241	1.960	1.00	1.00	1.00	1.41	1.000	1.5/5	0.040	0.0345	0.0059	0.34	0.30	0.26	0.0361
	1	1.241	1.960	1.00	1.00	1.00	1.41	1.000	1.5/5	0.030	0.0268	0.0077	0.36	0.28	0.27	0.0290
	8	2.481	1.960	2.00	2.00	2.00	2.83	1.000	1.5/5	0.072	0.0559	0.0022	0.44	0.48	0.35	0.0603
	8	2.481	1.960	2.00	2.00	2.00	2.83	1.000	1.5/5	0.063	0.0503	0.0026	0.42	0.40	0.34	0.0538
	8	2.481	1.960	2.00	2.00	2.00	2.83	1.000	1.5/5	0.049	0.0410	0.0067	0.37	0.38	0.33	0.0433
	27	3.722	1.960	3.00	3.00	3.00	4.24	1.000	1.5/5	0.082	0.0617	0.0028	0.56	0.53	0.42	0.0671
	27	3.722	1.960	3.00	3.00	3.00	4.24	1.000	1.5/5	0.069	0.0538	0.0047	0.56	0.51	0.42	0.0578
	27	3.722	1.960	3.00	3.00	3.00	4.24	1.000	1.5/5	0.053	0.0437	0.0081	0.61	0.47	0.45	0.0464
	64	4.963	1.960	4.00	4.00	4.00	5.66	1.000	1.5/5	0.089	0.0654	0.0030	0.59	0.54	0.48	0.0714
	64	4.963	1.960	4.00	4.00	4.00	5.66	1.000	1.5/5	0.046	0.0389	0.0081	0.60	0.71	0.47	0.0500
	64	4.963	1.960	4.00	4.00	4.00	5.66	1.000	1.5/5	0.044	0.0374	0.0128	0.62	0.54	0.49	0.0413
	125	6.204	1.960	5.00	5.00	5.00	7.07	1.000	1.5/5	0.088	0.0651	0.0030	0.63	0.62	0.43	0.0711
	125	6.204	1.960	5.00	5.00	5.00	7.07	1.000	1.5/5	0.052	0.0430	0.0081	0.69	0.75	0.46	0.0578
	125	6.204	1.960	5.00	5.00	5.00	7.07	1.000	1.5/5	0.045	0.0381	0.0138	0.70	0.68	0.48	0.0453

Table B-1: (Continued)

	V (cm^3)	d_s (cm)	γ_s (g/cm^3)	a (cm)	b (cm)	c (cm)	L (cm)	SF $f(a,b,c)$	t/b	h (m)	R (m)	S	V_{vc} (m/s)	V_{cc} (m/s)	V_{bc} (m/s)	R_b (m)
SPHERICAL PARTICLES	1	1.241	1.960	1.24	1.24	1.24	1.24	0.806	1.5/5	0.054	0.0444	0.0032	0.43	0.41	0.35	0.0490
	1	1.241	1.960	1.24	1.24	1.24	1.24	0.806	1.5/5	0.041	0.0352	0.0083	0.37	0.40	0.35	0.0332
	1	1.241	1.960	1.24	1.24	1.24	1.24	0.806	1.5/5	0.032	0.0284	0.0123	0.42	0.37	0.32	0.0261
	8	2.481	1.960	2.48	2.48	2.48	2.48	0.806	1.5/5	0.090	0.0662	0.0021	0.48	0.50	0.39	0.0670
	8	2.481	1.960	2.48	2.48	2.48	2.48	0.806	1.5/5	0.067	0.0528	0.0033	0.45	0.42	0.39	0.0567
	8	2.481	1.960	2.48	2.48	2.48	2.48	0.806	1.5/5	0.044	0.0374	0.0073	0.53	0.39	0.42	0.0430
	27	3.722	1.960	3.72	3.72	3.72	3.72	0.806	1.5/5	0.083	0.0623	0.0040	0.57	0.55	0.45	0.0678
	27	3.722	1.960	3.72	3.72	3.72	3.72	0.806	1.5/5	0.067	0.0528	0.0093	0.60	0.54	0.47	0.0486
	27	3.722	1.960	3.72	3.72	3.72	3.72	0.806	1.5/5	0.052	0.0430	0.0161	0.61	0.50	0.49	0.0398
	64	4.963	1.960	4.96	4.96	4.96	4.96	0.806	1.5/5	0.087	0.0645	0.0058	0.66	0.80	0.50	0.0677
	64	4.963	1.960	4.96	4.96	4.96	4.96	0.806	1.5/5	0.065	0.0516	0.0093	0.68	0.79	0.54	0.0553
	64	4.963	1.960	4.96	4.96	4.96	4.96	0.806	1.5/5	0.055	0.0451	0.0149	0.71	0.70	0.55	0.0479
	125	6.204	1.960	6.20	6.20	6.20	6.20	0.806	1.5/5	0.069	0.0541	0.0088	0.78	0.86	0.57	0.0620
	125	6.204	1.960	6.20	6.20	6.20	6.20	0.806	1.5/5	0.056	0.0458	0.0118	0.79	0.83	0.59	0.0590
	125	6.204	1.960	6.20	6.20	6.20	6.20	0.806	1.5/5	0.047	0.0393	0.0169	0.81	0.80	0.60	0.0545

Table B-1: (Continued)

	V (cm^3)	d_s (cm)	γ_s (g/cm^3)	a (cm)	b (cm)	c (cm)	L (cm)	SF $f(a,b,c)$	t/b	h (m)	R (m)	S	V_{vc} (m/s)	V_{cc} (m/s)	V_{bc} (m/s)	R_b (m)
RECTANGULAR ARTICLES	8	2.481	1.960	4.00	1.00	2.00	4.12	1.250	1.5/5	0.051	0.0424	0.0052	0.36	0.40	0.29	0.0448
	8	2.481	1.960	4.00	1.00	2.00	4.12	1.250	1.5/5	0.039	0.0337	0.0081	0.38	0.44	0.33	0.0353
	8	2.481	1.960	4.00	1.00	2.00	4.12	1.250	1.5/5	0.031	0.0276	0.0133	0.47	0.45	0.39	0.0286
	27	3.722	1.960	4.50	2.00	3.00	4.92	1.083	1.5/5	0.072	0.0559	0.0019	0.51	0.50	0.30	0.0671
	27	3.722	1.960	4.50	2.00	3.00	4.92	1.083	1.5/5	0.056	0.0458	0.0048	0.56	0.49	0.31	0.0486
	27	3.722	1.960	4.50	2.00	3.00	4.92	1.083	1.5/5	0.041	0.0352	0.0111	0.60	0.43	0.32	0.0369
	64	4.963	1.960	5.33	3.00	4.00	6.12	1.042	1.5/5	0.088	0.0651	0.0019	0.53	0.50	0.37	0.0711
	64	4.963	1.960	5.33	3.00	4.00	6.12	1.042	1.5/5	0.071	0.0553	0.0034	0.51	0.49	0.38	0.0596
	64	4.963	1.960	5.33	3.00	4.00	6.12	1.042	1.5/5	0.045	0.0381	0.0096	0.59	0.56	0.42	0.0401
	125	6.204	1.960	6.25	4.00	5.00	7.42	1.025	1.5/5	0.103	0.0729	0.0016	0.53	0.49	0.40	0.0770
	125	6.204	1.960	6.25	4.00	5.00	7.42	1.025	1.5/5	0.066	0.0522	0.0045	0.56	0.46	0.38	0.0560
	125	6.204	1.960	6.25	4.00	5.00	7.42	1.025	1.5/5	0.047	0.0396	0.0120	0.59	0.45	0.37	0.0417

Table B-1: (Continued)

	V (cm^3)	d_s (cm)	γ_s (g/cm^3)	a (cm)	b (cm)	c (cm)	L (cm)	SF $f(a,b,c)$	t/b	h (m)	R (m)	S	V_{vc} (m/s)	V_{cc} (m/s)	V_{bc} (m/s)	R_b (m)
RECTANGULAR ARTICLES*	8	2.481	1.960	2.00	1.00	4.00	2.24	0.375	1.5/5	0.107	0.0749	0.0050	0.81	0.91	0.60	0.0787
	8	2.481	1.960	2.00	1.00	4.00	2.24	0.375	1.5/5	0.093	0.0678	0.0096	0.82	0.85	0.62	0.0648
	8	2.481	1.960	2.00	1.00	4.00	2.24	0.375	1.5/5	0.080	0.0606	0.0127	0.83	0.82	0.62	0.0624
	27	3.722	1.960	3.00	2.00	4.50	3.61	0.556	1.5/5	0.110	0.0764	0.0048	0.83	1.03	0.61	0.0848
	27	3.722	1.960	3.00	2.00	4.50	3.61	0.556	1.5/5	0.090	0.0662	0.0088	0.85	1.00	0.62	0.0724
	27	3.722	1.960	3.00	2.00	4.50	3.61	0.556	1.5/5	0.075	0.0577	0.0147	0.87	0.97	0.65	0.0624
	64	4.963	1.960	4.00	3.00	5.33	5.00	0.656	1.5/5	0.100	0.0714	0.0081	0.79	1.05	0.63	0.0787
	64	4.963	1.960	4.00	3.00	5.33	5.00	0.656	1.5/5	0.093	0.0678	0.0099	0.82	1.02	0.63	0.0743
	64	4.963	1.960	4.00	3.00	5.33	5.00	0.656	1.5/5	0.075	0.0577	0.0141	0.89	0.99	0.65	0.0657
	125	6.204	1.960	5.00	4.00	6.25	6.40	0.720	1.5/5	0.080	0.0605	0.0169	0.83	1.09	0.67	0.0657
	125	6.204	1.960	5.00	4.00	6.25	6.40	0.720	1.5/5	0.079	0.0597	0.0147	0.88	1.02	0.68	0.0743
	125	6.204	1.960	5.00	4.00	6.25	6.40	0.720	1.5/5	0.071	0.0553	0.0094	0.96	0.99	0.69	0.0787

* These particles are placed in the most stable position.

Table B-1: (Continued)

	V (cm^3)	d_s (cm)	γ_s (g/cm^3)	a (cm)	b (cm)	c (cm)	L (cm)	SF $f(a,b,c)$	t/b	h (m)	R (m)	S	V_{vc} (m/s)	V_{cc} (m/s)	V_{bc} (m/s)	R_b (m)
IRREGULAR PARTICLES	8	2.481	1.960	4.37	1.00	2.63	4.48	0.905	1.5/5	0.071	0.0553	0.0025	0.44	0.45	0.36	0.0596
	8	2.481	1.960	4.37	1.00	2.63	4.48	0.905	1.5/5	0.056	0.0458	0.0052	0.48	0.40	0.40	0.0486
	8	2.481	1.960	4.37	1.00	2.63	4.48	0.905	1.5/5	0.044	0.0374	0.0081	0.53	0.37	0.41	0.0393
	27	3.722	1.960	5.68	2.00	3.42	6.02	0.995	1.5/5	0.088	0.0651	0.0016	0.52	0.52	0.38	0.0711
	27	3.722	1.960	5.68	2.00	3.42	6.02	0.995	1.5/5	0.069	0.0541	0.0040	0.51	0.49	0.40	0.0582
	27	3.722	1.960	5.68	2.00	3.42	6.02	0.995	1.5/5	0.053	0.0437	0.0074	0.58	0.44	0.44	0.0464
	64	4.963	1.960	7.14	3.00	4.30	7.74	1.044	1.5/5	0.079	0.0600	0.0030	0.51	0.49	0.43	0.0651
	64	4.963	1.960	7.14	3.00	4.30	7.74	1.044	1.5/5	0.062	0.0497	0.0055	0.58	0.46	0.39	0.0531
	64	4.963	1.960	7.14	3.00	4.30	7.74	1.044	1.5/5	0.040	0.0345	0.0141	0.59	0.50	0.45	0.0391
	125	6.204	1.960	8.65	4.00	5.20	9.53	1.077	1.5/5	0.087	0.0645	0.0030	0.53	0.61	0.42	0.0705
	125	6.204	1.960	8.65	4.00	5.20	9.53	1.077	1.5/5	0.060	0.0485	0.0071	0.54	0.71	0.46	0.0567
	125	6.204	1.960	8.65	4.00	5.20	9.53	1.077	1.5/5	0.045	0.0381	0.0110	0.62	0.65	0.47	0.0479

Table B-2: Experimental data.

	V (cm^3)	d_s (cm)	γ_s (g/cm^3)	a (cm)	b (cm)	c (cm)	L (cm)	SF $f(a,b,c)$	t/b	h (m)	R (m)	S	V_{vc} (m/s)	V_{cc} (m/s)	V_{bc} (m/s)	R_b (m)
CUBIC PARTICLES	1	1.241	2.360	1.00	1.00	1.00	1.41	1.000	1.5/5	0.046	0.0389	0.0049	0.45	0.35	0.45	0.0409
	1	1.241	2.360	1.00	1.00	1.00	1.41	1.000	1.5/5	0.041	0.0352	0.0059	0.43	0.30	0.49	0.0369
	1	1.241	2.360	1.00	1.00	1.00	1.41	1.000	1.5/5	0.034	0.0299	0.0077	0.49	0.29	0.50	0.0311
	8	2.481	2.360	2.00	2.00	2.00	2.83	1.000	1.5/5	0.054	0.0444	0.0065	0.79	0.52	0.61	0.0471
	8	2.481	2.360	2.00	2.00	2.00	2.83	1.000	1.5/5	0.050	0.0417	0.0081	0.82	0.49	0.62	0.0441
	8	2.481	2.360	2.00	2.00	2.00	2.83	1.000	1.5/5	0.043	0.0367	0.0111	0.76	0.46	0.64	0.0385
	27	3.722	2.360	3.00	3.00	3.00	4.24	1.000	1.5/5	0.079	0.0600	0.0044	0.67	0.56	0.69	0.0651
	27	3.722	2.360	3.00	3.00	3.00	4.24	1.000	1.5/5	0.066	0.0522	0.0065	0.77	0.58	0.69	0.0560
	27	3.722	2.360	3.00	3.00	3.00	4.24	1.000	1.5/5	0.055	0.0451	0.0094	0.88	0.56	0.72	0.0479
	64	4.963	2.360	4.00	4.00	4.00	5.66	1.000	1.5/5	0.061	0.0490	0.0091	0.91	0.80	0.69	0.0524
	64	4.963	2.360	4.00	4.00	4.00	5.66	1.000	1.5/5	0.053	0.0437	0.0117	0.93	0.78	0.72	0.0464
	64	4.963	2.360	4.00	4.00	4.00	5.66	1.000	1.5/5	0.047	0.0396	0.0147	0.97	0.76	0.78	0.0417
	125	6.204	2.360	5.00	5.00	5.00	7.07	1.000	1.5/5	0.108	0.0754	0.0035	0.99	0.87	0.74	0.0836
	125	6.204	2.360	5.00	5.00	5.00	7.07	1.000	1.5/5	0.059	0.0477	0.0123	1.02	0.91	0.76	0.0509
	125	6.204	2.360	5.00	5.00	5.00	7.07	1.000	1.5/5	0.048	0.0403	0.0185	1.07	0.93	0.79	0.0425

Table B-2: (Continued)

	V (cm^3)	d_s (cm)	γ_s (g/cm^3)	a (cm)	b (cm)	c (cm)	L (cm)	SF $f(a,b,c)$	t/b	h (m)	R (m)	S	V_{vc} (m/s)	V_{cc} (m/s)	V_{bc} (m/s)	R_b (m)
SPHERICAL PARTICLES	1	1.241	2.360	1.24	1.24	1.24	1.24	0.806	1.5/5	0.052	0.0430	0.0050	0.55	0.42	0.53	0.0456
	1	1.241	2.360	1.24	1.24	1.24	1.24	0.806	1.5/5	0.046	0.0389	0.0064	0.57	0.39	0.57	0.0409
	1	1.241	2.360	1.24	1.24	1.24	1.24	0.806	1.5/5	0.038	0.0330	0.0079	0.54	0.35	0.61	0.0345
	8	2.481	2.360	2.48	2.48	2.48	2.48	0.806	1.5/5	0.083	0.0623	0.0035	0.68	0.71	0.65	0.0678
	8	2.481	2.360	2.48	2.48	2.48	2.48	0.806	1.5/5	0.067	0.0528	0.0053	0.70	0.63	0.69	0.0567
	8	2.481	2.360	2.48	2.48	2.48	2.48	0.806	1.5/5	0.056	0.0458	0.0084	0.72	0.54	0.70	0.0486
	27	3.722	2.360	3.72	3.72	3.72	3.72	0.806	1.5/5	0.077	0.0589	0.0065	0.99	0.92	0.75	0.0638
	27	3.722	2.360	3.72	3.72	3.72	3.72	0.806	1.5/5	0.071	0.0553	0.0083	0.99	0.90	0.79	0.0596
	27	3.722	2.360	3.72	3.72	3.72	3.72	0.806	1.5/5	0.064	0.0510	0.0110	0.98	0.87	0.81	0.0546
	64	4.963	2.360	4.96	4.96	4.96	4.96	0.806	1.5/5	0.070	0.0547	0.0108	1.10	1.09	0.87	0.0589
	64	4.963	2.360	4.96	4.96	4.96	4.96	0.806	1.5/5	0.064	0.0510	0.0123	1.07	1.06	0.89	0.0546
	64	4.963	2.360	4.96	4.96	4.96	4.96	0.806	1.5/5	0.059	0.0477	0.0149	1.07	1.00	0.90	0.0509
	125	6.204	2.360	6.20	6.20	6.20	6.20	0.806	1.5/5	0.067	0.0528	0.0141	1.19	1.19	0.88	0.0567
	125	6.204	2.360	6.20	6.20	6.20	6.20	0.806	1.5/5	0.062	0.0497	0.0171	1.13	1.16	0.90	0.0531
	125	6.204	2.360	6.20	6.20	6.20	6.20	0.806	1.5/5	0.056	0.0458	0.0203	1.17	1.16	0.94	0.0486

Table B-2: (Continued)

	V (cm^3)	d_s (cm)	γ_s (g/cm^3)	a (cm)	b (cm)	c (cm)	L (cm)	SF $f(a,b,c)$	t/b	h (m)	R (m)	S	V_{vc} (m/s)	V_{cc} (m/s)	V_{bc} (m/s)	R_b (m)
RECTANGULAR ARTICLES	8	2.481	2.360	4.00	1.00	2.00	4.12	1.250	1.5/5	0.057	0.0464	0.0047	0.59	0.47	0.51	0.0494
	8	2.481	2.360	4.00	1.00	2.00	4.12	1.250	1.5/5	0.049	0.0410	0.0059	0.64	0.40	0.52	0.0433
	8	2.481	2.360	4.00	1.00	2.00	4.12	1.250	1.5/5	0.041	0.0352	0.0091	0.60	0.37	0.57	0.0369
	27	3.722	2.360	4.50	2.00	3.00	4.92	1.083	1.5/5	0.077	0.0589	0.0029	0.58	0.50	0.60	0.0638
	27	3.722	2.360	4.50	2.00	3.00	4.92	1.083	1.5/5	0.059	0.0477	0.0058	0.60	0.49	0.62	0.0509
	27	3.722	2.360	4.50	2.00	3.00	4.92	1.083	1.5/5	0.048	0.0403	0.0078	0.65	0.44	0.69	0.0425
	64	4.963	2.360	5.33	3.00	4.00	6.12	1.042	1.5/5	0.061	0.0490	0.0067	0.86	0.67	0.69	0.0524
	64	4.963	2.360	5.33	3.00	4.00	6.12	1.042	1.5/5	0.054	0.0444	0.0084	0.88	0.62	0.72	0.0471
	64	4.963	2.360	5.33	3.00	4.00	6.12	1.042	1.5/5	0.047	0.0396	0.0107	0.91	0.60	0.77	0.0417
	125	6.204	2.360	6.25	4.00	5.00	7.42	1.025	1.5/5	0.106	0.0744	0.0025	0.80	0.78	0.70	0.0824
	125	6.204	2.360	6.25	4.00	5.00	7.42	1.025	1.5/5	0.061	0.0490	0.0083	0.83	0.71	0.71	0.0524
	125	6.204	2.360	6.25	4.00	5.00	7.42	1.025	1.5/5	0.050	0.0413	0.0123	0.90	0.66	0.73	0.0437

Table B-2: (Continued)

	V (cm^3)	d_s (cm)	γ_s (g/cm^3)	a (cm)	b (cm)	c (cm)	L (cm)	SF $f(a,b,c)$	t/b	h (m)	R (m)	S	V_{vc} (m/s)	V_{cc} (m/s)	V_{bc} (m/s)	R_b (m)
RECTANGULAR ARTICLES*	8	2.481	2.360	2.00	1.00	4.00	2.24	0.375	1.5/5	0.070	0.0547	0.0133	1.13	1.12	0.88	0.0589
	8	2.481	2.360	2.00	1.00	4.00	2.24	0.375	1.5/5	0.065	0.0516	0.0147	1.11	1.11	0.90	0.0553
	8	2.481	2.360	2.00	1.00	4.00	2.24	0.375	1.5/5	0.059	0.0477	0.0195	1.07	1.09	0.92	0.0509
	27	3.722	2.360	3.00	2.00	4.50	3.61	0.556	1.5/5	0.079	0.0600	0.0117	1.19	1.20	0.89	0.0651
	27	3.722	2.360	3.00	2.00	4.50	3.61	0.556	1.5/5	0.068	0.0535	0.0165	1.15	1.18	0.90	0.0575
	27	3.722	2.360	3.00	2.00	4.50	3.61	0.556	1.5/5	0.058	0.0471	0.0211	1.10	1.17	0.98	0.0502
	64	4.963	2.360	4.00	3.00	5.33	5.00	0.656	1.5/5	0.089	0.0656	0.0097	1.13	1.27	0.89	0.0718
	64	4.963	2.360	4.00	3.00	5.33	5.00	0.656	1.5/5	0.076	0.0583	0.0138	1.18	1.25	0.96	0.0631
	64	4.963	2.360	4.00	3.00	5.33	5.00	0.656	1.5/5	0.063	0.0503	0.0217	1.20	1.20	0.98	0.0538
	125	6.204	2.360	5.00	4.00	6.25	6.40	0.720	1.5/5	0.085	0.0634	0.0122	1.24	1.29	0.93	0.0691
	125	6.204	2.360	5.00	4.00	6.25	6.40	0.720	1.5/5	0.079	0.0600	0.0141	1.17	1.28	1.02	0.0651
	125	6.204	2.360	5.00	4.00	6.25	6.40	0.720	1.5/5	0.073	0.0565	0.0177	1.18	1.26	1.01	0.0610

* These particles are placed in the most stable position.

Table B-2: (Continued)

	V (cm^3)	d_s (cm)	γ_s (g/cm^3)	a (cm)	b (cm)	c (cm)	L (cm)	SF $f(a,b,c)$	t/b	h (m)	R (m)	S	V_{vc} (m/s)	V_{cc} (m/s)	V_{bc} (m/s)	R_b (m)
IRREGULAR PARTICLES	8	2.481	2.360	4.37	1.00	2.63	4.48	0.905	1.5/5	0.074	0.0571	0.0033	0.56	0.41	0.60	0.0617
	8	2.481	2.360	4.37	1.00	2.63	4.48	0.905	1.5/5	0.062	0.0497	0.0042	0.59	0.40	0.65	0.0531
	8	2.481	2.360	4.37	1.00	2.63	4.48	0.905	1.5/5	0.053	0.0437	0.0060	0.64	0.37	0.62	0.0464
	27	3.722	2.360	5.68	2.00	3.42	6.02	0.995	1.5/5	0.073	0.0565	0.0044	0.65	0.57	0.65	0.0610
	27	3.722	2.360	5.68	2.00	3.42	6.02	0.995	1.5/5	0.064	0.0510	0.0057	0.77	0.50	0.69	0.0546
	27	3.722	2.360	5.68	2.00	3.42	6.02	0.995	1.5/5	0.055	0.0451	0.0077	0.83	0.49	0.72	0.0479
	64	4.963	2.360	7.14	3.00	4.30	7.74	1.044	1.5/5	0.099	0.0709	0.0025	0.77	0.59	0.63	0.0781
	64	4.963	2.360	7.14	3.00	4.30	7.74	1.044	1.5/5	0.061	0.0490	0.0072	0.88	0.65	0.68	0.0524
	64	4.963	2.360	7.14	3.00	4.30	7.74	1.044	1.5/5	0.049	0.0410	0.0103	0.92	0.57	0.70	0.0433
	125	6.204	2.360	8.65	4.00	5.20	9.53	1.077	1.5/5	0.113	0.0778	0.0023	0.75	0.64	0.67	0.0866
	125	6.204	2.360	8.65	4.00	5.20	9.53	1.077	1.5/5	0.068	0.0535	0.0069	0.80	0.71	0.69	0.0575
	125	6.204	2.360	8.65	4.00	5.20	9.53	1.077	1.5/5	0.044	0.0374	0.0151	0.88	0.78	0.70	0.0393